Enhancing Power System Resilience through Computational Optimization

by

Georgios Patsakis

A dissertation submitted in partial satisfaction of the

requirements for the degree of

Doctor of Philosophy

in

Engineering - Industrial Engineering and Operations Research

in the

Graduate Division

of the

University of California, Berkeley

Committee in charge:

Professor Shmuel Oren, Chair
Professor Alper Atamturk
Professor Duncan Callaway

Spring 2020

Enhancing Power System Resilience through Computational Optimization

Abstract

Enhancing Power System Resilience through Computational Optimization

by

Georgios Patsakis

Doctor of Philosophy in Engineering - Industrial Engineering and Operations Research

University of California, Berkeley

Professor Shmuel Oren, Chair

In this dissertation we develop models, solution techniques, and derive policy implications for a number of important applications in improving power system resilience and flexibility: black start allocation and power system restoration, optimal islanding, stochastic unit commitment and flexible wind dispatch. The models we employ are predominantly mixed integer programs (MIPs), i.e. optimization problems in which some of the variables must take integer values. These problems are NP-hard in general, so there is no guarantee that we will be able to obtain solutions within acceptable time and accuracy as the scale of the problem increases. For that reason, we also develop or utilize specialized computational techniques, which broadly fall into one of the following categories: decomposition algorithms that exploit the problem structure (sparsity), reformulations of the problem constraints, and customized heuristics.

We start by exploring the problem of restoring the normal operation of the power system after a blackout. The restoration of the system builds around specific units with the ability to start autonomously (black start units). We formulate a planning problem for deciding the allocation of these units on the grid - black start allocation (BSA) - in an optimal way, while simultaneously optimizing over the possible restoration plans. We include, among others, considerations for thermal limits of lines, alleviating overvoltages, and constraints to model the startup curves of generators. Due to the size and complexity of the resulting MIP, commercial solvers are unable to tackle it directly. We construct a randomized heuristic based on linear programming relaxations of the optimization problem and an understanding of the underlying physics of the power grid to aid the solvers. The heuristic execution is parallelized and implemented on a high-performance computing environment. We are able to obtain solutions with optimality guarantees within reasonable times for test power systems with a few hundred buses.

We proceed to extract a substructure of the feasible region from any problem in power systems that employs reconfiguration of the physical topology (i.e. switching on/off of generators, branches, and buses): each energized island in the power system needs to contain at least one energized generator. We explore reformulations that describe the feasible region corresponding to this require-

ment. We employ two families of valid inequalities to strengthen the formulation, both exponential in size, but separable in polynomial time. We study polyhedral properties of the integer hull and the strength of some of these inequalities under simplifying assumptions. We proceed to conduct computational experiments for two problems in which the substructure appears: the optimal islanding problem and a simplified version of the BSA problem. We are able to observe significant computational benefits by using suitable reformulations for both problems. Finally, we describe an approach to obtain solutions with an optimality guarantee for a simplified model of BSA in a synthetic test case with 2000 nodes representative of Texas.

We extend the modeling framework of the BSA problem to accommodate for uncertainty in the power outages. Specifically, we consider optimal allocations of the black start units over a number of scenarios of partial or total outages. These scenarios may also include irreparable damage caused to components of the system. The resulting stochastic mixed integer program exhibits sparsity, so we employ a decomposition algorithm by scenario to solve instances of the problem.

We then return to the optimal islanding problem to examine it in more detail. We observe that, despite the formulation improvements, the branch and cut algorithm is still fairly slow for an online application of that scale, which requires to act within seconds to prevent a cascaded outage of the system. For that reason, we propose a heuristic based on a reformulation of the optimization into a problem in graph theory. We utilize an algorithm to obtain heuristic solutions with high computational efficiency and good quality compared to state-of-the-art techniques.

To conclude this dissertation, we introduce a framework for evaluating the cost of priority dispatch for wind power. Renewable generation is commonly considered a must-take resource in power systems, despite the technical capabilities of current wind turbines to dispatch at levels lower than their available output. The cost of that policy compared to one that instead optimizes over the available wind output is evaluated for a reduced California system, by employing a two-stage stochastic program for stochastic unit commitment. A scenario decomposition algorithm for the resulting large-scale MIP, parallelized on a high-performance computing environment, enables us to obtain near optimal solutions and calculate the difference in cost between the two policies.

To my extended family

Contents

List of Figures

List of Tables

Acknowledgments

I want to offer my heartfelt thanks to my PhD advisor, professor Shmuel Oren, for his support throughout my graduate life. After my meetings with him, I felt appreciated and motivated to continue working on my research. He was always available whenever I asked for help or advice. His support and trust were not just words, but rather explicitly tangible: He nominated me to be the next instructor for a Berkeley course when he stepped down from teaching it, which ended up being one of the most enjoyable things I did while at UC Berkeley. He encouraged me to take internships without imposing any constraints, so as to best explore my interests. He even supported me when I had a crisis in my personal life by offering probably the most useful advice anyone had offered me at the time. He is always present in my happy academic moments, often being more excited than I am. He was even fully supportive when, contrary to his expectations, I decided to continue my career outside academia after my graduation. My advisor has been a fatherly figure in my life over the past five years.

I would like to express my gratitude to my collaborators, Deepak Rajan and Ignacio Aravena. When Deepak got to know me through his course on integer programming and asked me to join him for an internship at the Lawrence Livermore National Laboratory, I did not expect that the outcome of this collaboration would shape my interests and deeply influence my PhD. I owe a great part of my current knowledge, personality, and goals to his teaching, mentoring, and friendship. He was an outstanding mentor, always available and interested in my research progress, and always offering useful advice. Through my internships at the lab, I also got to know Ignacio. Ignacio offered me invaluable technical help and guidance on high performance computing and research during my first steps. Our frequent formal and informal research meetings at random (though arguably with a concentrated distribution) cafes across the US were among the most enjoyable parts of my PhD experience. At this point, I consider Deepak, Ignacio, and their families, to be very close friends.

I would like to thank the members of my PhD committee, professor Alper Atamturk and professor Duncan Callaway, for their time and for their useful comments.

I would like to thank professor Javad Lavaei. He included me in his group meetings throughout my PhD and I learned a lot from being both on the presenting and on the attending side. His mathematical intuition was always impressive and helped me gain understanding on many areas of optimization outside my research focus. He also gave me the opportunity to serve as a guest lecturer in his graduate course, for which I am also grateful.

I would like to thank Anthony Papavasiliou, who was the person who convinced me to come to UC Berkeley for my PhD among my different choices at the time, and for his support during my first steps of research.

I would like to thank professor Dorit Hochbaum for a very interesting course that deeply influenced me and my interests, including part of the work in this thesis. Her algorithm for approximating the normalized cut is used in Chapter 5.

I would like to thank Jenny Rios from PG&E for her invaluable help and guidance in understanding the important considerations during the power system restoration process and for inviting me to the restoration drills of PG&E.

I would like to thank professor Rhonda Righter and professor Phil Kaminsky for their individual support, for our enjoyable interactions, and for being wonderful people.

I would like to thank Richard Chen for the creative experience of working with him during my time at Amazon.

I would like to thank Robert Phillips for our pleasant conversations and for agreeing to serve as a guest speaker in my course.

I would like to thank Stavros Papathanassiou, Costas Vournas, and Nikos Hatziargyriou, my beloved professors from my undergraduate studies, with whom I still keep in touch. I would also like to thank Petros Karamanakos, who was the person who introduced me to scientific research, and Sotirios Nanou who was my collaborator in my undergraduate thesis research.

I would like to express my gratitude to the late Shabbir Ahmed, who was one of the nicest people I had the pleasure to talk to and get advice from, and deeply influenced my work.

I would like to thank the Farkas Boys (Salar Fattahi, Pedro Hespanhol, Matt Olfat) and the Greek Squad (Chris Adamopoulos, Harry Andreades, Fotis Iliopoulos, Georgios Moschidis, Vrettos Moulos, Paris Siminelakis, Panos Zarkos) for being like a family to me at Berkeley.

Among my friends during my time at Berkeley, I would also like to thank Jiaying Shi, Chen Chen, Paula Lipka, Clay Campaigne, Zhu Yang, Dean Grosbard, Richard Zhang, Cedric Josz, Alfonso Lobos, Igor Molybog, Han Feng, Sang Woo Park, Yuhao Ding, Quico Spaen, Kevin Li, Arman Jabbari, Vasiliki Kouva, Christina Alamana, Areti Papakonstantinou, Dimitris Tsipras, Kyriakos Axiotis, George Charitos, Eleni Antonelli, Aristotelis Magganas, Grace Jiang, George Papadopoulos, Theodora Zagoriti, Antonis Manousis, Orestis Vassios, Rose Falanga, Cy Silver, Yonatan Mintz, and Andres Gomez for the time we spent together. I would also like to thank my friends in Greece, who made my vacation time so much more enjoyable and helped me recharge to continue my PhD.

This thesis is dedicated to my extended family: my parents, my brother, my aunts and uncles, my grandparents, my cousins, my close friends, and all the people who contributed to my upbringing and shaped me to become the person I am today.

I would like to acknowledge the Onassis Foundation for financially supporting me throughout my PhD. I would also like to acknowledge the Tsinghua-Berkeley Shenzhen Institute (TBSI), the Power Systems Engineering Research Center (PSERC), the Lawrence Livermore National Laboratory (LLNL), and the Army Research Office (ARO grant W911NF-17-1-0555) for funding different parts of this research.

Chapter 1

Introduction

1.1 Abstract

In this dissertation we consider a number of applications in the power systems literature and practice, related to enhancing the resilience or flexibility of the system: power system restoration and black start allocation, optimal islanding, stochastic unit commitment. Our goal is to develop tools to make operational or planning decisions, and in order to do so we need to utilize a number of techniques to solve instances of these problems. In this introduction, we first briefly define resilience, reliability, and flexibility in the context of power systems. We motivate each application, its importance, and the modeling choices made, at the chapter we first introduce it. However, the techniques we employ for all the applications fall into the same few general categories: customized heuristics, reformulations, decomposition algorithms. We motivate the use of such techniques in the introduction. The introduction is by no means a complete treatment of computational and theoretical considerations regarding combinatorial optimization or mixed integer programming techniques - we merely present some results that will become useful in the chapters that follow. We conclude this chapter by giving a general outline of the dissertation. The target audience of the presentation has a background in power systems and basic optimization knowledge at a graduate level.

1.2 Power System Resilience, Reliability, and Flexibility

Electricity supply is such a ubiquitous commodity, that the full extent of the consequences from a sustained electricity outage are often not fully comprehensible. These vary from the interruption of house and public lighting, refrigeration and the internet, to the shutdown of banking and ATM systems, the water supply, raw sewage processing, cell phone communications, and farming operations. All of the above occurred during the Northeast blackout of August 2003 [95], which affected tens of millions of people for weeks. Such concerns are amplified due to a rapid transformation in the power grid: The generation mixture moves away from the traditional paradigm due to the introduction of renewables, distributed generation, electric vehicles, micro-grids, and storage. The power system infrastructure, built to a large extent about half a century ago, is aging. The climate is changing and extreme events (wildfires, hurricanes) are becoming more frequent. Cyber-security threats are becoming an important concern for a power system that relies increasingly more on the information infrastructure and automation. All of these factors have led to a widespread interest for enhancing power system resilience.

Resilience refers to the ability of the system to withstand and reduce the magnitude or duration of disruptive events, such as natural disasters [116, 141]. A typical example, also considered in this thesis, is the ability of the system to restart after an extended blackout (black start). Another example we will consider is intentional islanding, where in order to prevent a widespread system outage after a large disturbance, the operator switches off lines in the system to create smaller islands that can be easily controlled.

A related term to resilience is power system reliability [52], which refers to the ability of the grid to provide uninterrupted power to the customers. One difference between resilience and reliability in the rarity and intensity of the events considered as interruptions. For example, local outages that get resolved within minutes, or faults in a few lines that may lead to small scale power interruptions, lie within the realm of reliability - in fact such events are pretty common and operators deal with them on a daily basis. On the contrary, an earthquake or hurricane that can take out a very large part of the grid is fairly rare, but its consequences are far more serious. Such an event will not be part of a reliability study, but falls within the realm of resilience.

In this dissertation, we will briefly address reliability concerns when we talk about stochastic unit commitment. In that problem, the operator seeks for a generation dispatch a day before operation, and considers to that end a number of possible scenarios for the day ahead. Scenarios include renewable energy outcomes, but also possible system faults (such as faults in a few lines or generators). Because of that, the resulting generation dispatch will be able to satisfy the load (or at least will incur small load shed) even if a few lines or generators suffer failures (at least in the case this scenario was included in the optimization). Examples of essential reliability services include voltage support, operating reserves, frequency services, and reactive power support.

One more difference between resilience and reliability is that the former usually has an integral time component to it, which is also reflected in the metrics used to measure resilience. To be more precise, we are interested in how the system performs over time before, during, and after the large scale disturbance. For example, in the case of restoration, we will be interested in the proportion of the system restored over time, or in the loss of load over time.

Yet another concern for the power system is its flexibility [117]. Flexibility is a term mostly used for the measures taken to ensure that, as the generation mix moves away from traditional generation sources to new ones (distributed generation, renewables, microgrids, storage, electric cars), the grid will still be able to adapt and satisfy the demand economically and reliably. Flexibility concerns include how the power system can adapt over different time scales, such as ensuring voltage stability and frequency response in the short term, or facing a potential long term rise in gas prices. One example of a paradigm change that can lead to increased grid flexibility, and is considered in this dissertation, is the utilization of the advanced controls of current wind turbines to improve the economic operation of the system. Specifically, instead of fully injecting all available wind generation to the system through priority dispatch as is the case in Europe, optimizing the output of the wind turbines over the available range can lead to increased economic efficiency.

Optimization models have a central role in evaluating and implementing operational changes in the grid. Many power systems applications that involve in particular enhancing the resilience, reliability, and flexibility of the system are modeled using mixed integer programming. These applications often need to describe discontinuous phenomena, such as changes in the state of different components. The use of binary variables is a convenient modeling tool for that purpose. Since this dissertation heavily uses such models, the next three sections are devoted to briefly summarizing the most important concepts necessary to understand part of the main text of the dissertation.

1.3 Mixed Integer Linear Programming

One common point between all of the applications we consider in this thesis is that they can be formulated as large scale mixed integer linear programs (MILPs). More specifically, we only consider optimization problems with rational coefficients that require that some of the variables are restricted to be binary (i.e. belong to the set $\mathbb{B} = \{0, 1\}$). A general form for these types of problems is:

$$\begin{aligned} \underset{\boldsymbol{x},\boldsymbol{y}}{\text{minimize}} \quad & \boldsymbol{c}_x^T \boldsymbol{x} + \boldsymbol{c}_y^T \boldsymbol{y} \\ \text{subject to} \quad & \boldsymbol{A}\boldsymbol{x} + \boldsymbol{B}\boldsymbol{y} \geq \boldsymbol{b} \\ & \boldsymbol{x} \in \mathbb{B}^n \\ & \boldsymbol{y} \in \mathbb{R}^p \end{aligned} \tag{1.1}$$

where $\boldsymbol{A} \in \mathbb{Q}^{m \times n}$, $\boldsymbol{B} \in \mathbb{Q}^{m \times p}$, $\boldsymbol{c}_x \in \mathbb{Q}^n$, $\boldsymbol{c}_y \in \mathbb{Q}^p$, $\boldsymbol{b} \in \mathbb{Q}^m$, and at least one variable is restricted be binary ($n \geq 1$). For the case where $n = 0$, optimization (1.1) corresponds to a linear program (minimizing a linear objective over a polyhedron) and can be solved efficiently both in theory and in practice. On the other hand, MILPs are NP-hard in general, so it is not (yet) known if an efficient (polynomial in the input size) algorithm exists to solve them. There are, however, algorithms that, under mild technical conditions, are guaranteed to yield an optimal solution of the optimization problem if one exists, in finite time. Such algorithms are: branch and bound, the cutting plane algorithm, and a combination of the two, branch and cut, which is the state of the art in solving MILPs in any commercial software. These algorithms, as well as all of the concepts discussed in sections 1.3 and 1.4, are described in any textbook on integer programming [33, 151].

Branch and cut proceeds by updating lower bounds (LB) and upper bounds (UB) for the problem objective (i.e. values that are guaranteed to be lower and higher respectively than the optimal objective). Termination typically comes when the bounds come sufficiently close to each other, according to a desired accuracy. This accuracy is commonly calculated for a minimization problem as $\frac{\text{UB}-\text{LB}}{|\text{UB}|}$, a quantity referred to as the optimality gap guarantee. The algorithm relies on the fact that solving linear programs can be done reliably and efficiently. We especially care about the linear program (LP) that arises from relaxing the integrality requirement. Specifically, define the region:

$$S = \{(\boldsymbol{x}, \boldsymbol{y}) \in [0,1]^n \times \mathbb{R}^p : \boldsymbol{A}\boldsymbol{x} + \boldsymbol{B}\boldsymbol{y} \geq \boldsymbol{b}\} \tag{1.2}$$

Using this notation, optimization (1.1) is expressed:

$$\begin{aligned} z_{\text{MIP}} = \underset{\boldsymbol{x},\boldsymbol{y}}{\text{minimize}} \quad & \boldsymbol{c}_x^T\boldsymbol{x} + \boldsymbol{c}_y^T\boldsymbol{y} \\ \text{subject to} \quad & (\boldsymbol{x}, \boldsymbol{y}) \in S \\ & \boldsymbol{x} \in \mathbb{Z}^n \end{aligned} \tag{1.3}$$

We refer to S as a formulation for (1.3). We define the LP relaxation of (1.3) corresponding to formulation S to be:

$$\begin{aligned} z_{\text{LP}}(S) = \underset{\boldsymbol{x},\boldsymbol{y}}{\text{minimize}} \quad & \boldsymbol{c}_x^T\boldsymbol{x} + \boldsymbol{c}_y^T\boldsymbol{y} \\ \text{subject to} \quad & (\boldsymbol{x}, \boldsymbol{y}) \in S \end{aligned} \tag{1.4}$$

Solving the LP relaxation provides a lower bound ($z_{\text{LP}}(S) \leq z_{\text{MIP}}$) to (1.3) (since we relaxed the integrality constraints) and is one of the first steps in branch and cut. The algorithm, after possibly introducing additional inequalities, proceeds to "branch" by creating two or more subproblems and solving the LP relaxations of each. Based on this process, the lower bound is updated.

1.4 Reformulations and Valid Inequalities

Now consider a set $\tilde{S} = \{(\boldsymbol{x}, \boldsymbol{y}) \in [0,1]^n \times \mathbb{R}^p : \tilde{\boldsymbol{A}}\boldsymbol{x} + \tilde{\boldsymbol{B}}\boldsymbol{y} \geq \tilde{\boldsymbol{b}}\}$ for some rational matrices $\tilde{A}, \tilde{B}, \tilde{b}$ such that $\tilde{S} \subset S$ (i.e. the set $\tilde{S}$ is a subset of S) and the restriction of the set to only integer values of $\boldsymbol{x}$ yields the same region H, i.e $H = \{(\boldsymbol{x}, \boldsymbol{y}) \in \tilde{S} : \boldsymbol{x} \in \mathbb{Z}^n\} = \{(\boldsymbol{x}, \boldsymbol{y}) \in S : \boldsymbol{x} \in \mathbb{Z}^n\}$. We refer to $\tilde{S}$ as a stronger formulation for H than S. It also holds from (1.4) that $z_{\text{LP}}(\tilde{S}) \geq z_{\text{LP}}(S)$, which means that a stronger formulation yields at least as good a bound for problem (1.3). Since continuous relaxations are solved at every step of the algorithm and the quality of lower bounds plays a significant role to the termination of the algorithm, a strong formulation is likely to lead to a smaller search space. On the other hand, it is often the case that strong formulations require the solution of larger LP problems (more variables or constraints), which may adversely influence the execution time of the algorithm - the trade-off is usually decided based on computational experiments for every instance.

Among all strong formulations, the convex hull $\text{conv}(H)$ of the feasible region H, which consists of all convex combinations of points in H, is the strongest (it is a subset of all convex formulations). It can be shown that $\text{conv}(H)$ is also a (rational) polyhedron (Meyer 1974). The notion

of the convex hull is important because solving a linear program over conv(H) turns out to yield the same optimal value as the (non-convex) optimization over H.

The problem is that in most cases it is hard or impractical to find a description for conv(H). Even if we are able to find a description, it will likely contain a very large number of constraints. In fact, if our original optimization problem is NP-hard, the linear constraints necessary to describe the convex hull are at least exponential in the input size, unless $P = NP$. On the other hand, if we are able to describe the convex hull using linear constraints of size pollynomially bounded by the input size, the optimization over H can be solved in polynomial time. A statement even more general than that holds true: if we can solve the separation problem for conv(H) in polynomial time, then the optimization over H can be solved in polynomial time (by an argument that uses the ellipsoid method) [151]. The separation problem is the following: given a point, either verify that it belongs to conv(H) or provide a linear inequality that separates it from conv(H), i.e. an inequality that is satisfied by all points in conv(H) but is violated by the given point.

A linear inequality $\boldsymbol{\alpha}^T\boldsymbol{u} \geq \beta$ that is satisfied by all points $\boldsymbol{u} \in H$ (hence also by all points in conv(H)) is called valid for H. These inequalities are important since they often help obtain a stronger formulation for H. A set F is called a face of conv(H) if there exists a valid inequality $\boldsymbol{\alpha}^T\boldsymbol{u} \geq \beta$ for conv(H) such that $F = \{\boldsymbol{u} \in \text{conv}(H) : \boldsymbol{\alpha}^T\boldsymbol{u} = \beta\}$. That is, the valid inequality is satisfied with equality at F. In some sense, the size of F gives an indication of how close the inequality is to the the set conv(H) - a large set F indicates that the inequality is tightly close to the convex hull.

To express the last statement in mathematical terms, we first need the notion of the dimension of a polyhedron P (the relevant polyhedron in our case is conv(H)). The dimension of P, dim(P), is given by the largest k such that we can find $k+1$ affinely independent points in P. If the dimension of the variable space is equal to the dimension of P, P is called full dimensional. A face of P is also a polyhedron. A face F is called a facet if $\dim(F) = \dim(P) - 1$. The corresponding valid inequality is called facet-defining. In some sense, a facet-defining inequality is the strongest valid inequality we can devise.

A more general and careful treatment of strong formulations and the theory of valid inequalities can be found in [144] and [33], as well as most textbooks on integer programming.

1.5 Heuristics

The solver obtains lower bounds of the minimization problem (1.3) by solving suitable LP relaxations, as we mentioned. The upper bounds of the algorithm, on the other hand, correspond to integer feasible points for the full problem (points in H) and come from two main sources: either the LP relaxation of a node solve turns out to be integer feasible, or a heuristic algorithm is used to obtain a feasible point. The solver maintains the best upper bound found so far and the corresponding point (incumbent). Good upper bounds in combination with strong formulations help with pruning: if a node relaxation yields an optimal objective that is worse than the incumbent objective, we need not explore this node any further.

Solvers use numerous types of heuristics to obtain good solutions. Simple rounding heuristics try to obtain feasible points by rounding the variable values of an LP relaxation solution at a node. Diving heuristics combine fixing some variables to global entries and reoptimizing. Local search heuristics do a search around feasible or infeasible points (usually by changing the values for a subset of variables) to obtain feasible points with possibly better objective.

It is generally not known in advance how effective particular heuristics will be in obtaining good feasible points. Therefore, it is often the case that the default heuristic strategies of commercial solvers will not be effective for certain problem classes or instances. That is why, in some cases, knowing the structure of a problem can help construct specialized heuristics that will be effective to get good feasible points for the particular application. MIP solvers allow user heuristics or user initialization points to be incorporated in the branch and cut algorithm to accommodate for such cases.

Heuristics of course do not have to be tied to a branch and bound framework. Any algorithm that can potentially obtain feasible points to the optimization is a heuristic. Effective heuristics have small execution times and usually use the structure of the problem to obtain feasible points with a good objective. However, there is typically no guarantee for the performance of a heuristic - it is unknown how close the obtained objective is to the optimal one.

1.6 Decomposition Algorithms

Large-scale optimization problems derived from applications can often prove hard to solve directly. For example, in the case of MILPs, a large number of variables may lead to slow LP solves, or the poor quality of lower and upper bounds may lead to a large branch and bound tree. Often, however, the problem exhibits structure (which is commonly caused by a specific sparsity pattern of the constraint matrix) that can be exploited to give rise to a decomposition algorithm. The purpose of a decomposition algorithm in general is to solve smaller optimization problems that iteratively approximate the solution of the original optimization problem, usually by providing lower and/or upper bounds for the original optimization problem. These smaller problems usually come from omitting part of the variables or constraints of the problem (often after first reformulating the problem) and using a modified objective.

There are multiple decomposition techniques used in the literature, often directed towards specific applications. The most commonly used are variations of Lagrangian relaxation, Dantzig-Wolfe decomposition, and Benders decomposition [151]. It should be noted that most decomposition algorithms are not solution techniques solely for MIPs, but rather general techniques that may take a specific form for MIP applications. In this dissertation, we will mainly use decomposition techniques for stochastic programs. We introduce the relevant general framework below.

Stochastic Programming

Stochastic programming is a framework for optimization problems that involve uncertainty. While there are many modeling approaches, in this work we only deal with problems that have

the following format. We assume we are given a finite set of scenarios S, with a corresponding probability π_s for the realization of scenario $s \in S$. We wish to make a decision $\boldsymbol{x} \in X$, which will lead to a bounded cost $f_s(\boldsymbol{x})$ if scenario s is realized. Note that the cost $f_s(\boldsymbol{x})$ may come from the solution of a subsequent optimization problem, to which $\boldsymbol{x}$ and the scenario s are inputs. We want to make a decision $\boldsymbol{x}$ that minimizes the expected cost over the scenarios. This can be formulated as the following optimization problem:

$$\begin{aligned} \underset{\boldsymbol{x}}{\text{minimize}} \quad & \sum_{s \in S} \pi_s f_s(\boldsymbol{x}) \\ \text{subject to} \quad & \boldsymbol{x} \in X \end{aligned} \tag{1.5}$$

Solving this optimization might be computationally intractable due to the number of scenarios. We can equivalently reformulate the problem as follows, by adding variables $\boldsymbol{x}_s$:

$$\begin{aligned} \underset{\boldsymbol{x}_s, \boldsymbol{x}}{\text{minimize}} \quad & \sum_{s \in S} \pi_s f_s(\boldsymbol{x}_s) \\ \text{subject to} \quad & \pi_s \boldsymbol{x}_s = \pi_s \boldsymbol{x}, s \in S \\ & \boldsymbol{x}_s \in X, s \in S \end{aligned} \tag{1.6}$$

We refer to the constraints $\pi_s \boldsymbol{x}_s = \pi_s \boldsymbol{x}$ as the *non-anticipativaty* constraints. By relaxing them, we obtain a lower bound to the original optimization [16] for any value of the Lagrangian multiplier $\boldsymbol{w} = \{\boldsymbol{w}_s\}_{s \in S}$:

$$\begin{aligned} g(\boldsymbol{w}) \; = \underset{\boldsymbol{x}_s, \boldsymbol{x}}{\text{minimize}} \quad & \sum_{s \in S} \pi_s \left(f_s(\boldsymbol{x}_s) + \boldsymbol{w}_s^T \boldsymbol{x}_s \right) - \sum_{s \in S} \pi_s \boldsymbol{w}_s^T \boldsymbol{x} \\ \text{subject to} \quad & \boldsymbol{x}_s \in X, s \in S \end{aligned} \tag{1.7}$$

We can decompose this optimization problem by scenario. The best possible bound comes from maximizing over possible values of $\boldsymbol{w}$:

$$\begin{aligned} \underset{\boldsymbol{w}}{\text{maximize}} \; g(\boldsymbol{w}) \; = \quad & \underset{\boldsymbol{w}_s}{\text{maximize}} \; \sum_{s \in S} \pi_s g_s(\boldsymbol{w}_s) \\ & \text{subject to} \; \sum_{s \in S} \pi_s \boldsymbol{w}_s = 0 \end{aligned} \tag{1.8}$$

where we define for every scenario $s \in S$:

$$\begin{aligned} g_s(\boldsymbol{w}_s) \; = \underset{\boldsymbol{x}_s}{\text{minimize}} \quad & f_s(\boldsymbol{x}_s) + \boldsymbol{w}_s^T \boldsymbol{x}_s \\ \text{subject to} \quad & \boldsymbol{x}_s \in X \end{aligned} \tag{1.9}$$

Note that the constraint $\sum_{s \in S} \pi_s \boldsymbol{w}_s = 0$ is explicitly imposed to ensure that the objective of the minimization problem remains bounded (since $\boldsymbol{x}$ is unconstrained). For any feasible $\boldsymbol{w}$, we obtain a lower bound to our original problem (1.5) by solving $|S|$ independent optimization problems.

In order to improve the bound, a projected subgradient optimization algorithm can be used for maximizing g (since it is convex but not necessarily differentiable).

We can also obtain upper bounds to (1.5) by evaluating its objective for the feasible points $\boldsymbol{x}_s$ possibly found when solving (1.9) for the different scenarios. Without further assumptions on the structure of f_s, there is no guarantee that the lower bounds and upper bounds obtained will come sufficiently close. For certain applications where exact optimization is not necessary and the quality of the bounds obtained is satisfactory, this might not be an issue. In chapter 6 of this thesis, we will use for our computations a modified algorithm based on these ideas, but with a theoretical guarantee for convergence to the optimum.

1.7 Organization of this Dissertation

This section gives an brief summary of the chapters that follow. An effort has been made so that each chapter is self contained and can be read independently. As a result, there will be some overlap between the chapters.

The remainder of this dissertation is organized as follows:

- **Chapter 2.** Large scale outages (blackouts) of the power system can be caused by equipment failures, natural disasters, human errors, or malicious attacks. These events are rare, but they can result in loss of human life, as well as economic losses of billions of dollars. An important consideration in the recovery process from these events is that not all generators of the power system can restart without already being connected to an energized grid - in fact the operator relies on a few units (black start units) to restart the system. These units can start autonomously and the restoration process builds around them. However, the technical upgrades, maintenance, and testing associated with allocating these units, as well as the fact that their use as black start units will be infrequent, impose budget constraints on the allocation of these units across the grid. In chapter 2, we develop a model for the allocation of black start units, subject to such a budget constraint.

  Our optimization model captures successive snapshots of the restoration state of the power system for time steps within a finite time horizon, with consideration for a number of constraints: generator startup curves, active power balance, reactive power balance and overvoltages, and line flows. Binary variables are associated with the restoration of each component in the system (buses, branches, generators), for a fixed time horizon. Commercial solvers had difficulty finding feasible solutions to the optimization for the instances considered, so we used the underlying physics of the problem to develop a randomized heuristic based on relaxations of the problem. Specifically, we energize the system in steps, checking reactive power compensation to energize transmission lines and prevent overvoltages, and active power compensation to energize new generators. Multiple instances of the heuristic are executed in parallel on a high performance computing environment. While the heuristic can be used independently to find restoration sequences, we instead feed these feasible solutions as initialization to the branch and cut algorithm. A commercial solver is then used to obtain

restoration sequences better than (or at least as good as) the initialization. Finally, since we used simplified models of ac power flow in the optimization models, a verification step must also be performed in the end to ensure that the solutions we found correspond to feasible operational points. These ideas were used to obtain solutions for test systems with a few hundred buses. The work presented in this chapter has been published in [115].

- **Chapter 3.** Equivalent reformulations of the constraints of a MIP often lead to a very different computational performance. Motivated by this observation, we identify a substructure that arises in two power systems applications: the optimal islanding problem and the black start allocation problem. These problems have the common characteristic that nodes, branches, and potentially generators can be on or off, giving rise to a number of possible reconfigurations of the power grid. Regardless of the power system configuration, each energized island needs to have at least one energized generator, a requirement which we refer to as the Island Energization (IE) constraint. In chapter 3, we explore different reformulations of this constraint and how they impact the computations for our two applications.

  Specifically, we define the feasible region that satisfies the IE constraints and write two families of valid inequalities for that region. These families are exponential in size, but both can be separated in polynomial time. Under simplifying assumptions, we can show that some of the inequalities we introduced define facets of the convex hull of the feasible region. We then study the computational performance of the formulations. We first extract a formulation of the optimal islanding problem from recent literature in power systems. Our best performing reformulation solves the problem at least one order of magnitude faster than the original formulation for large instances of the problem. We then examine a simplified version of the black start allocation problem. Again, we obtain a significant difference between our best performing reformulation and the one most commonly used in the power systems literature. Finally, we present a model and a solution approach to obtain a black start allocation for an industrial size system of a few thousand buses. Part of the computational aspects of these results have been published in [114]. The reformulations of the IE constraints are also used within a general framework to solve a power system restoration problem (where the black start units are known and fixed in advance and the goal is to restore the system to normal operation) described in [9], which utilizes a more detailed modeling of the nonlinear ac power flows described in [8].

- **Chapter 4.** In this chapter we extend our modeling approach for the black start allocation problem to accommodate for stochasticity. Specifically, the black start units are chosen in a way that optimizes their performance over a number of possible scenarios. These scenarios include outages (partial or total blackouts) of the power system, as well as unavailability of components (branches, buses) after the outage. We observe that, since the characteristics of the generators (startup curves, capacities, and location) do not change across scenarios, a unit that is a good black start candidate for one scenario will likely be a good candidate for different scenarios. Based on this observation, we suggest the use of a decomposition algorithm from the literature that is expected to perform well for such a setup. As a proof

of concept, we provide simulations on a small scale system. The results of this chapter have been published in [109].

- **Chapter 5.** In this chapter, we dive slightly more into the details of the intentional controlled islanding problem. We already introduced the problem in chapter 3, but there are two main concerns with our treatment there: First, the MIP model presented assumed that the set of coherent generators (which was an input to the optimization problem) is known. Second, even with the improved formulation, the computational times obtained were not satisfactory for a real time algorithm that needs to act within seconds to prevent a cascaded outage. In this chapter, we focus on presenting a heuristic to both obtain coherent generator sets and a line switching action, within acceptable times. In order to develop such an algorithm, we briefly present the small signal system analysis of the power system, through which generator coherency is evaluated. We transform the islanding problem into a normalized cut problem. Then, we use an algorithm from the literature to obtain a heuristic solution. The resulting approach exhibits high computational efficiency and allows for a natural integration of further islanding requirements. The results of this chapter have been published in [112].

- **Chapter 6.** This chapter is devoted to a computational study with policy implications. Renewable energy, such as wind generation, is commonly treated as a must-take resource in power systems (i.e. it is prioritized over other types of generation). This seems reasonable, since wind generation comes at (almost) zero marginal cost. Furthermore, traditional wind generation had limited controlability of its output. However, most current technologies for wind generation offer the ability to control the output at practically any level below the maximum available wind generation. We want to evaluate the (expected) benefit from exploiting this capability for the power system, as the wind integration levels increase.

  In order to motivate this work, we first construct a number of small example power systems that illustrate scenarios in which spilling wind generation leads to a lower cost operation of the system, even though wind generation itself has zero cost. The causes of this behavior in our toy examples are technical minima, startup costs, ramping constraints, or congestion. We further proceed to evaluate the difference in cost between the two policies (must-take and flexible wind generation) in a stochastic unit commitment setup for a simplified California model. For the solution of the resulting large scale mixed integer program, we use a decomposition algorithm based on projected subgradient descent and global cuts, parallelized in a high performance computing environment. In the case of high wind integration, we observe a significant cost benefit, since the additional flexibility offered by wind generation allows more extended use of inflexible, cheap sources of energy. The results of this work have been published in [113].

- **Chapter 7.** The last chapter of the dissertation is devoted to extensions and future directions of research. Some of the work in this dissertation, and especially the models and optimization related to black start allocation, are still at a relatively early stage in the literature. That means there are a number of possible ways that these models can be extended or modified,

and understanding their structure still requires a significant research effort. Other parts of the work, such as the flexible wind dispatch study of chapter 6, were based on well established models and solution techniques, but relaxing the model assumptions in different ways could provide further opportunities for research.

Chapter 2

Optimal Black Start Allocation for Power System Restoration

2.1 Abstract

Equipment failures, operator errors, natural disasters and cyber-attacks can and have caused extended blackouts of the electric grid. Even though such events are rare, preparedness for them is critical because extended power outages endanger human lives, compromise national security, or result in economic losses of billions of dollars. Since most of the generating units cannot restart without connecting to an energized grid, the system operator relies on a few units with the ability to start autonomously, called Black Start (BS) units, to restore the power system. Allocating and maintaining these units is costly and can severely impact the restoration security and time. We formulate an optimization problem to optimally allocate BS units in the grid, while simultaneously optimizing over the restoration sequence.

In this chapter, we first present the main considerations behind black start allocation (BSA) and power system restoration modeling and optimization. We then extend existing optimal BSA models by including grid considerations such as active power nodal balance, transmission switching, nodal reactive power support and voltage limits. In order to aid the branch and bound tree that solves the resulting large scale Mixed Integer Program (MIP), we propose a randomized heuristic that is executed multiple times in parallel on a high-performance computing environment to find feasible solutions. We proceed to solve the IEEE-39, the IEEE-118 and a simplified WECC system with 225 nodes and 136 generators to near optimality.

Nomenclature

Sets

N Set of buses.

E Set of branches (ordered pairs of buses).

G Set of generators.

$G(i)$ Set of generators connected to bus $i \in N$.

T Set of consecutive integer time instances, starting from $1 \in T$.

Variables

δ_i^t Voltage phase of bus $i \in N$ at time $t \in T$.

f_{ij}^t Network flow for energizing paths for branch $(ij) \in E$ at time $t \in T$.

f_g^t Network flow for energizing paths from generator $g \in G$ at time $t \in T$.

$p_{SH_i}^t$ Active power load shed at bus $i \in N$ and time $t \in T$.

p_g^t Active power generation of generator $g \in G$ at time $t \in T$.

p_{ij}^t, q_{ij}^t Active/reactive power flow of branch $(ij) \in E$ at time $t \in T$.

u_{BS_g} Binary variable indicating generator $g \in G$ is a BS generator.

u_g^t, u_i^t, u_{ij}^t Binary variable indicating generator $g \in G$, bus $i \in N$, branch $(ij) \in E$ energized at time $t \in T$ (zero indicates not energized).

v_i^t Voltage magnitude of bus $i \in N$ at time $t \in T$.

Parameters

$\underline{\delta}, \overline{\delta}$ Lower/upper bounds for voltage phases.

ϵ Trade-off coefficient for line energization.

μ Trade-off coefficient for inertia.

B Total budget for BS generator installations.

$B_{SH_{ij}}$ Shunt susceptance of branch $(ij) \in E$.

b_{ij}, g_{ij} Susceptance/conductance for branch $(ij) \in E$.

C_{BS_g} Cost of turning $g \in G$ to a BS generator.

C_i Cost of load shed in bus $i \in N$.

$\cos(\phi_{D_i})$ Power factor of load at bus $i \in N$.

J_g Inertia of generator $g \in G$.

K_{R_g} Ramping rate of generator $g \in G$.

P_{CR_g} Cranking power required to be provided to generator $g \in G$ to initiate its start-up.

$\underline{P}_g, \overline{P}_g$ Minimum and maximum active power generation from generator $g \in G$ after the decomposition.

$P_g^{\min}, P_g^{\max}$ Minimum and maximum active power generation from generator $g \in G$ before the decomposition.

P_{D_i} Available load at bus $i \in N$.

p_g^0 Initial active power of generator $g \in G$.

$\underline{Q}_g$ Minimum reactive power generation from generator $g \in G$.

Q_{SH_i} Shunt reactor for bus $i \in N$.

$\overline{S}_{ij}$ Maximum flow limit for branch $(ij) \in E$.

T_{CR_g} Time between generator $g \in G$ being energized until it can increase its active power from zero.

T_{CRIT_g} Maximum critical time for generator $g \in G$.

u_g^0, u_i^0, u_{ij}^0 Binary parameter indicating the initial state of generator $g \in G$, bus $i \in N$, branch $(ij) \in E$.

$\underline{V}, \overline{V}$ Lower/upper bounds for voltage magnitude.

2.2 Introduction

On August 24, 2003 a fault of a high-voltage power line in Ohio initiated an extended blackout that affected 50 million people for up to two days. The blackout contributed to at least 11 deaths and its cost was estimated at $\$6$ billion [95]. On September 8, 2011 an operator error caused an outage in California and Arizona that deprived 2.7 million people of electricity for up to 12 hours [107]. Natural phenomena, like earthquakes and wind storms, are also usual causes of extended outages; just in 2017 there have been multiple incidents nationwide (3.8 million customers without power due to Hurricane Irma in Florida in September, $800,000$ customers due to a wind storm in Michigan

in March, $500,000$ homes in California in March). Recently, cyber attacks on the grid have been added to the concerns for a blackout, after hackers caused $225,000$ customers to lose power on December 23, 2015, in Ukraine. The North American Electric Reliability Corporation (NERC) and the Electricity Information Sharing and Analysis Center (E-ISAC) have worked to analyze the attack [85] and a lot of research is currently focused on the cyber-security of the power grid. However, in the event where counter measures fail, we need to restore the grid as fast as possible; especially since a hostile attack will try to take advantage of the moments after an outage where security is compromised.

The process of restoring the system back to normal operation involves crucial steps and considerations [54, 89]. Most of the generating units of the grid do not have the ability to restart by themselves, i.e. unless there is already an existing energized grid to connect to. For that reason, the system operators rely on a few units, called Black Start (BS) units, that can start independently. Clearly, the location and technical specifications of these units will directly affect the restoration time and security of the power grid. However, engaging a new generator as a BS unit is costly (in the order of millions of dollars) and is also associated with regular maintenance and testing costs (in the order of hundreds thousands of dollars) [73]. The Electric Reliability Council of Texas (ERCOT) has a biennial BS procurement process that typically procures 14-18 units [128]. The California Independent System Operator (CAISO) recently (May 2017) [18] identified a need for immediately procuring additional BS resources. So far there is no concrete optimization problem utilized to aid the process. The optimal allocation of BS units in the grid is the primary purpose of this chapter.

The main considerations checked by the operators during the restoration process are: restoring critical loads as fast as possible, building paths to energize the non BS units, while maintaining frequency stability and avoiding voltage violations. The power system restoration optimization problem, that incorporates the aforementioned concerns to generate valid restoration sequences, has received some attention recently. In [71, 90], the authors propose a step-wise strategy based on achieving specific milestones in the restoration process. In [134] an optimization problem that includes the generator active power capabilities is considered. However, the grid power flows are neglected and reactive power compensation, which constitutes a major concern for restoration, is not included. In [74] an aggregate reactive power constraint is utilized, but the grid flows are not. These considerations are addressed afterwards through heuristic modifications of the resulting sequence, however the changes undermine the optimality of the final solution. A different modeling approach that includes reactive power considerations is adopted in [22], aiming to motivate the use of microgrids for the BS procedure, which is applied at a 6-bus system. A mixed integer non linear program is formulated in [27] and is heuristically solved using Ant Colony Optimization. Instead of the complete restoration, the sectionalization problem is solved in [146] using binary decision diagrams. An effort to integrate wind power in restoration is made in [61]. Literature reviews of relevant approaches are provided in [23, 157].

Even though the optimization of the restoration sequence is an interesting problem by itself, the need for restoration is a rare event in which the operators expect to base the restoration steps on their experience rather than software output not tested against actual restoration events. However, the allocation and contracting of BS units is a process that usually happens yearly for every

operator, so the decisions associated with preparedness for the rare extended outages constitute an important problem that needs to be solved on a regular basis, even if the actual outage rarely occurs. General guidelines and methodologies for selecting BS units exist both in literature [75, 125, 133] and in restoration manuals [118]. There is limited research, however, on formulating an optimization problem to address the allocation. Recently, in [122], a minimum cost BS procurement problem was formulated, without considering the restoration sequence. In [121] the allocation optimization problem is enhanced by considering active power considerations of the restoration sequence, but not thermal line limits or reactive power compensation.

In this chapter, we formulate and solve the black start allocation (BSA) problem, while also introducing innovations to the modeling of the restoration sequence formulation. The main contributions of this work are the following:

1. We introduce a new modeling approach utilizing one energization binary variable for every time step and one BSA binary variable to capture the widely used capability curves for BS and non BS generating units by decomposing them into two parts, which allows us to formulate the allocation problem in combination with the corresponding power system restoration problem.

2. We solve a BSA problem with a more detailed modeling of the restoration process than existing BSA literature, which is achieved by including constraints on the thermal limits of lines for the steps of the restoration sequence (by employing an approximation for the active and reactive power flows), constraints to alleviate overvoltage (through manipulation of active power flows, reactive power compensation or de-energization of transmission lines), and constraints that ensure the consistency of the grid at every step (allowing de-energization of transmission lines to alleviate overvoltages).

3. Due to the size and structure of the resulting optimization problem, commercial solvers encounter difficulties in identifying feasible solutions to it. For that purpose, we propose a randomized heuristic that is guided by linear programming (LP) relaxations to generate feasible solutions to the optimization problem and aid the solvers.

The energization sequences generated by the optimization problem are checked for ac feasibility in the final step, as in [31, 74]. However, since most of the considerations have already been integrated in the optimization, the changes necessary to achieve ac feasibility are minimal.

The rest of the chapter is organized as follows. In section 2.3, the main concerns of the Power System Restoration Process are mentioned. In section 2.4, the proposed model constraints and objective are outlined. In section 2.5 the proposed heuristic is outlined, and in section 2.6 simulation results for three test cases, the IEEE-39, the IEEE-118, and a simplified WECC system are presented. Finally, in section 2.7 conclusions are drawn and the topics of the subsequent two chapters are motivated. The work of this chapter has been published in [115].

2.3 Power System Restoration

The restoration planning for most systems consists of constructing a plan that incorporates the priorities of the operators to ensure a secure system revival. Usually this plan is associated with the worst-case scenario, i.e. restoration from full blackout. In this section, we go through the basic considerations of the restoration process. Later, we present an optimization model that integrates most of these concerns.

System Identification and Preparation

The first step after a major outage is identifying and assessing the stability and safety of the remaining grid (if any), mitigating equipment and rating issues (voltage and thermal limits for the stable islands), and identifying equipment availability in order to build a restoration plan. Our ability to assess the system state can vary with the design of the protection system, SCADA penetration on both the transmission and distribution systems, and visibility of data, because of the disturbance. Most breakers of the transmission system are (remotely or manually) opened and the distribution is disconnected. Usually, the renewables are also disconnected, due to their intermittency.

Setting Priorities

The strategy for system restoration, whether from a BS resource or from a surviving island, is based on priorities that are dictated by reliability standards and are usually specific to the utility. For example, NERC Reliability Standard EOP-005-2 has identified restoration of off-site power to nuclear power plants as a priority of restoration. Providing power for auxiliary loads in order to energize non BS generating plants, restoration of fast starting units, station service batteries, control centers, major transmission lines, and restoration of stabilizing loads are all restoration priorities to technically support voltage and frequency of the grid during restoration. The ultimate restoration goal is to return the grid to normal operations (e.g. eliminate islands, restore inter-ties and customer load) quickly without compromising safety and reliably.

Reactive Power and Voltage Limits

Energizing transmission lines when served load is low (common during the restoration process) yields Ferranti rise considerations. More specifically, the capacitances of high voltage transmission lines inject reactive power into the system which leads to overvoltages in the endpoints of the energized transmission system, since loads that could induce an opposing voltage drop are not served. Reactive power compensation, to prevent limit violations, is achieved through shunt reactors or other VAR compensation connected to high voltage transmission lines, or synchronous generators that can absorb reactive power after being energized. In addition, grid operators engage in a few standard practices throughout the restoration process in order to keep voltages under check: picking up load with lagging power factor or de-energizing transmission lines.

Active Power and Frequency Regulation

Active power balance for all the islands is important during restoration to ensure the frequency remains within tolerances throughout the process. Frequency stability is directly influenced by the inertia of energized generators. In order to energize more generators, load must be picked up to ensure the generating units can ramp up (especially when technical minima of units must be satisfied). Loads with rotating masses, such as induction machines, may also be preferred during the restoration process for the same reasons.

2.4 Optimization Model

As already mentioned, a BS unit has the ability to start on its own, without being connected into the grid. After a blackout, the BS units are responsible for partly energizing the grid by also providing cranking power to the units that do not possess BS capability. We represent the allocation of BS units using binary decision variables u_{BS_g}, for every generator $g \in G$. The typical way to achieve that is to install a smaller (often diesel) unit that will provide the cranking power. Generators that are already BS units can have a preassigned binary value of 1. If a generator cannot be chosen as a BS unit due to technical considerations, the binary variable is a priori set to zero. The restoration process is signified through binary variables for the various grid components (buses, lines and generators). A value of 1 indicates an energized component. In what follows, we describe the physical constraints and the objective for the BSA problem.

Black Start Allocation Budget Constraint

Costs are assigned for utilizing each one of the generating units as a BS resource. These costs could be set by the system operator (for example, ISO New England offers specific tariffs based on the ratings of generators [73]) or could be the bid of a generator after a call from the operator. The cost reflects not only the dedicated, usually diesel, generating unit used to restart the generator, but also the costs of testing and preserving the capability. For the purposes of modeling, we assume that the annual payments for BS services are converted into a one time capital cost:

$$\sum_{g \in G} C_{BS_g} u_{BS_g} \leq B \tag{2.1}$$

Bus Active Power Balance

The bus balancing constraint has the form:

$$\begin{aligned} &\sum_{j:(ji)\in E} p^t_{ji} + \sum_{g \in G(i)} \left(p^t_g + P_{CR_g}(u_{BS_g} - u^t_g)\right) \\ &- \sum_{j:(ij)\in E} p^t_{ij} = P_{D_i} - p^t_{SH_i}, \forall i \in N, \forall t \in T \end{aligned} \tag{2.2}$$

Constraint (6.6b) stipulates the active power conservation at bus $i \in N$ every time instant $t \in T$. If a generator is chosen to be BS ($u_{BS_g} = 1$), then its cranking power is provided for (by an external source), so it can be immediately energized ($u_g^t = 1$). However, if we want a non BS generator g to be energized, the constraint introduces a negative term $-P_{CR_g}$, so the cranking power needs to be provided for either by a different generator or by flows into the bus. In the initial phases of the restoration, this constraint will ensure that only the generators that are assigned to be BS can actually be energized (i.e. have $u_g^t = 1$).

The load is modeled through a shedding variable that is equal to the total load in the case the bus is not energized:

$$(1 - u_i^t)P_{D_i} \leq p_{SH_i}^t \leq P_{D_i}, \forall i \in N, \forall t \in T \tag{2.3}$$

We note that it is not easy to know the maximum load P_{D_i} of a bus. When load is picked up after an outage, the demand is often greater than before, a phenomenon known as cold load pickup [126]. However, during restoration load is used as a controlable tool to accommodate voltage limits, ensure stable operation of the islands, or satisfy the minimum active power requirements of generators, so its actual maximum value is not central. We are also usually capable to pick it up in small chunks, so we assume a continuous load shedding variable, that can move between zero and maximum value; similar to the approach in [31]. The model currently has no constraints for the rate of load pickup. In the power system restoration literature, the problem of restoring the load is often solved after the restoration sequence is acquired [57, 120], so that more detailed load pickup models can be used. Frequency stability issues become important when the actual load pickup actions are considered [87, 91].

Bus Reactive Power Constraint

Reactive power capacity is important in maintaining the voltages of the power system within reasonable limits. Since the main concern during the restoration process is the capability of the system to absorb the reactive power generated by the high capacitance of the lines, we only consider a single directional constraint approximating the capability of the system units to absorb reactive power. The following constraint is introduced at every bus:

$$\begin{aligned} &\sum_{j:(ji)\in E} q_{ji}^t - \sum_{j:(ij)\in E} q_{ij}^t + \sum_{g\in G(i)} \underline{Q}_g u_g^{\max\{0,t-T_{CR_g}-1\}} \\ &+ \sum_{j:(ji)\in E} \frac{1}{2} B_{SH_{ji}} u_{ij}^t + \sum_{j:(ij)\in E} \frac{1}{2} B_{SH_{ij}} u_{ij}^t + Q_{SHi} u_i^t \\ &\leq (P_{D_i} - p_{SH_i}^t) \tan(\phi_{D_i}), \forall i \in N, \forall t \in T \end{aligned} \tag{2.4}$$

A line injects reactive power $\frac{1}{2} B_{SH_{ij}} V^2 u_{ij}^t$ at each of the buses it connects to, if energized, where the bus voltage V is assumed close to one for this constraint, to allow for a linear formulation. The reactive power can be absorbed by either generators that have been energized at least $T_{CR_g} + 1$ time units in advance, or by reactive compensation connected to the bus Q_{SH_i}, or by loads

with lagging power factor ($\tan(\phi_{D_i}) > 0$). The load is assumed picked up at a constant power factor, as in [31] and [22]. While not a precise approximation, the reactive power constraints ensure that: (i) Every island formed during the restoration process has adequate reactive power absorption capability. To see why this is true, one can add all of the equations (6.6c) for the nodes of an island that may arise in the restoration process. The reactive flows that lead outside the island are set to zero by (2.7). The reactive flows that are within the island cancel each other. What remains is the constraint that the total (aggregate) reactive power absorption capacity of the island exceeds the total reactive power injection by the lines. (ii) There is no reactive power sink (i.e. the reactive power generated by transmission lines must be absorbed by some component of the system). The equations may allow for fictitious reactive power generation, but this is an inferior concern for restoration, since the system typically operates under excessive reactive power generation.

Generator Model

A typical generator startup curve is assumed, as in [74,134], see figure 2.1. The curve is decomposed into two parts, as shown in 2.1. The binary variable u_g^t is associated with the energization state of generator $g \in G$ (i.e. it is 1 for $t \geq t_{start}$). This variable is exogenously defined based on the availability of active power or BS unit assignment in (6.6b). That requirement corresponds to figure 2.1c. The modeling of the generator output in figure 2.1b will now be defined based on the following constraints:

$$0 \leq p_g^\tau \leq \overline{P}_g u_g^t, \forall g \in G, \forall \tau \in \{t, t+1, \ldots, t+T_{CR_g}+1\}, \quad \forall t \in T \cup \{0\} \tag{2.5a}$$

$$p_g^t - p_g^{t-1} \leq K_{R_g}, \forall g \in G, \forall t \in T \tag{2.5b}$$

$$p_g^{t-1} - p_g^t \leq K_{R_g}, \forall g \in G, \forall t \in T \tag{2.5c}$$

Constraint (2.5a) makes sure that the active power can not become positive for at least T_{CR_g} units of time after the generator is energized, both for BS and for NBS generators. Also, the maximum active power limit is imposed at all time instances that the generator has positive active power production. The ramping rate capability is imposed through the constraints (2.5b) and (2.5c). Next, the following constraint for a generator $g \in G$ would ensure that the minimum active power generation limit $\underline{P}_g$ is satisfied, after the cranking time has passed and the generator has ramped up to $\underline{P}_g$.

$$p_g^\tau \geq \underline{P}_g u_g^t\,,\ \forall\, \tau\ \geq (t + T_{CR_g} + {}^{\underline{P}_g}/_{K_{R_g}})\,, \forall t \in T \tag{2.6}$$

Finally, some non BS generators have critical hot times [134], so in these cases a constraint for unit $g \in G$ can be introduced to ensure that the unit will be energized by that time, imposing $u_g^t = 1\,, \forall t \geq T_{CRIT_g}$.

Line Switching

In order to model the formation of islands, a constraint that stipulates that active and reactive flows can only go through lines that are energized needs to be enforced. For that purpose, the ideas

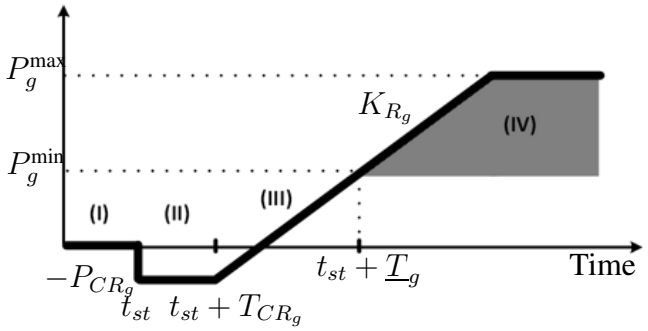

(a) A disconnected generator $g \in G$ (phase I) gets energized at time t_{st} (i.e. u_g^t becomes 1 at $t = t_{st}$) and needs to be cranked for a period of T_{CR_g} (phase II). During the cranking period, the generator absorbs the cranking power P_{CR_g}. (negative generation). The generator then starts to ramp up to its technical minimum $\underline{P}_g$ (phase III) at time $t_{st} + \underline{T}_g$, where $\underline{T}_g = T_{CR_g} + {}^{(P_{CR_g}+P_g^{\min})}/_{K_{R_g}}$. Afterwards, generation can freely move between $P_g^{\min}$ and $P_g^{\max}$, within the ramping capability K_{R_g}. This model appears in other works, such as in [71] and [74]. For the purposes of this work, we decompose the model as the superposition of the two curves below.

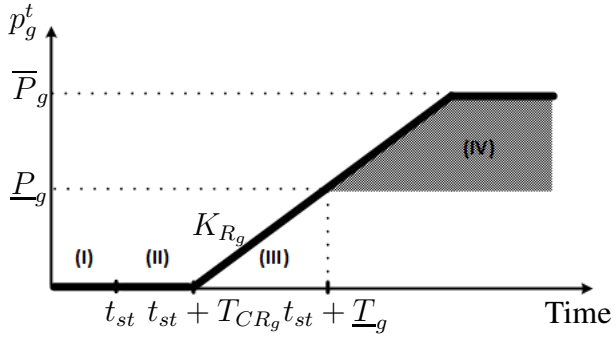

(b) The first part of the decomposed generator model. The generation levels in the graph are defined as $\underline{P}_g = P_g^{\min} + P_{CR_g}$ and $\overline{P}_g = P_g^{\max} + P_{CR_g}$.

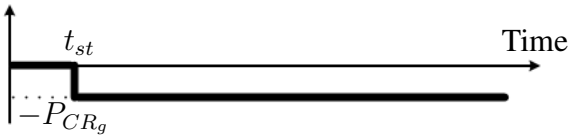

(c) The second part of the decomposed generator model. This is essentially a negative step function to the cranking power of the generating unit at the time of energization ($u_g^t = 1$). The allocation of the BS units allows for u_g^t to become 1, even if there is no external power fed to the unit.

Figure 2.1: Typical generator active power curve and its decomposition into two parts. The parameters vary depending on the type of generator.

from transmission switching [66] are utilized, with a modification to accommodate for reactive power. The same ideas have been utilized in other works on restoration and islanding as well [139].

$$|p_{ij}^t| + |q_{ij}^t| \leq u_{ij}^t \overline{S}_{ij}, \forall (ij) \in E, \forall t \in T \tag{2.7}$$

Constraint (2.7) is an approximation of the constraint $\sqrt{(p_{ij}^t)^2 + (q_{ij}^t)^2} \leq u_{ij}^t \overline{S}_{ij}$ in the following way: if the line is not energized, both equations set its active and reactive power flow to zero. If the line is energized, an apparent power limit is imposed on the line. Due to the inequality $\sqrt{(p_{ij}^t)^2 + (q_{ij}^t)^2} \leq |p_{ij}^t| + |q_{ij}^t|$, constraint (2.7) is tighter than the physical limit (L-1 ball instead of the L-2 ball with the same radius). The two constraints are in disagreement mainly in the area of simultaneously large values of both active and reactive flow, a setting that we rarely expect to occur during the initial steps of restoration (the load is at most 10-20% restored by the end of the time horizon we are considering). Constraint (2.7) is eventually substituted by four linear constraints to eliminate the absolute values.

$$p_{ij}^t = -b_{ij}(\delta_i^t - \delta_j^t) u_{ij}^t, \forall (ij) \in E, \forall t \in T \tag{2.8a}$$

$$q_{ij}^t = \left(-b_{ij}(v_i^t - v_j^t) - g_{ij}(\delta_i^t - \delta_j^t)\right) u_{ij}^t, \forall (ij) \in E, \forall t \in T \tag{2.8b}$$

$$\underline{\delta} \leq \delta_i^t \leq \overline{\delta}, \forall i \in N, \forall t \in T \tag{2.8c}$$

$$\underline{V} \leq v_i^t \leq \overline{V}, \forall i \in N, \forall t \in T \tag{2.8d}$$

Constraints (2.8a) and (2.8b) set the active and reactive power flow of line $(ij) \in E$ to zero, if the line is not energized ($u_{ij}^t = 0$), and impose a linearized approximation of the active and reactive power flows otherwise. Both line susceptances and conductances are considered for reactive power, since eliminating overvoltages during the restoration process is commonly performed not only through reactive power compensation, but also by picking up load to induce active flows. These equations are linearized via a big-M reformulation, as in [66], which combined with (2.7), yields the same feasible region as (2.8a) and (2.8b). For example, constraint (2.8a) yields:

$$b_{ij}(\delta_i^t - \delta_j^t) + p_{ij}^t \leq (1 - u_{ij}^t) M_{ij}, \forall (ij) \in E, \forall t \in T \tag{2.9a}$$

$$b_{ij}(\delta_i^t - \delta_j^t) + p_{ij}^t \geq (u_{ij}^t - 1) M_{ij}, \forall (ij) \in E, \forall t \in T \tag{2.9b}$$

where $M_{ij} = |b_{ij}|(\overline{\delta} - \underline{\delta})$.

Consistency of Energized Grid

A series of constraints need to be imposed to ensure consistency of the grid at any given time point. More specifically, we need to enforce that all the energized buses of the grid at any time instant are connected to an energized generator through a path of energized lines. We will later in

this dissertation refer to this constraint as the island energization constraint.

$$0 \leq f_g^t \leq u_g^t, \forall g \in G, \forall t \in T \tag{2.10a}$$

$$-u_{ij}^t \leq f_{ij}^t \leq u_{ij}^t, \forall (ij) \in E, \forall t \in T \tag{2.10b}$$

$$\sum_{j:(ji)\in E} f_{ji}^t - \sum_{j:(ij)\in E} f_{ij}^t + \sum_{g\in G(i)} f_g^t = \frac{1}{N} u_i^t, \quad \forall i \in N, \forall t \in T \tag{2.10c}$$

(2.10a), (2.10b) and (2.10c) impose a feasibility problem given fixed values of u_g^t, u_{ij}^t and u_i^t for the flows f_{ij}^t and f_i^t. A bus can be energized ($u_i^t = 1$) if there is a feasible flow from one or more of the generators with $u_g^t = 1$, flowing only through branches with $u_{ij}^t = 1$, such that a fictitious load on that bus of $\frac{1}{N} u_i^t$ can be satisfied. Otherwise, the state of that bus has to be $u_i^t = 0$.

Additional constraints that ensure the consistency of the grid are also necessary. If a generator connected to a bus is energized, then the bus is considered energized:

$$u_g^t \leq u_i^t \, , \forall i \in N, \forall g \in G(i), \forall t \in T \tag{2.11}$$

A line can get energized at a time step only if one of the buses connected to it was energized at the previous time step:

$$u_i^t \leq u_i^{t-1} + u_j^{t-1} \, , \forall (ij) \in E, \forall t \in T \tag{2.12}$$

Also, when a branch gets energized, both of the buses connected to it are energized:

$$u_{ij}^t \leq u_i^t, u_{ij}^t \leq u_j^t \, , \forall (ij) \in E, \forall t \in T \tag{2.13}$$

Finally, we assume that buses and generators are picked up only once:

$$u_g^t \geq u_g^{t-1} \, , \forall g \in G, \forall t \in T \tag{2.14a}$$

$$u_i^t \geq u_i^{t-1} \, , \forall i \in N, \forall t \in T \tag{2.14b}$$

Note the same assumption is not made for lines. The reason is that de-energizing lines is a standard practice included in the restoration guidelines that some grid operators have developed to alleviate overvoltages, so our modeling allows for such operating practice. Allowing line de-energization is what makes constraints (2.10a)-(2.10c) necessary in our formulation.

Optimization Objective

The objective of the problem in general will highly depend on the priorities set by the characteristics of each particular system. A generic form can be the following:

$$\text{minimize} \sum_{t\in T} \left(\sum_{i\in N} C_i^t p_{SH_i}^t - \mu \sum_{g\in G} u_g^t J_g - \epsilon \sum_{(ij)\in E} u_{ij}^t \right) \tag{2.15}$$

(4.14) penalizes the load shed (depending on the criticality of the load), incentivizes increasing the total inertia of the energized system, and encourages the complete energization of the grid. The final form of the objective ultimately depends on the priorities of the particular system; a vital load will carry high cost, or energizing a generating plant or government or industrial consumer will be considered more important.

2.5 A Heuristic

We used a commercial solver (FICO Xpress Optimizer [62]) to handle the optimization problem formulated in the previous section. We observed that the solver struggled to find feasible solutions to the problem using its own heuristics, even when an increased number of threads was devoted to that purpose. For that reason, we developed a custom heuristic that utilizes the time-staging structure of the problem, is guided by LP relaxations and tries to identify feasible solutions. Randomization is used at various parts of the heuristic, so that multiple executions can yield different solutions. The solutions are then fed to the solver to aid the branch and bound tree. Multiple runs of the heuristic can be launched in parallel in a high performance computing environment to speed up the process. The heuristic consists of two phases. In the BS Allocation Phase, the BS units are assigned and the value of u_{BSg} is fixed to an integer for the next phase. In the Restoration Sequence Phase, the restoration sequence based on the BS units is fixed. Both phases use the function RANDOMRANK (given in figure 2.2), which takes a list of fractional values as input, perturbs them by noise (by adding αX, where X is uniformly distributed in $[0, 1]$ and α a controllable parameter that influences how much randomness will be injected in the LP relaxation solution), and returns a ranked list. We also allow the solver to tighten the relaxation by exploiting the integral nature of the variables.

In the BS Allocation Phase, the LP relaxation of the full problem is solved. From the solution ($u^{LP}_{BSg} \in [0, 1]$), the generators are ranked (using RANDOMRANK with $\alpha = \alpha_{BS}$) and picked based on the ranking, up to the available budget B. For the rest of the heuristic the BS allocation is considered fixed, i.e. the binary decision variables u_{BSg} are fixed to integral values. The Restoration Sequence Phase adopts the following pattern: At every step τ in the time horizon an LP relaxation is solved. Then, based on the relaxed values obtained from the assignment variables of lines $u^{\tau,LP}_{ij}$ and generators $u^{\tau,LP}_{g}$ at this time step, all binary variables for time τ are fixed to integral values for the next steps, and the process is repeated. However, a simple randomized rounding scheme would not work because it is very easy to construct an infeasible combination. Instead, at every step we make intelligent fixings by tracking the islands that are formed, and labeling every bus, line and generator by the index of the island they belong to (unlabeled if not yet energized). This phase of the algorithm has two parts: the Line Selection part defines the topology, i.e. which lines and buses are going to be introduced, whereas the Generator Selection part defines which generators will be energized.

In the Line Selection part, a ranking of the lines is again formed (using RANDOMRANK with $\alpha = \alpha_E$) based on the LP relaxation values. However, only lines with positive relaxation values $u^{\tau,LP}_{ij}$ are considered in the ranking, since these are guaranteed to be lines connected to at least one

Black Start Allocation Phase
$t \leftarrow 0$
Solve LP relaxation. Get $u^{LP}_{BS_g} \in [0,1], \forall g \in G$
Pick generators in order RANDOMRANK $(\{u^{LP}_{BS_g}\}_{g\in G}, \alpha_{BS})$ as BS (fix u_{BS_g} , $\forall g \in G$) up to budget B.
Based on fixing of BS, ramping rates and active and reactive power limitations, update active and reactive power capabilities of the generators $\forall t \in T$.
Initialize islands, generator and node labels corresponding to the BS units.
Restoration Sequence Phase
for $\tau \in T$ **do**
    Solve LP with u_{BS_g} and u^t_g, u^t_{ij}, u^t_i fixed for $t \leq (\tau - 1)$.
    Line Selection
    repeat
        Pick next line $(i', j') \in E$ based on RANDOMRANK $(\{u^{\tau,LP}_{ij}\}_{(ij)\in E}, \alpha_E)$ with $u^{\tau,LP}_{i'j'} > 0$
        if New Reactive Power Capability in Island of $(i', j') \geq R_Q$ **then**
            Add line (fix $u^\tau_{i'j'} = 1$) and corresponding nodes (fix $u^\tau_{i'} = 1$ or $u^\tau_{j'} = 1$) if necessary.
            Update islands
            Update node, line and generator labels.
        end if
    until all lines with $u^{\tau,LP}_{i'j'} > 0$ tested
    Generator Selection
    repeat
        Pick next generator $g' \in G$ based on RANDOMRANK $(\{u^{\tau,LP}_g\}_{g\in G}, \alpha_G)$ with $u^{\tau,LP}_{g'} > 0$ and connected to an energized node.
        if New Active Power Capability in Island of $g' \geq R_P$ **then**
            Add generator (fix $u^\tau_{g'} = 1$).
            Update generator labels.
            Based on ramping rate and active and reactive power limitations, update active and reactive power capability of g' $\forall t \in T$.
        end if
    until all connected generators with $u^{LP}_{g'} > 0$ tested
end for

function RANDOMRANK $(\{u_k\}_{k\in K}, \alpha)$
    $r_k \leftarrow u_k + \alpha X_k$, where $X_k \sim$ Unif$(0, 1)$
    Rank elements of K based on r_k: Let $R : \{1, \ldots, |K|\} \mapsto K$ be a bijection s.t. $i > j \iff r_{R(i)} \leq r_{R(j)}$
    return R
end function

Figure 2.2: Randomized heuristic for feasible point search.

bus energized at the previous time step, due to constraint (2.12). Then, the lines are sequentially introduced according to their ranking. Since the main concern with energizing lines is the reactive power they inject into the system (which could cause overvoltage problems due to the Ferranti effect), the reactive power capability of the island that would be created if the line was connected is checked before deciding to introduce the line. At the same time, given that the constraint is only checked at an island level, a higher threshold R_Q may be used to possibly account for not considering the local effect for that line. In the Generator Selection phase, the LP relaxation again yields a ranking of the generators (using RANDOMRANK with $\alpha = \alpha_G$). A similar test is performed to qualify introducing the generator; in this case, the main concern is whether or not the island possesses adequate active power capacity to provide for the cranking power of the generator, plus some slack of R_P to accommodate for only checking this constraint on an island level. If the generator has a minimum stable operational limit $\underline{P}_g$, then the load capability of the island to accommodate for this generation is also tested.

2.6 Experimental Results

All the simulations are performed on the Cab cluster of the Lawrence Livermore National Laboratory. The Cab cluster consists of 1296 nodes with 20736 cores, with an Intel Xeon E5-2670 processor at 2.6 GHz and 32 GB per node. For the simulations, Mosel $4.0.4$ was used with Xpress [62]. The heuristic simulations were parallelized at 6 nodes by utilizing Mosel, with 4 jobs per node and 4 threads per job.

Unit	P_{CR_g} [MW]	$\underline{Q}_g$ [MVar]	K_{R_g} [MW/h]	C_{BS_g} $(B = 30)$
G1	6	-400	215	13.5
G2	8	-300	246	15.5
G3	7	-300	236	14.5
G4	5	0	198	12.5
G5	8	0	244	15.5
G6	6	-300	214	13.5
G7	6	0	210	13.5
G8	13	0	346	20.5
G9	15	-300	384	22.5
G10	1	-300	162	8.5

Table 2.1: Data used for the IEEE-39 system. All the cranking times are set to $T_{CR_g} = 30$min, except $T_{CR_{10}} = 10$min.

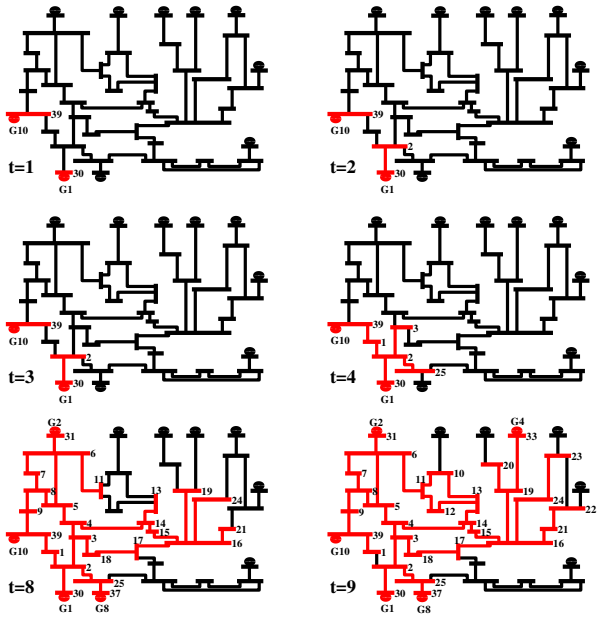

Figure 2.3: Sampled steps of the restoration process. Generators 1 and 10 are chosen by the optimization problem as BS units, so they get energized first. The rest of the grid is gradually restored. The time unit is 5min. Note that the line connecting buses 2 and 30 is picked up immediately after energization, because it has no shunt capacitance in the model. However, the generators cannot pick further transmission lines immediately, since they can not change their reactive power setpoint up until one period after the cranking is over (i.e. after time 3 for G1). Notice also that the line connecting buses 1 and 39 gets de-energized at time $t = 9$. Forcing energization of the line at this time point leads to ac infeasibility, which means that the flexibility of de-energizing lines (enabled by the model) is utilized.

Simulation of the IEEE-39 Bus System

In order to illustrate the effectiveness of the proposed model, a small test case is initially considered. The IEEE-39 bus system consists of 39 buses, 10 generators and 34 branches [11]. The most important parameters for the problem are given in Table 2.1; most of the cranking powers and cranking times for that system are taken from [74]. The parameters for generator 10 are purposefully chosen in a way that favors turning it into a BS unit (i.e. small cranking power of 1MW and a small cranking time of 10 minutes). The cost of load shedding at every bus is set to $(5000 + 50 * i)$\$/MWh, where i is the bus number of the load. Both μ and ϵ are set to comparatively small values (equal to 100). The length of the time horizon is set to $T = 40$ time units, with a 5 minutes time step. The problem has 36058 constraints and 16380 variables, of which 3810 are binary.

Xpress struggles to find feasible solutions to the problem. After 30 minutes, only one feasible solution was found, with an optimality gap of 43.30%. Gurobi performs better for this small problem, by finding a solution with 1% gap within 20 minutes.

As an alternative, we launch parallel heuristic executions in Xpress until 100 feasible solutions

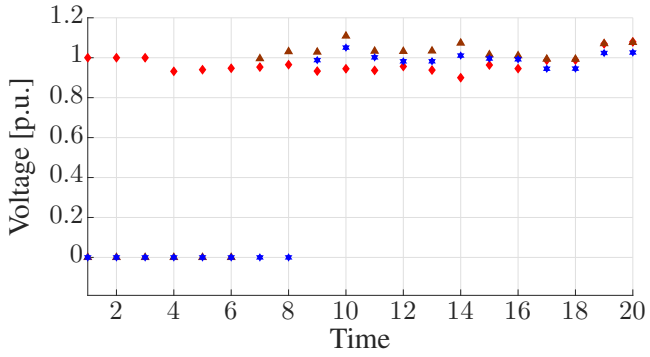

Figure 2.4: Voltages of three buses from the ac simulations. Bus 16 (brown triangles) is on the edges of the transmission system and suffers from overvoltages (in fact at time $t = 10$ we need to relax the voltage limit to 1.12p.u. for one time step). Bus 30 (red diamonds) is a generator bus and its value is set as low as possible, to accomodate for reactive power transfer to the transmission system. Finally, the voltage of bus 20 is depicted with blue hexagrams. The transition from zero to nonzero values indicates the time step that a node is energized.

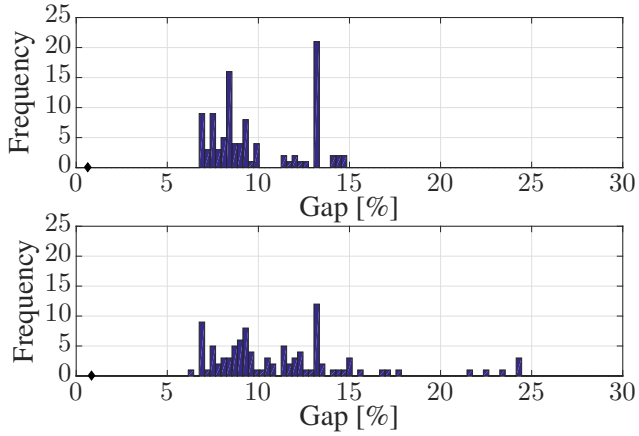

Figure 2.5: Gap for 100 feasible solutions generated by the heuristic, for two different settings of the value of α_{BS}, i.e. $\alpha_{BS} = 0$ (plot above) and $\alpha_{BS} = 1.5$ (plot below). The values of α_E and α_G are set to 0.5. The heuristic solutions were fed to the optimizer, which solved the problem within 1% tolerance. The gap for that solution is shown with a diamond on the plots. Increased randomness (meaning the heuristic moves randomly away from the LP relaxation solution) leads to worse feasible solutions in general, but may also get lucky and find a better feasible solution.

are found (which takes approximately 15 minutes). The feasible solutions are then fed to Xpress and the solver usually achieves the desired 1% gap within 15 minutes. The purpose of the heuristic is therefore not to completely substitute the optimization solver, but to guide it.

In the optimal allocation, generators 1 and 10 (as expected) are chosen. Generator 1 was selected due to its high reactive capability (which is important for that system that has no reactors for compensation). Some steps of the restoration process are presented in figure 2.3.

We also check the restoration sequence for ac feasibility. For that, an ac feasible point is sought for the grid configuration at every step and given the various unit capabilities, as in [31,74]. The islands are identified at every step and an ac optimal power flow (OPF) is performed using the software Matpower [159]. The load is initially considered fixed at the value provided by the optimization problem. If this does not yield an feasible point, the load is perturbed by no more than 10% around that value. This was adequate for finding feasible points at all time instances, apart from three in which the upper voltage limit had to be relaxed from 1.1 to 1.12; see figure 2.4. A systematic way to perform this task is described in [120].

Finally, in figure 2.5, heuristic executions for two different settings of the parameter α_{BS} are shown. Note that none of the heuristic executions gets very close to the best integer solution found. This is due to the fact that the final integer allocation assigns a generator (G1) with a very small u_{BS_g} value in the LP relaxation, so the heuristic is unlikely to make this assignment. Furthermore, the heuristic by construction lacks some characteristics that the optimal solution could have, such as the ability to de-energize lines. Such modifications are left for the local search of the solvers to identify.

Simulation of the IEEE-118 Bus System

The IEEE-118 bus system consists of 118 buses, 186 branches and 54 generators. The data from [148] were used for cranking powers, ramping rates and cranking times of the generating units. The allocation costs were assumed to have two parts: 70% of the cost was assumed the same for all units and the remaining 30% was assumed proportional to the BS unit's cranking power. The total budget is assumed 15% of the cost of assigning all the units as BS. For the 345kV lines, reactive compensation equal to approximately 45% of their capacitance was assumed connected to each of their endpoints (reactive compensation of this size appears in actual systems to alleviate the Ferranti rise). The cost of load shed was set in the same way as for the IEEE-39 bus system. A time resolution of 15 minutes was considered, for 20 time steps.

The optimization problem has 70704 constraints and 30028 variables, of which 7214 are binary. When the problem is fed to the Xpress Optimizer, the solver is unable to identify a feasible solution within a 5 hour time limit. Gurobi can only find the feasible solution corresponding to setting all binaries to zero (i.e. making no actions to restore the power system) within the same time limit. Executions of the heuristic identify feasible solutions, as well as eventually the optimal solution (verified by the solver due the the termination of the branch and bound tree search), and the performance with respect to time is depicted in Table 2.2. Six generators are assigned as BS units (G21, G22, G25, G28, G45 and G51). In order to signify the importance of the voltage constraints, figure 2.6 indicates the buses at which voltages are set to their maximum or minimum

Parameters	Time for M feasible points [s]			
$(\alpha_{BS}, \alpha_E, \alpha_G)$	$M = 5$	$M = 50$	$M = 100$	$M = 1000$
$(0.8, 0.5, 0.5)$	218	791	1133	10045
$(0.8, 1.5, 0.5)$	242	688	1263	10656
$(0.8, 0.5, 1.5)$	228	653	1110	10808
$(0.8, 1.5, 1.5)$	236	701	1193	11304

Table 2.2: Time for the heuristic to find the designated number of feasible solutions for the IEEE-118 system, depending on the randomness parameters. For many executions ($M = 1000$), increased randomness yields higher computational times, due to more points identified by the heuristic being infeasible; the difference is in general not observable for fewer executions.

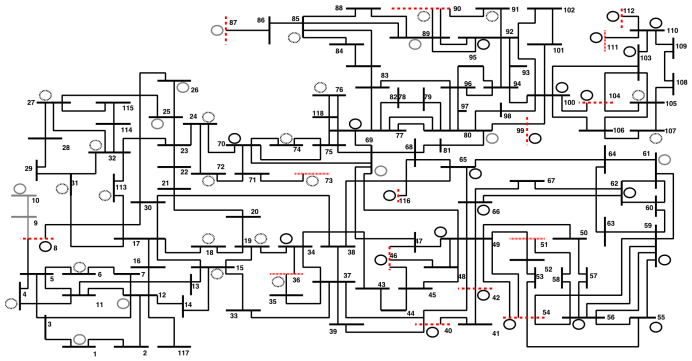

Figure 2.6: Snapshot of the IEEE-118 system ($t = 10$). The non energized part is depicted in gray, generators with bold black line have nonzero output, whereas dotted generators are being cranked. Red dotted bus lines and red dashed bus lines indicate buses at their maximum and minimum voltage respectively. Note that buses of generators with reactive power support (such as 46) are usually set to the minimum voltage (in order to absorb reactive power), whereas some buses at the edges of transmission (such as 51) are set to the maximum.

limits from the optimization. The resulting solution is also tested for ac feasibility at every time step.

Simulation of the Reduced WECC System

As a final test case, we consider a reduced model of the Western Electricity Coordinating Council (WECC) system [156] with 225 buses, 371 lines, 130 conventional generators and 6 hydro units. The same model is used in [105][1]. The generation mix in terms of type, number of generators and total capacity is shown in Table 2.3. The renewable energy generation is assumed disconnected

[1]Data available at the following link: `https://drive.google.com/drive/u/2/folders/1F3u6yq-noQhv8APZKaa45mM0q1I9_-cy`.

Type	**U**nits	**C**apacity [MW]
Nuclear	2	4499
Gas	101	21781
Coal / Oil	3 /1	199 / 121
Dual Fuel	23	4679
Hydro	6	8613

Table 2.3: Generator mix for the WECC test system.

during the restoration, with the exception of hydro. The imports are also assumed disconnected. A time horizon of 18 steps with 15 minute resolution was considered.

One of the crucial priorities when energizing the grid is providing power to the nuclear power plants, due to security considerations. For this reason, a penalty was associated in the objective with u_g^t for the nuclear power plants to ensure their quick restoration. The total budget is assumed 4% of the total cost for allocating all the units. Nuclear power plants are excluded from serving as black starts (by setting the corresponding binary allocation variable to zero).

The optimization problem has 131470 constraints and 55418 variables, of which 13597 are binary. Xpress and Gurobi were unable to find any feasible solutions within the 5 hour time limit imposed. The heuristic is launched and finds 20 feasible solutions within 40 minutes. The optimization problem is then solved within 6.7% optimality gap in Xpress, after 2 hours of execution. The power plants allocated were three hydro plants, which is expected due to their small cranking power and cranking time (they constitute ideal BS units), as well as one gas station at McCall. The gas station was allocated due to its proximity to the nuclear power plant at Diablo Canyon (since none of the hydro units are in the vicinity). The sequence was also tested for ac feasibility.

2.7 Conclusions

In this chapter, we formulated and solved the optimal BSA problem. We enhanced existing literature on the topic with a new modeling approach and sets of constraints to accommodate for some of the most important considerations during restoration. Based on our understanding of the problem structure, we proposed a heuristic guided by the LP relaxation of the optimization. The feasible solutions generated by the heuristic are then fed into commercial solvers, which can then provide global guarantees for optimality.

In the following chapters, tighter reformulations of the constraints of the problem will be developed and the benefit from their use will be explored. Furthermore, since the initial state of the system (i.e. the stable islands after a blackout) is a parameter to our problem, a BS allocation that can accommodate for a number of scenarios can be achieved by solving a two-stage stochastic program. In this case, the first stage decision will be the BS allocation, the scenarios will be a

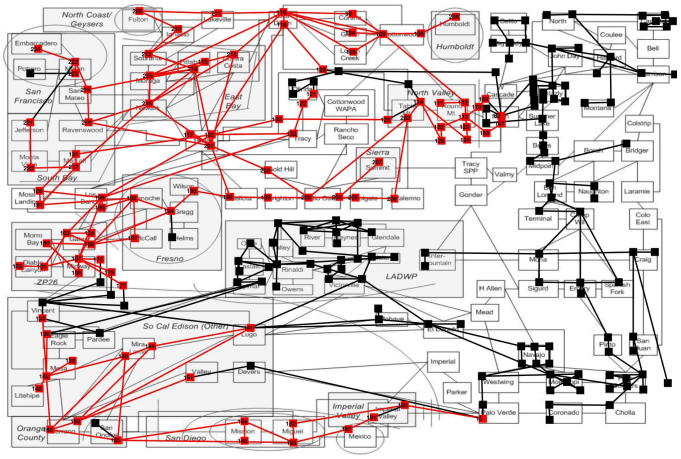

Figure 2.7: Snapshot of the restoration for the WECC system (restored part in red).

number of possible outages (defined by experts), and the second stage will be the restoration steps according to the scenario.

Chapter 3

Formulations and Valid Inequalities for Power System Islanding and Restoration

3.1 Abstract

Reformulating the constraints of a Mixed Integer Linear Program (MILP) can lead to a better computational performance when off-the-shelf software is used to solve the problem. The process involves identifying subsets or substructures among the problem constraints, obtaining a strong or more compact formulation for them, and then solving the original problem with the modifications to observe if the computational performance has improved. This section explores a substructure that appears in two problems within the power systems literature that involve reconfiguration of the power system topology: Intentional Controlled Islanding (ICI) and Black Start Allocation (BSA).

A key consideration in both of these problems is that each island that appears after a reconfiguration must have at least one energized generator. We examine three alternative MILP formulations for this restriction and examine their relative strength in terms of their linear programming relaxation. In order to further strengthen the formulations, we introduce a family of exponentially many valid cuts that can be separated in polynomial time. Under simplifying assumptions, we show that the integer hull of the feasible region is a full dimensional polyhedron, and prove that some of the constraints we introduced define facets of the integer hull. We draw a connection of this region with the one resulting from the rooted maximum weight connected subgraph problem.

Since the time to solve MILPs can vary significantly between equivalent formulations, we present computational experiments on various systems for the ICI and BSA problems. The ICI problem modeling is obtained from publications in the power systems literature and the optimization problem is reformulated to exhibit a strictly better computational performance. For the BSA problem, a simplified model is presented with the goal to solve systems of larger scale than the ones of the previous chapter. An implementation using lazy constraint generation through integer callbacks for an exponential in size reformulation of the problem exhibits the best performance in solving the problem. An approach to obtain near optimal solutions for a synthetic test case of the Texas system (2000 buses, 3206 branches, 544 generators) is described.

3.2 Introduction

Mixed integer programs (MIPs) and in particular mixed integer linear programs (MILPs), i.e. optimization models with linear constraints that involve integer as well as real variables, are becoming ubiquitous in power systems applications (unit commitment, power system restoration, capacity expansion planning, optimal islanding). The main reasons for their popularity are that they offer broad modeling capabilities and that specialized commercial MILP solvers have improved significantly over the past years, making MILPs tractable for many practical applications. In these applications, binary variables are used to represent commitment, scheduling, time dependencies, component energization, as well as to approximate nonlinear curves with piecewise linear functions. Two of the problems that have been formulated as MILPs in power systems are Intentional Controlled Islanding (ICI) and Black Start Allocation (BSA).

ICI is a measure employed to prevent cascading power system outage by splitting the grid into smaller, stable and easily controllable islands via switching off lines [3, 34, 38, 41, 43, 44, 50, 58, 59, 81, 137–139, 147, 152, 158]. One straightforward approach to model the problem is to represent the switching decisions with binary variables and formulate an optimization problem [38, 43, 44, 50, 58, 59, 81, 137–139, 158]. The optimization objective and constraints embody the requirements that the splitting should satisfy, such as minimum power flow disruption, size and capacity of the resulting islands and isolating or grouping generators in coherent sets.

The BSA for Power System Restoration (PSR) problem [27, 71, 72, 74, 89, 115, 120–122, 132, 134] aims to allocate Black Start (BS) resources in the grid in an efficient way, in order to ensure a successful restoration of the power system after an outage. The problem is often modeled as a MIP, with binary decisions representing the BS unit allocation and the restoration of generators/branches/buses of the system [72, 74, 115, 120–122, 132, 134]. The optimization objective is to maximize the energization of the system components over a time horizon, or to minimize the load shedding for critical loads, whereas the constraints ensure that the allocation and restoration plans are feasible.

Both of the aforementioned problems, and possibly others, allow the switching of lines of the power system. It is therefore often necessary to include a constraint to ensure that at all times each island has at least one generator to set up the voltage. More abstractly, the constraint ensures that a graph is partitioned into connected subgraphs, each of which contains a special type of node. In the power systems context, this node is one with an energized generator or corresponding to a set of coherent generators. We will refer to this constraint as the *island energization* (IE) constraint. An example of a system state that violates this requirement is depicted in figure 3.1. Network commodity flow formulations have been used to explicitly enforce this requirement [38, 43, 44, 50, 58, 81, 115, 121, 122] and this is currently the most common approach for power systems applications.

The underlying structure of the problem resembles, after a suitable tranformation, that of the rooted maximum weight connected subgraph problem [84], with weights (positive or negative) on edges and nodes, for an undirected graph. We will make the connection more formal subsequently in this chapter. The directed graph version of the problem is what mostly appears in the literature, since it can give rise to stronger formulations. In practice, this problem is most commonly studied

in the space of either only nodes or only edges, since the connectivity requirements can be equivalently reformulated with only nodes or only edge variables to obtain more compact formulations. However, in our power systems applications, we need to utilize node, bus, and generator variables, since they all get involved in other constraints introduced through the power systems interpretation of the components.

A similar requirement to the IE constraint appears in other contexts as well. For instance, in [40], the authors propose three formulations to obtain a connected subgraph that includes a set of terminal nodes in a graph, and provide computational results to test the comparative performance and strength of the different formulations. In their problem, they must select a single connected subgraph that includes certain terminal nodes. In our case, we can select multiple connected subgraphs (islands) that must contain at least one generator. While projections of the feasible region of the two problems can be shown to be equivalent using the appropriate network transformations, one of their formulations restricts the connected subgraphs to be trees. Similarly, our problem differs from the Steiner Tree problem and multiple generalizations of it (such as the Prize Collecting Steiner Tree Problem [63]), because these problems restrict their connected subgraphs to be trees, whereas our islands can include cycles.

The motivation for studying equivalent reformulations of the same set of constraints is that, despite the continuous improvements of MILP solvers, the solution times highly depend on the problem formulation employed. As a result, equivalent reformulations of the same requirement can lead to very different solver performances. For a minimization problem, the lower bounds found by the solvers of a MILP are based on solving successive continuous relaxations of the problem, i.e. optimization problems that relax the integrality requirement of some variables. Therefore, equivalent reformulations of the problem with tighter continuous relaxations can lead to better lower bounds and hence a smaller branch and bound (B&B) tree. Unfortunately, tighter formulations usually come at the expense of more variables and/or constraints. As a result, there is a computational trade-off between the use of different formulations that has to be resolved based on theoretical and computational results for every particular problem.

The main contributions of this work are the following:

1. We present three different formulations of the IE constraint using binary variables for generators, buses and branches: a single-commodity flow formulation F_1, a multi-commodity flow formulation F_2, and an exponential in size, cut-set formulation F_3 and we examine their relative strength. Formulation F_3 employs an exponential number of constraints (which we will refer to as *Type I* cuts), but can be separated in polynomial time. We also introduce a new set of exponentially many valid inequalities (*Type II* cuts), separable in polynomial time. We present a polyhedral analysis for the simplified case of a complete graph to show that some of the valid inequalities we presented define facets of the integer hull. We describe the connection of the feasible region to the one of the rooted maximum weight connected subgraph problem.

2. We present a new formulation for the variant of the optimal ICI problem considered in [81]. Our formulation has fewer variables and constraints and exhibits a better computational performance for the instances examined.

3. We present an alternative model for BSA that is tailored for power systems of realistic size. Modifications are introduced to, among others, the objective, the generator start-up curves, and the power flows.

4. We demonstrate through computational experiments that: (i) For both problems (ICI and BSA), the size of F_2 makes it impractical to use in realistic applications; (ii) For the optimal BSA problem, the use of the Type I and Type II inequalities, part of them introduced through integer callbacks, seems to offer the best computational performance for the instances tested; (iii) For the optimal ICI problem, Type I and Type II constraints perform no better than F_1 in the instances we tried, mainly due to the computational overhead of separating the constraints.

The largest test system used for BSA is a synthetic Texas test case (2000 buses, 3206 branches, 544 generators), which leads to an optimization with more than a million constraints and hundreds of thousand binary variables. An adaptation of the heuristic presented in the previous chapter is used to obtain feasible solutions. We perform numerical experiments with different problem formulations in order to obtain a good optimality guarantee.

The rest of this chapter is organized as follows: section 3.3 sets up the notation for the chapter; section 3.4 gives the equivalent reformulations of the IE constraints; section 3.5 proves the formulation equivalence and relative strength; section 3.6 presents a family of valid cuts; section 3.7 includes a polyhedral analysis under simplifying assumptions; section 3.8 draws the connection to graph theory; section 3.9 describes the model for large scale BSA; sections 3.10 contains simulation results, and section 3.11 concludes the chapter. The Appendix contains descriptions of the islanding formulations used in the simulations of section 3.10.

3.3 Notation

Let (N, E) be the undirected graph derived from the physical graph of the power system, where buses correspond to nodes (set N) and branches to undirected edges (set E). Let A be a directed edge set corresponding to E, with the direction of each edge defined by arbitrarily picking a "From Bus" and "To Bus" for every system branch, as is common in the power systems literature. Note that $|A| = |E|$. Let G be the set of all generators, $G(i)$ the set of generators that are connected to bus $i \in N$, and $G(S)$ the set of generators connected to a node $i \in S$, where $S \subseteq N$. For the case where a single generator is connected to i, we will denote this generator by $g(i)$, i.e. $G(i) = \{g(i)\}$. Let u_i denote the energization status of bus $i \in N$ (where $u_i = 1$ indicates an energized bus, whereas $u_i = 0$ indicates a de-energized bus), u_{ij} denote the energization status of branch $(ij) \in E$ (or $(ij) \in A$ by a slight abuse of notation, since there is a bijective correspondence between E and A), and u_g the energization status of generator $g \in G$. The energization state of the system is completely described by the binary vector $\mathbf{u} \in \mathbb{B}^{|N|\times|E|\times|G|}$. We will denote $d = |N| \times |E| \times |G|$.

We also use auxiliary variables $\boldsymbol{f}$, corresponding to energization network flows (not power flows), in the definition of the single- and multi-commodity flow formulations. Finally, if S is a

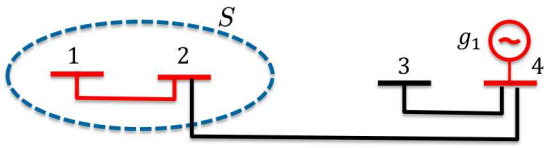

Figure 3.1: A small power system with four buses, three branches and one generator. Red color indicates an energized component, whereas black color indicates de-energized components. Note that nodes 1 and 2 and branch $(1, 2)$ form an energized island without any generator, hence this is an infeasible topology that violates the IE constraint.

subset of the nodes $S \subseteq N$, the undirected cut-set $\delta(S)$ is defined as the set that contains all the edges in E with one node in S and one node in $N \setminus S$.

3.4 Formulations for the Island Energization Constraint

The power system restoration (PSR) problem, which is solved for a given allocation of BS units in the system, aims to gradually restore a power system to an operational state after a complete or partial outage. The optimal ICI problem deals with temporarily reconfiguring the grid, by switching lines on and off, as a measure to improve the system security. Both problems involve a series of stepwise actions (usually switchings of lines and generators), while the system moves through a number of different states. Each state can be captured through the status of every bus, line or generator (on or off, i.e. energized or de-energized), as well as through other system characteristics (power flows, generation, etc).

Every step of the process in both problems should respect the island energization (IE) constraint. This requirement may be obvious to the experts that actually perform the switching operations to reconfigure the grid, but when an optimization model is employed to determine a switching plan, the IE constraint has to be imposed. If the ac power flow equations are utilized to model the power system in the optimization model, the IE constraint is implicitly imposed (shunt elements will force node voltage to zero). However, in order to achieve tractability or obtain optimality guarantees, the power flow equations are often relaxed or substituted with approximations and relaxations in the resilience literature which can violate the IE constraint. In such cases, the IE constraint must be explicitly imposed, as in [38, 43, 44, 50, 58, 81, 115, 121, 122].

The IE constraint formulations we examine in this chapter are valid for distribution systems as well. However, for distribution systems one can exploit the graph structure even more, due to the mostly radial nature of the system. As a result, for these systems, there already exist specialized constraints that impose the connectivity requirement, such as the ones used in [24, 25, 119, 136]. These formulations are specific for distribution systems and do not work for general networks. Our formulations are tailored for general networks, aiming to allow cycles, which are common in transmission systems.

In this section, we present three different formulations to impose the IE constraint, F_1, F_2, and F_3. We will denote the feasible region of the points satisfying the IE constrain by H. Constraints (3.1) and (3.2) are included in all the formulations:

1. If a generator $g \in G$ connected to node $i \in N$ is energized, then the node is considered energized.
$$u_g \leq u_i, g \in G(i), i \in N \tag{3.1}$$

2. If a branch is energized, both the nodes at its endpoints are considered energized.
$$u_{ij} \leq u_i, u_{ij} \leq u_j, \ (ij) \in E \tag{3.2}$$

Single-Commodity Flow Formulation

The first formulation (F_1) is given by:

$$\begin{aligned} F_1 = &\{\mathbf{u} \in [0,1]^d : \exists f_g \ \forall g \in G, f_{ij} \ \forall (ij) \in A : \\ &\text{(3.1), (3.2), (3.4a)-(3.4c)}\} \end{aligned} \tag{3.3}$$

where:

$$0 \leq f_g \leq u_g, \ g \in G \tag{3.4a}$$
$$-u_{ij} \leq f_{ij} \leq u_{ij}, \ (ij) \in A \tag{3.4b}$$
$$\sum_{j:(ji)\in A} f_{ji} - \sum_{j:(ij)\in A} f_{ij} + \sum_{g \in G(i)} f_g = \frac{1}{|N|} u_i, \ i \in N \tag{3.4c}$$

Given the definition of F_1 above, we define the feasible region of the IE problem to be $H = F_1 \cap \mathbb{B}^d$. In the definition of F_1, a set of auxiliary network flow variables f_g, $g \in G$ and f_{ij}, $(ij) \in A$, are employed. An energized node (i.e. $u_i = 1$) will act as a sink of $\frac{1}{|N|}$ amount of network flow, captured in the right hand side of (3.4c). Network flow can only be generated from energized generators, due to (3.4a). Finally, it can only flow through energized branches due to (3.4b). This ensures that there will be a path from any energized node to an energized generator that uses only energized lines (this is the path that the network flow follows to move from the energized generator to the energized node). For example, the topology of figure 3.1 is infeasible, since node 1 would act as a sink of $1/4$ amount of network flow, but network flow can only be generated at node 4 by the energized generator g_1 and cannot pass through the de-energized line $(2, 4)$. Note that the size of the sinks is $\frac{1}{|N|}$, so that the topology where a single generator (that can generate up to 1 unit of network flow) energizes all the nodes of a (connected) power system belongs in F_1. The single-commodity flow formulation is the one most commonly used in power systems applications [38,43,44,50,58,81,115,121,122]. The formulation has $|G| + |E|$ flow variables and $|N| + |E| + |G|$ constraints (excluding (3.1) and (3.2)).

Multi-Commodity Flow Formulation

An alternative formulation approach, following the same logic, would be to consider a different type of flow corresponding to the energization of each node. This would lead to the following

formulation

$$\begin{aligned} F_2 =&\{\mathbf{u} \in [0,1]^d : \exists f_g^k \; \forall k \in N \; \forall g \in G, \\ & f_{ij}^k \; \forall k \in N \; \forall (ij) \in A : (3.1), (3.2), (3.6a)\text{-}(3.6d)\} \end{aligned} \tag{3.5}$$

where:

$$0 \leq f_g^k \leq u_g, \; k \in N, g \in G \tag{3.6a}$$

$$-u_{ij} \leq f_{ij}^k \leq u_{ij}, \; k \in N, (ij) \in A \tag{3.6b}$$

$$\sum_{j:(ji)\in A} f_{ji}^k - \sum_{j:(ij)\in A} f_{ij}^k + \sum_{g\in G(i)} f_g^k = u_i, \quad k \in N, i \in N : i = k \tag{3.6c}$$

$$\sum_{j:(ji)\in A} f_{ji}^k - \sum_{j:(ij)\in A} f_{ij}^k + \sum_{g\in G(i)} f_g^k = 0, \quad k \in N, i \in N : i \neq k \tag{3.6d}$$

The idea behind this formulation is that each node is treated separately and is associated with its own type of network flow and constraints. If node $k \in N$ is energized, then one or more of the energized generators will need to generate the type k network flow, that needs to pass through energized lines. The only sink for that type of network flow is node k, which means that the network flow of type k is preserved at every other node $i \neq k$. In this case, the normalization of $\frac{1}{|N|}$ is not necessary in (3.6c), since a single energized generator can generate all $|N|$ types of network flows to energize all the nodes. This formulation has $|N| \cdot (|G| + |E|)$ network flow variables and $|N| \cdot (|N| + |E| + |G|)$ constraints (excluding (3.1) and (3.2)).

Cut-Set Formulation

The third formulation only employs the binary variables. More specifically,

$$F_3 = \{\mathbf{u} \in [0,1]^d : (3.1), (3.2), (3.8)\} \tag{3.7}$$

where:

$$\sum_{(ij)\in\delta(S)} u_{ij} + \sum_{i\in S} \sum_{g\in G(i)} u_g \geq u_n, \; n \in S, S \subseteq N \tag{3.8}$$

We will refer to the family of inequalities (3.8) as *Type I* constraints. The idea behind this formulation is that, given any subset S of the nodes, if any node in that subset is energized (i.e. if u_n in the right hand side of (3.8) is equal to 1 for some $n \in S$), then an energized generator must be providing the energizing flow. Therefore, either one generator within the set S should be energized (i.e. $\sum_{i\in S} \sum_{g\in G(i)} u_g \geq 1$ in the left hand side of (3.8)), so that the energizing flow comes from that generator, or at least one edge in the cut-set should be energized (i.e. $\sum_{(ij)\in\delta(S)} u_{ij} \geq 1$ in the left hand side of (3.8)), so that the energizing flow comes from a generator outside the set S. For example, the topology of figure 3.1 is infeasible, since if we pick the set $S = \{1, 2\}$ and the node

$n = 1$ with $u_1 = 1$, the left hand side of (3.8) is zero (since there are no generator nodes in S and the only edge in the cut-set has $u_{24} = 0$), while the right hand side is one. Finally, for every node $n \in N$, there are $2^{|N|-1}$ subsets S of N that contain it, so the formulation has a total of $|N| \cdot 2^{|N|-1}$ constraints (excluding (3.1) and (3.2)), which is exponential in the size of $|N|$.

3.5 Formulation Equivalence and Strength

Formulation Equivalence

We proceed to show that the three formulations restricted to $\mathbb{B}^d$ represent the same region.

Proposition 1. *Formulations F_1, F_2 and F_3 restricted to $\mathbf{u} \in \mathbb{B}^d$ are equivalent, i.e. $H = F_1 \cap \mathbb{B}^d = F_2 \cap \mathbb{B}^d = F_3 \cap \mathbb{B}^d$.*

Proof. Let $H_1 = F_1 \cap \mathbb{B}^d$, $H_2 = F_2 \cap \mathbb{B}^d$, and $H_3 = F_3 \cap \mathbb{B}^d$. We show that $H_1 \subseteq H_3$, $H_3 \subseteq H_2$, and $H_2 \subseteq H_1$.

Part 1. $\mathbf{u} \in H_1 \implies \mathbf{u} \in H_3$

Assume for contradiction that $\mathbf{u} \in H_1$ but $\mathbf{u} \notin H_3$. Based on (3.8), that means $\exists S_0 \subseteq N, \exists n_0 \in S_0 : \sum_{(ij)\in\delta(S_0)} u_{ij} + \sum_{i\in S_0} \sum_{g\in G(i)} u_g < u_{n_0}$. Since the right hand side is binary, and the left hand side is integer, the only way for strict inequality to hold is if $\sum_{(ij)\in\delta(S_0)} u_{ij} + \sum_{i\in S_0} \sum_{g\in G(i)} u_g = 0$ and $u_{n_0} = 1$. Since the first equality is a sum of non-negative terms equal to zero, each one of them has to equal zero, so we obtain that:

$$u_{ij} = 0,\ (ij) \in \delta(S_0) \tag{3.9a}$$
$$u_g = 0,\ g \in G(i), i \in S_0 \tag{3.9b}$$
$$u_{n_0} = 1 \tag{3.9c}$$

Now, since $\mathbf{u} \in F_1$, by summing over equations (3.4c) for $i \in S_0$, we obtain:

$$\sum_{i\in S_0} \left(\sum_{j:(ji)\in A} f_{ji} - \sum_{j:(ij)\in A} f_{ij} \right) + \sum_{i\in S_0} \sum_{g\in G(i)} f_g = \frac{1}{|N|} \sum_{i\in S_0} u_i$$

The left hand side (LHS) can be simplified by observing that the sum of the flows inside the set S_0 will cancel each other, while the flows on branches that have only one node in S_0 (i.e. belong in $\delta(S_0)$), are all zero, due to (3.4b) and (3.9a).

$$\begin{aligned} \text{LHS} &= \sum_{i\in S_0} \left(\sum_{j:(ji)\in A} f_{ji} - \sum_{j:(ij)\in A} f_{ij} \right) + \sum_{i\in S_0} \sum_{g\in G(i)} f_g \\ &= \sum_{i\in S_0} \sum_{g\in G(i)} f_g \leq \sum_{i\in S_0} \sum_{g\in G(i)} u_g = 0 \end{aligned}$$

where the last line uses (3.4a) and (3.9b). On the other hand, the right hand side (RHS) yields:

$$\text{RHS} \quad \geq \frac{1}{|N|} u_{n_0} = \frac{1}{|N|}$$

where we used that $n_0 \in S_0$ and the rest of the binary variables in the summation are non negative, together with (3.9c). Based on the inequalities for the LHS and RHS, we obtain $0 \geq \frac{1}{|N|}$, which is a contradiction.

Part 2. $\mathbf{u} \in H_3 \implies \mathbf{u} \in H_2$

Based on $\mathbf{u}$, construct a directed graph with nodes $N \cup \{t\}$, where t is a dummy node, and edges: for each node $i \in N$ that has at least one generator (i.e. $G(i) \neq \emptyset$), add a directed edge from t to i with capacity $\sum_{g \in G(i)} u_g$, and for each directed edge $(ij) \in A$, add two directed edges, one from i to j and one from j to i, both with capacity u_{ij}. Now pick a node $k \in N$. For $T \subseteq N$ and $S = N \setminus T$, the capacity of any t-k cut is given by (see figure 3.2):

$$C(T \cup \{t\}, S) = \sum_{(ij) \in \delta(S)} u_{ij} + \sum_{i \in S} \sum_{g \in G(i)} u_g \tag{3.10}$$

which is greater than or equal to u_k, since $k \in S$ and $\mathbf{u} \in H_3$. Therefore, the min-cut has capacity $v \geq u_k$, which means the max-flow has capacity v. We can scale all the flows of the max-flow by the positive quantity $\frac{u_k}{v}$, which is no greater than one, to obtain flows that retain feasibility and inject u_k amount of network flow at node k. Define f_g^k based on the flow on the edge t-i, where $g \in G(i)$ (if more than one generators are connected to bus i, assign to each f_g^k flow proportional to the capacity u_g). For every edge $(ij) \in E$, assign f_{ij}^k equal to the difference of the flows on the arcs in the graph we created, which is guaranteed to be in $[-u_{ij}, u_{ij}]$ due to the feasibility of the max-flows. We can repeat this process for every node $k \in N$, and hence generate feasible flows for formulation F_2, which shows that $\mathbf{u} \in H_2$.

Part 3. $\mathbf{u} \in H_2 \implies \mathbf{u} \in H_1$

Since $\mathbf{u} \in H_2$, based on the multi-commodity flows of formulation F_2, let:

$$\begin{aligned} f_g &= \frac{1}{|N|} \sum_{k \in N} f_g^k, g \in G \\ f_{ij} &= \frac{1}{|N|} \sum_{k \in N} f_{ij}^k, (ij) \in E \end{aligned}$$

By summing over all $k \in N$ the constraints of formulation F_2, one can observe that the flows defined above satisfy the constraints of formulation F_1. □

Formulation Strength

As we saw in the introduction of this dissertation, when comparing two MILP formulations F_i and F_j, we say that F_i is (strictly) stronger than F_j if F_i is a (strict) subset of F_j. A stronger formulation yields better bounds in the execution of B&B.

The following propositions give a result for the relative strength of the three formulations.

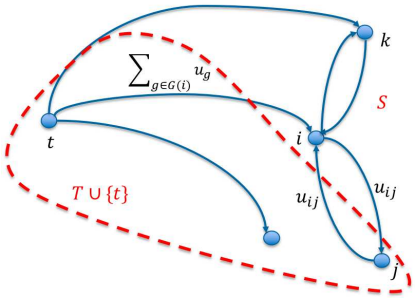

Figure 3.2: Graph used in the proofs of Proposition 1, Proposition 3, and Proposition 4.

Proposition 2. *F_2 is strictly stronger than F_1.*

Proof. We first need to show that $\mathbf{u} \in F_2 \implies \mathbf{u} \in F_1$. To see that, note that the proof employed in Part 3 of Proposition 1 did not use the integrality of the variables in $\mathbf{u}$. Therefore, the same proof can be used to show the inclusion in this case.

To see the strictness of the inclusion, consider a graph with two nodes $N = \{1, 2\}$, one line $E = \{(1, 2)\}$, and one generator $G = \{g(1)\}$ connected to node 1. Consider the point $(u_1, u_2, u_{12}, u_{g(1)}) = (1, 1, 1/2, 1)$. Picking $f_{g(1)} = 1, f_{12} = 1/2$, we can see that $(1, 1, 1/2, 1) \in F_1$. However, the point does not belong in F_2, since for $k = 2$ the line capacity of $1/2$ prevents the 1 unit of type 2 flow to pass from the generator to the sink in node 2. □

Proposition 3. *F_2 and F_3 are equally strong, i.e. $F_2 = F_3$.*

Proof. To see that $\mathbf{u} \in F_3 \implies \mathbf{u} \in F_2$, notice that the proof in Part 2 of Proposition 1 did not use the integrality of the variables $\mathbf{u}$. Therefore the same proof can be employed to show this result as well.

To see that $\mathbf{u} \in F_2 \implies \mathbf{u} \in F_3$, for each $k \in N$, consider the max-flow problem from t to k in the graph of figure 3.2. Due to the constraints in F_2, a feasible flow of at least u_k exists. Therefore, the maximum flow is at least u_k, which means that the minimum cut is at least u_k. That implies that any other cut, whose capacity has the form (3.10), will be greater than or equal to the minimum cut, so greater than or equal to u_k. Since this holds for all $k \in N$, the constraints of F_3 are satisfied. □

The constraints in formulation F_3 are exponentially many. Even though we cannot include all of them in the model that is passed to commercial optimization software, we can actually efficiently identify a violated constraint of F_3, based on the following proposition. Therefore, we can use solver callbacks to dynamically add the constraints at any point the solver reaches (fractional or not), only if they are violated.

Proposition 4. *Given a point $\mathbf{u} \in [0, 1]^d$, we can identify a violated constraint from F_3 or verify that none exists (separation problem), in polynomial time.*

Proof. Given a point $\mathbf{u} \in [0,1]^d$, for every $k \in N$, construct the graph from figure 3.2. Then find the minimum $t-k$ cut in this graph and compare the value to u_k. Given the fact that the capacity of a cut in that graph has the form (3.10), there are two cases for the capacity of the minimum cut C^k_{min}:

1. If $C^k_{\text{min}} < u_k$, for some $k \in N$, then node k and the minimum cut set S_{min} yield a violated constraint in F_3.

2. If $C^k_{\text{min}} \geq u_k$, for all $k \in N$, then all constraints in (F_3) are satisfied.

Since the min-cut problems can be solved in polynomial time, and we only need to solve at most $|N|$ of them, the separation problem can be solved in polynomial time. Note that, if the point is integral, a graph traversal to identify the islands and check if there exists one without a generator, is enough to identify if all constraints are satisfied in linear time (if we find an island with no generator, we can then generate a violated constraint with S corresponding to that island). Note we assume 3.1) and (3.2 are satisfied, since we can simply check if they are violated.

□

3.6 A Family of Valid Cuts

We define the following function of the binary vector $\boldsymbol{u}$ and the subset $S \subseteq N$:

$$f_S(\boldsymbol{u}) = \sum_{(ij)\in E: i,j\in S} u_{ij} + \sum_{(ij)\in\delta(S)} u_{ij} + \sum_{g\in G(S)} u_g - \sum_{i\in S} u_i \tag{3.11}$$

Define the following inequalities, which we will refer to as *Type II* inequalities:

$$f_S(\boldsymbol{u}) \geq 0, \forall S \subseteq N \tag{3.12}$$

Proposition 5. *Constraints* (3.12) *are valid for the feasible region* H.

Proof. Let $\boldsymbol{u}$ be an feasible point for H (binary vector). We will show that for all $S \subseteq N$, constraints (3.12) are satisfied at $\boldsymbol{u}$. The proof is by induction in the size of the set S. For $|S| = 1$, the constraints reduce to the Type I constraints (3.8) with $|S| = 1$, which are valid. Now assume that all constraints for sets with $|S| = k$ are valid. Take an arbitrary set of cardinality $k+1$ and assume it has the form $\hat{S} \cup \{i_0\}$, where $i_0 \notin \hat{S}$ is an arbitrary node in that set. By the induction hypothesis we have for the set $\hat{S}$: $f_{\hat{S}}(\boldsymbol{u}) \geq 0$. It suffices to show that $f_{\hat{S}\cup\{i_0\}}(\boldsymbol{u}) \geq 0$.

We consider two cases. First, assume that $f_{\hat{S}}(\boldsymbol{u}) \geq 1$. Consider the difference:

$$f_{\hat{S}\cup\{i_0\}}(\boldsymbol{u}) - f_{\hat{S}}(\boldsymbol{u}) = \sum_{j\in N\setminus(\hat{S}\cup\{i_0\}):(i_0 j)\in E} u_{i_0 j} + \sum_{g\in G(\{i_0\})} u_g - u_{i_0} \tag{3.13}$$

Due to the binary nature of the variables in equation (3.13) we have $f_{\hat{S}\cup\{i_0\}}(\boldsymbol{u}) - f_{\hat{S}}(\boldsymbol{u}) \geq -1$. Since $f_{\hat{S}}(\boldsymbol{u}) \geq 1$, we obtain $f_{\hat{S}\cup\{i_0\}}(\boldsymbol{u}) \geq 0$.

Now assume that $f_{\hat{S}}(\boldsymbol{u}) = 0$. If $u_{i_0} = 0$, by (3.13), we obtain $f_{\hat{S}\cup\{i_0\}}(\boldsymbol{u}) - f_{\hat{S}}(\boldsymbol{u}) \geq 0$, which yields $f_{\hat{S}\cup\{i_0\}}(\boldsymbol{u}) \geq 0$. If $u_{i_0} = 1$, define $\sum_{i\in\hat{S}} u_i = \bar{k}$. Consequently, the following equality holds using that $f_{\hat{S}}(\boldsymbol{u}) = 0$:

$$\sum_{(ij)\in E: i,j\in\hat{S}} u_{ij} + \sum_{(ij)\in\delta(\hat{S})} u_{ij} + \sum_{g\in G(\hat{S})} u_g = \bar{k} \tag{3.14}$$

Denote $\bar{S}$ the subset of $\hat{S}$ corresponding to energized nodes: $\bar{S} = \{i \in \hat{S} : u_i = 1\}$, with $|\bar{S}| = \bar{k}$. Define the undirected graph $\bar{G}$ with node set $V_{\bar{G}} = \bar{S} \cup \{i_0\} \cup \{s\}$, where s is a dummy super-node which corresponds to all generators and to nodes $N \setminus (\hat{S} \cup \{i_0\})$, and edge set $E_{\bar{G}}$. For $E_{\bar{G}}$, we add an edge between $i \in \bar{S} \cup \{i_0\}$ and $j \in \bar{S} \cup \{i_0\}$ if $u_{ij} = 1$. Between $i \in \bar{S} \cup \{i_0\}$ and s we add $\sum_{j\in N\setminus(\hat{S}\cup\{i\}):(ij)\in E} u_{ij} + \sum_{g\in G(\{i\})} u_g$ edges. Note that the value of the left hand side of equation (3.14) is exactly the number of edges of $\bar{G}$ that have at least one endpoint in the set $\bar{S}$. To see that, note that even though $\bar{G}$ contains no edges associated with generator variables or edge variables of the nodes in $\hat{S} \setminus \bar{S}$, the corresponding variables will all be zero due to inequalities (3.1) and (3.2) and since the nodes in $\hat{S} \setminus \bar{S}$ are de-energized.

Since the vector $\boldsymbol{u}$ is feasible, there is a path from every energized node to an energized generator in the associated energized graph. In the context of graph $\bar{G}$, that means there exists a path from every node in $\bar{S} \cup \{i_0\}$ to node s. That implies that graph $\bar{G}$ is connected. The graph has $\bar{k} + 2$ nodes, so it must have at least $\bar{k} + 1$ edges. Exactly $\bar{k}$ edges have at least one endpoint in $\bar{S}$, due to (3.14). Therefore, there is at least one edge with no endpoints in $\bar{S}$, i.e. there is an edge between i_0 and the dummy node s. By the construction of the edge set of the graph, this implies $\sum_{j\in N\setminus(\hat{S}\cup\{i_0\}):(i_0j)\in E} u_{i_0j} + \sum_{g\in G(\{i_0\})} u_g \geq 1$, which together with (3.13) and $f_{\hat{S}}(\boldsymbol{u}) = 0$ leads to $f_{\hat{S}\cup\{i_0\}}(\boldsymbol{u}) \geq 0$. This concludes the proof by induction. □

This family of cuts is neither stronger nor weaker than the family of Type I cuts we introduced before. To see that, first consider a graph with two nodes $N = \{1, 2\}$, one branch $E = \{(1, 2)\}$, and two generators, $g(1)$ connected to node 1 and $g(2)$ connected to node 2. Consider the point $(u_1, u_2, u_{12}, u_{g(1)}, u_{g(2)}) = (1, 1, 1/2, 1/2, 1/2)$. This point satisfies all the Type I constraints. However, it violates the Type II constraint for $S = \{1, 2\}$, i.e. $u_{g(1)} + u_{g(2)} + u_{12} \geq u_1 + u_2$.

Conversely, consider the graph with $N = \{1, 2, 3\}$, edges $E = \{(1, 2), (1, 3), (2, 3)\}$ and one generator $g(1)$ connected to node 1. The point with values: $(u_1, u_2, u_3, u_{12}, u_{13}, u_{23}, u_{g(1)}) = (1/2, 1/2, 1/2, 1/2, 1/2, 1/2, 0)$ satisfies all constraints of Type II, but violates $u_{g(1)} \geq u_1$, the Type I constraint for $S = N$ for node $1 \in S$.

Proposition 6. *For a given, possibly fractional, $\boldsymbol{u} \in [0, 1]^d$, $f_S(\boldsymbol{u})$ is a submodular function of $S \subseteq N$.*

Proof. Consider two sets $A, B \subseteq N$ with $A \subseteq B$ and $i_0 \notin B$. We will show that $f_{A\cup\{i_0\}}(\boldsymbol{u}) - f_A(\boldsymbol{u}) \geq f_{B\cup\{i_0\}}(\boldsymbol{u}) - f_B(\boldsymbol{u})$. Using (3.13), the above inequality reduces to:

$$\sum_{j\in N\setminus(A\cup\{i_0\}):(i_0j)\in E} u_{i_0j} + \sum_{g\in G(\{i_0\})} u_g - u_{i_0} \geq \sum_{j\in N\setminus(B\cup\{i_0\}):(i_0j)\in E} u_{i_0j} + \sum_{g\in G(\{i_0\})} u_g - u_{i_0} \tag{3.15}$$

which is satisfied, since $A \subseteq B \implies N \setminus (A \cup \{i_0\}) \supseteq N \setminus (B \cup \{i_0\})$ and the variables u_{ij} are non negative. □

Corollary 1. *Constraints* (3.12) *can be separated in polynomial time.*

Proof. Given a fractional point $\boldsymbol{u}$, minimizing $f_S(\boldsymbol{u})$ over $S \subseteq N$ can be achieved in polynomial time (due to submodularity). If the optimal objective is negative, the minimizer S^* yields a violated constraint from (3.12). If the minimizer is non-negative, (3.12) is satisfied for all $S \subseteq N$. □

3.7 Polyhedral Analysis

For this section, we will assume for simplicity that the underlying (undirected) graph of the power system (N, E) is complete (i.e. there exists an edge between every two nodes) and that each node has a single generator (therefore, $|N| = |G|$). These assumptions are not realistic for actual power systems, but they allow for an easier analysis, with the aim of getting some insights on the strength of the inequalities introduced in the last two sections. We assume an arbitrary ordering of the nodes $\{1, \ldots, |N|\}$ (where the corresponding generators are $\{g(1), \ldots, g(|N|)\}$).

Proposition 7. *The convex hull conv(H) of the feasible region H is a full dimensional polyhedron.*

Proof. The convex hull is a polyhedron since the set of feasible points is finite. We will show that its dimension is $d = |N| + |E| + |G| = 2|N| + |E|$ by identifying $d + 1$ affinely independent points. Since the point $\boldsymbol{u} = 0$ is feasible, it suffices to find d linearly independent feasible points. Consider the following points:

1. $\boldsymbol{u}^{a_i}, i \in N$: Only node i and the corresponding generator $g(i)$ are energized ($|N|$ points):
2. $\boldsymbol{u}^{b_{ij}}, (ij) \in E$: Only two nodes i, j, the corresponding generators, and the edge connecting them are energized ($|E|$ points):
3. $\boldsymbol{u}^{c_{1j}}, j \in N \setminus \{1\}$: Only node 1 with generator $g(1)$, node j, and edge $(1j) \in E$ are energized ($|N| - 1$ points):
4. $\boldsymbol{u}^{d}$: Only node 1, node 2 with its generator, and edge (12) are energized (1 point).

We will show that the standard basis for $\mathbb{R}^d$ can be generated using linear combinations of the points above. Hence, the points span $\mathbb{R}^d$, and since there are d of them, they are linearly independent. To generate a vector $\boldsymbol{u}$ with only nonzero coordinate $u_g = 1$, for $g \in G(i), i \in N$: For $i = 1$, we simply need to subtract $\boldsymbol{u}^d$ from $\boldsymbol{u}^{b_{12}}$. For $i \neq 1$, we need to subtract $\boldsymbol{u}^{c_{1i}}$ from $\boldsymbol{u}^{b_{1i}}$. To generate a vector $\boldsymbol{u}$ with only nonzero coordinate $u_i = 1$ for $i \in N$, we can simply subtract the standard basis vector with only $u_g = 1, g \in G(i)$, generated previously, from $\boldsymbol{u}^{a_i}$. Finally, to generate a vector with only nonzero coordinate $u_{ij} = 1$, $(ij) \in E$, we form $\boldsymbol{u}^{b_{ij}} - \boldsymbol{u}^{a_i} - \boldsymbol{u}^{a_j}$. This completes the proof.

□

Proposition 8. *Constraints* (3.8) *with* $|S| = 1$*, i.e.:*

$$\sum_{j \in N} u_{nj} + u_{g(n)} \geq u_n, \quad n \in N \tag{3.16}$$

are facet defining for conv(H).

Proof. Since the convex hull of H is full dimensional, it suffices to find d affinely independent points in H that satisfy (3.16) with equality. One of them is the zero vector, so it suffices to find $d-1$ linearly independent points in H that satisfy (3.16) with equality. These are:

1. We will first consider points that have $u_n = 0$, $u_{g(n)} = 0$, and $u_{nj} = 0, j \in N$. Since these are the only variables in (3.16), the constraint is satisfied with equality. The variables corresponding to nodes $N \setminus \{n\}$, their generators, and the edges with both their endpoints between them (we will refer to these variables collectively by $\boldsymbol{u}_R$) can be chosen freely in a way that satisfies the IE constraints of a graph with $(|N| - 1)$ nodes and generators and $(|E| - |N| + 1)$ edges. Using the arguments in the proof of proposition 7, we can find $2(|N| - 1) + (|E| - |N| + 1) = |N| + |E| - 1$ feasible linearly independent points in this reduced space, which correspond to linearly independent points in the full space (where we have set the remaining variables equal to zero).

For the remaining points, the variables $\boldsymbol{u}_R$ are set equal to 1. We then choose:

2. For $j \in N \setminus \{n\}$, set $u_n = 1$, $u_{g(n)} = 0$, $u_{nj} = 1$, $u_{nk} = 0, k \in N \setminus \{n, j\}$. This yields $|N| - 1$ points that are linearly independent from each other and from all previous points since each one has a nonzero value at a position all previous ones did not have (i.e., u_{nj}).

3. Set $u_n = 1$, $u_{g(n)} = 1$, $u_{nj} = 0, j \in N \setminus \{n\}$. This yields 1 point linearly independent from the previous ones, since it is the only one that has $u_{g(n)} = 1$.

Therefore, we generated $(|N| + |E| - 1) + (|N| - 1) + 1 = 2|N| + |E| - 1 = d - 1$ linearly independent points in H, which concludes the proof.

□

Proposition 9. *Constraints* (3.8) *with* $S = N$*, i.e.:*

$$\sum_{i \in N} u_{g(i)} \geq u_n, \quad n \in N \tag{3.17}$$

are facet defining for conv(H).

Proof. We will prove the statement (without loss of generality) for $n = 1$. The zero vector satisfies (3.17) with equality, so we only need to find $d - 1$ linearly independent points in H that satisfy (3.17) with equality. We will generate d points (that are linearly dependent) and we will show they span a $d - 1$ dimensional subspace - hence there exists a subset of $d - 1$ points that are linearly independent. These points are:

1. $\boldsymbol{u}^{e_i}, i \in N$: Generator $g(1)$, nodes $1, 2, \ldots, i$, and edges $(1,2), (2,3), \ldots, (i-1, i)$ are energized. The rest of the system is de-energized. Note that $\boldsymbol{u}^{e_1}$ refers to the case where only $\boldsymbol{u}^{e_1}_{g(1)} = 1, \boldsymbol{u}^{e_1}_1 = 1$, and the rest of the network is de-energized. ($|N|$ points)

2. $\boldsymbol{u}^{f_i}, i \in N$: All nodes and edges are energized. Only the generator $g(i)$ (of node i) is energized and the others are not. ($|N|$ points)

3. $\boldsymbol{u}^{h_{ij}}, (ij) \in E$: All nodes are energized. All edges are energized, except edge (ij). Only generator $g(1)$ is energized and the rest are not. ($|E|$ points)

We will show the points above span a $d-1$ dimensional space by generating the columns of the following $d \times (d-1)$ full rank matrix:

$$\begin{array}{c} \\ \boldsymbol{u}_G \\ u_1 \\ \boldsymbol{u}_{N\setminus\{1\}} \\ \boldsymbol{u}_E \end{array} \begin{array}{c} \begin{array}{ccc} |G| & |N|-1 & |E| \end{array} \\ \begin{pmatrix} \boldsymbol{I}_{|G|} & \boldsymbol{0} & \boldsymbol{0} \\ \mathbb{1}_{1\times|G|} & \boldsymbol{0} & \boldsymbol{0} \\ 0 & \boldsymbol{I}_{|N|-1} & \boldsymbol{0} \\ \boldsymbol{0} & \boldsymbol{0} & \boldsymbol{I}_{|E|} \end{pmatrix} \end{array},$$

where $\boldsymbol{I}$ denotes the identity matrix and $\mathbb{1}$ the matrix of all ones. More specifically: to generate a vector with only nonzero coordinate $u_{ij} = 1$, for $(ij) \in E$, we form $\boldsymbol{u}^{f_1} - \boldsymbol{u}^{h_{ij}}$. To generate a vector with only nonzero coordinate $u_i = 1$, $i \in N \setminus \{1\}$, we form the vector $\boldsymbol{u}^{e_i} - \boldsymbol{u}^{e_{i-1}} + \boldsymbol{u}^{h_{i-1,i}} - \boldsymbol{u}^{f_1}$. Finally, we can generate a vector with only nonzero entries $u_{g(i)} = 1, u_1 = 1$, for some $i \in N$, by forming: $\boldsymbol{u}^{e_1} + \boldsymbol{u}^{f_i} - \boldsymbol{u}^{f_1}$. This completes the proof.

□

Proposition 10. *Constraints* (3.12) *with* $S = N$*, i.e.:*

$$\sum_{g\in G} u_g + \sum_{ij\in E} u_{ij} \geq \sum_{i\in N} u_i \tag{3.18}$$

are facet defining for conv(H).

Proof. We will assume without loss of generality that when we refer to an edge $(ij) \in E$, we have $i < j$. The zero vector satisfies (3.18) with equality, so we only need to find $d-1$ linearly independent points in H that satisfy (3.18) with equality. These are:

1. $\boldsymbol{u}^{a_i}, i \in N$: Only node i and the corresponding generator $g(i)$ are energized ($|N|$ points).

2. $\boldsymbol{u}^{k_{ij}}, (ij) \in E$: Only nodes i, j, edge (ij) and generator $g(i)$ are energized ($|E|$ points).

3. $\boldsymbol{u}^{l_i}, i \in N \setminus \{1\}$: Only nodes $1, i$, edge $(1i)$ and generator $g(i)$ are energized ($|N|-1$ points).

We will show these points span a $d-1$ dimensional subspace by showing we can use them to generate all columns of the full rank $d \times (d-1)$ matrix:

$$\begin{array}{c} \\ \boldsymbol{u}_G \\ u_1 \\ \boldsymbol{u}_{N\setminus\{1\}} \\ \boldsymbol{u}_E \end{array} \begin{array}{c} \begin{array}{ccc} |G| & |N|-1 & |E| \end{array} \\ \begin{pmatrix} \boldsymbol{I}_{|G|} & \mathbf{0} & \mathbf{0} \\ \mathbb{1}_{1\times|G|} & -\mathbb{1}_{1\times|N|-1} & \mathbb{1}_{1\times|E|} \\ 0 & \boldsymbol{I}_{|N|-1} & \mathbf{0} \\ \mathbf{0} & \mathbf{0} & \boldsymbol{I}_{|E|} \end{pmatrix} \end{array}.$$

To generate a column with $u_{g(i)} = 1, u_1 = 1$, for some $i \in N$, we form: $\boldsymbol{u}^{l_i} - \boldsymbol{u}^{k_{1i}} + \boldsymbol{u}^{a_1}$ for $i \neq 1$ and $\boldsymbol{u}^{a_1}$ for $i = 1$. To generate a column with $u_1 = -1, u_i = 1$, for $i \in N \setminus \{1\}$, we form $\boldsymbol{u}^{a_i} - \boldsymbol{u}^{a_1} - \boldsymbol{u}^{l_i} + \boldsymbol{u}^{k_{1i}}$. Finally, to generate a column with $u_1 = 1, u_{ij} = 1$, for some $(ij) \in E$, we form $\boldsymbol{u}^{k_{ij}} - \boldsymbol{u}^{a_i} - \boldsymbol{u}^{a_j} + \boldsymbol{u}^{a_1} + \boldsymbol{u}^{l_j} - \boldsymbol{u}^{k_{1j}}$. This concludes the proof. □

3.8 Connections to the Literature

The feasible region defined by the IE constraints can be transformed into the feasible region of the Rooted Maximum Weight Connected Subgraph Problem (RMWCS), with weights on edges and nodes. The problem appears in [84], where a decomposition algorithm is devised to solve it. The statement of the problem is as follows: consider an undirected graph with node set $\hat{N}$, edge set $\hat{E}$, and a given node $r \in \hat{N}$. Weights are associated with nodes and edges of the graph. We seek to find a maximum weight connected subgraph that contains r. This problem is a modification of the maximum weight connected subgraph problem.

The feasible region of the IE constraints can be transformed to the one of RMWCS. To see that, consider the underlying undirected graph of the power system, with edges E and nodes N. We introduce a dummy node r. We then add one edge between r and node i for every generator in $G(i)$. Edges connected to the root r correspond to the generator variables $u_g, g \in G$. The remaining edges correspond to the branch variables $u_{ij}, ij \in E$, and the nodes correspond to the bus variables $u_i, i \in N$. Since the root node r must be included in the subgraph, and the subgraph needs to be connected, every energized element has to be connected to r with one edge variable (which corresponds to the energized generator).

MIP formulations for the RMWCS have been studied in [40] for the directed graph version of the problem. In this version, each node in the subgraph must be reachable from the root via a directed path. The authors present a single commodity and a multi-commodity flow formulation, similar to the ones in our work. They also present a cut-set formulation, but with the further restriction that the subgraph forms an arborescence: for every node there exists a unique directed path from the root node.

In [45] the authors transform the undirected, node weighted, unrooted, connected subgraph problem to the Steiner tree problem, using the fact that the subgraph can without loss of generality be chosen to be a tree for the case of only node weights. Using this transformation, they employ algorithms for the Steiner tree problem to solve instances in protein–protein interaction networks.

Note that edge weights can also be accommodated in this framework by adding a node with the corresponding weight of every edge.

In [12] the feasible region for the unrooted, undirected version of the problem is formulated in the space of only edges. A new set of constraints is introduced, namely the matching partition inequalities. These inequalities define facets of the integer hull under some assumptions. A convex hull description is given for cycles and trees. Constraints similar to (3.8) are used, with the only difference that the in the right hand side edge variables appear instead of node variables - this actually leads to a weaker constraint, due to (3.2), but the node variables are eliminated.

In [6] the authors formulate the RMWCS for the directed and undirected case in the space of only nodes and present a polyhedral analysis for that polyhedron as well as a comparison of the strength of the formulation with the edge-based formulation. They use a set of inequalities based on node-separators. The formulation at the space of nodes can be strengthened using lifting of the node separator inequalities [5, 150] and one more family of inequalities, the in-degree inequalities, as shown in [150], to become as strong as the edge-based formulation.

Multiple publications have dealt with the computational aspects of solving the problem in applications outside the power systems domain. In [123], reduction techniques and other computational tools are used for exact optimization. In [21] the model appears in a forestry planning application.

In most of the aforementioned literature, the problem is formulated either exclusively in the space of edges or in the space of nodes to reduce the number of variables. In our applications, however, we need both nodes and edges, since both types of variables appear in constraints other than the ones regarding connectivity. For example, the node energization variable is necessary to also indicate if this bus can support load or not. Edges appear in the switching models of the power flow equations, to regulate when the branches are open/closed. Edges also appear in the reactive power equations, since they are associated with the reactive power generation from long transmission lines.

It should also be noted that there are two ways to transfer results from the space of variables corresponding to arcs in a directed graph to the space corresponding to the edges of the undirected graph in the case of the RMWCS: the first one is to simply consider the undirected version of the constraints (i.e. omit the directions and substitute the in-neighbor set and out-neighbor set of a node with the undirected set of neighbors), if they remain valid. The second one is to consider each undirected graph as a directed graph with two edges, (ij) and (ji) with corresponding variables x_{ij} and x_{ji}, for every edge (ij) in the original undirected graph. Then, we set the variable of the undirected case u_{ij} equal to $u_{ij} = x_{ij} + x_{ji}$. This yields a strong formulation for the undirected graph (in fact, using the model from [6] together with this observation, we can get a stronger formulation than the formulations we considered in the previous sections, but in an extended variable space).

Formulation F_3 (i.e. the Type I constraints) is a straightforward extension of the common Steiner-tree based formulation for imposing an arborescence in directed graphs [40]. Our formulation differs from the formulations that impose the requirement for a spanning tree of the subgraph to ensure connectivity, such as in the vast literature on the prize collecting Steiner tree, in that the edge variables are allowed to form cycles in our case. Of course, the feasible region projected in the space of nodes is the same since connectivity of the subgraph is equivalent to the existence of

a spanning tree. To the best of our knowledge, the Type II constraints have not appeared in the literature for RMWCS. More importantly, identifying the connection to RMWCS for problems in the power systems literature is, to the best of our knowledge, first done in this work, and can lead to further explotation of this structure, potentially even for power systems applications that we did not consider with the same underlying requirements.

3.9 A Simplified BSA Model

The goal of this section is to provide a simplified model and a solution approach to obtain a candidate black start allocation (BSA) for large scale systems with optimality guarantees. Even after only retaining the basic structure of the BSA problem, for a system of a few thousand buses the resulting mixed integer program still contains millions of constraints and hundreds of thousands of binary variables, and solving the linear programming relaxation alone can take hours. The key idea described in what follows is to use a greedy heuristic to obtain a lower bound to the maximization problem and then reformulate the constraints to obtain a tight upper bound.

The Model

In this section, we present a version of the BSA problem that exhibits a better computational performance for large scale systems compared to the one presented in the previous chapter, while retaining the basic structure of the problem. Let t denote an integer time instance (T being the set of consecutive integer time instances starting from 0), g denote a generator in set G, i a bus (node) in set N, and (ij) a branch (edge) in set A. We use the binary variable u_{BS_g} to indicate, when set to 1, the allocation of generator $g \in G$ as a black start unit. The binary variables u_g^t, u_i^t, u_{ij}^t denote the energization (when set to 1) of generator g/bus i/branch (ij) at time t. Generator g is also associated with the binary cranking variable u_{CR_g}, which is 1 while the generator is cranking and the variable w_g^t which is equal to $u_g^t(1 - u_{BS_g})$. The variables f_g^t, f_{ij}^t denote the network flows of the F_1 formulation at time t, p_g^t is the active generation of generator g, p_{ij}^t is the active power flow on branch (ij), and $p_{SH_i}^t$ is the load shed at bus i. Finally, the parameters of the problem are the cost C_{BS_g} of allocating generator g to be a BS unit, the total allocation budget B, the number of allowable branch energizations per unit time K_{crew}, the generator active power maximum $P_g^{\max}$, active power minimum $P_g^{\min}$, cranking time T_{CR_g} (assumed to be a positive integer), cranking power P_{CR_g}, and minimum reactive power capability $\underline{Q}_g$, the bus load $P_{D_i} \geq 0$, angle ϕ_{D_i} and shunt reactance Q_{SH_i}, and the branch susceptance $B_{SH_{ij}}$ and branch power limit $\bar{S}_{ij}$. We define

the following optimization problem:

$$\text{maximize} \quad \sum_{(ij)\in A, t\in T} u_{ij}^t + \sum_{i\in N, t\in T} u_i^t + \lambda_G \sum_{t\in T} f(\boldsymbol{u}^t)$$

subject to

$$\sum_{g\in G} C_{BS_g} u_{BS_g} \leq B \tag{3.19a}$$

$$u_i^0 = 0,\ i \in N,\ u_g^t = 0,\ g \in G, t \in \{-T_{CR_g}, \ldots, -1\} \tag{3.19b}$$

$$u_g^t \geq u_g^{t-1},\ g \in G, t \in T \setminus \{0\} \tag{3.19c}$$

$$u_{CR_g}^t = u_g^t - u_g^{t-T_{CR_g}},\ g \in G, t \in T \tag{3.19d}$$

$$u_{ij}^t \leq u_i^{t-1} + u_j^{t-1}\ ,\ (ij) \in A,\ t \in T \setminus \{0\} \tag{3.19e}$$

$$\sum_{(ij)\in A} (u_{ij}^t - u_{ij}^{t-1})^+ \leq K_{\text{crew}},\ t \in T \setminus \{0\} \tag{3.19f}$$

$$u_{CR_g}^t \leq u_i^t + u_{BS_g},\ g \in G(i), i \in N \tag{3.19g}$$

$$u_g^t - u_{CR_g}^t \leq u_i^t\ ,\ i \in N,\ g \in G(i),\ t \in T \tag{3.19h}$$

$$u_{ij}^t \leq u_i^t,\ u_{ij}^t \leq u_j^t\ ,\ (ij) \in A,\ t \in T \tag{3.19i}$$

$$0 \leq f_g^t \leq u_g^t - u_{CR_g}^t,\ g \in G,\ t \in T, \tag{3.19j}$$

$$-u_{ij}^t \leq f_{ij}^t \leq u_{ij}^t,\ (ij) \in A,\ t \in T, \tag{3.19k}$$

$$\sum_{j:(ji)\in A} f_{ji}^t - \sum_{j:(ij)\in A} f_{ij}^t + \sum_{g\in G(i)} f_g^t = \frac{1}{|N|} u_i^t,\ i \in N,\ t \in T \tag{3.19l}$$

$$w_g^t + u_{BS_g} \geq u_g^t,\ g \in G, t \in T \tag{3.19m}$$

$$w_g^t \leq u_g^t,\ g \in G, t \in T \tag{3.19n}$$

$$w_g^t + u_{BS_g} \leq 1,\ g \in G, t \in T \tag{3.19o}$$

$$p_g^t \geq -P_{CR_g} w_g^t + (P_{CR_g} + P_g^{\min}) w_g^{t-T_{CR_g}},\ g \in G, t \in T \tag{3.19p}$$

$$p_g^t \leq P_g^{\max}(u_g^t - u_{CR_g}^t) - P_{CR_g}(w_g^t - w_g^{t-T_{CR_g}}),\ g \in G, t \in T \tag{3.19q}$$

$$-u_{ij}^t \bar{S}_{ij} \leq p_{ij}^t \leq \bar{S}_{ij} u_{ij}^t,\ (ij) \in A,\ t \in T \tag{3.19r}$$

$$\sum_{j:(ji)\in A} p_{ji}^t - \sum_{j:(ij)\in A} p_{ij}^t + \sum_{g\in G(i)} p_g^t = P_{D_i} - p_{SH_i}^t,\ i \in N,\ t \in T \tag{3.19s}$$

$$(1 - u_i^t) P_{D_i} \leq p_{SH_i}^t \leq P_{D_i},\ i \in N,\ t \in T \tag{3.19t}$$

$$\sum_{i\in N} \sum_{g\in G(i)} \underline{Q}_g u_g^{\max\{0, t-T_{CR_g}-1\}} + \sum_{(ij)\in A} B_{SH_{ij}} u_{ij}^t + \sum_{i\in N} Q_{SHi} u_i^t - \sum_{i\in N} P_{D_i} \tan(\phi_{D_i}) \leq 0,\ t \in T \tag{3.19u}$$

The objective is a measure of the energization state of the system at different time instances.

The first two objective terms encourage energization of grid branches and buses. We define $f(\boldsymbol{u}^t) = \min(\alpha_L \sum_{i \in N} P_{D_i}, \sum_{g \in G} u_g^t P_g^{\max})$. This definition is motivated by the fact that we want to energize generating units to support the power system, but since real power systems operate with large excess generation capacity we do not need to encourage unit energization after the total capacity of energized units exceeds a multiple α_L of the total load. The parameter λ_G is a trade-off coefficient.

Constraint (3.19a) imposes the black start allocation budget on the selection of black start units. The restoration of the system will start around these units. One simplified way to visualize the underlying optimization is as follows: We have a given budget to pick a few generators on the system (corresponding to particular nodes). We can then expand the system energization around these nodes in the power system graph over time. The objective metric corresponds roughly to how much of the system we were able to energize, measured at given time instances after the start of the process. Of course, the energization process needs to obey certain rules, such as operator switching limits, startup curves for the generators, power constraints for every island. We include some of these constraints in the optimization problem.

Constraint (3.19b) initializes the node and generator variables to zero (total blackout). Constraint (3.19c) stipulates that a generator can only be energized once. This assumption is only introduced to simplify the model - there is no actual system requirement for that. This assumption is not unreasonable though, since during the first steps of restoration (to which our optimization refers to), we usually tend to energize generators to stabilize the system and support more load, rather than turn them off. It is usually when the system returns to normal operation that costly units that were only energized for restoration purposes will be turned off again. (3.19d) defines the cranking variable (a generator is cranking if and only if it is currently energized but was not energized T_{CR_g} time units in the past).

(3.19e) and (3.19f) impose a limit on the rate for the energization. (3.19e) imposes that we can only energize an edge, if at least one of its buses was energized at the previous time step. (3.19f) is a physical constraint that comes from the fact that the operator has finite resources (people) to restore the system. We assume that each branch energization takes some time to happen (time that has to do with ensuring the feasibility of the energization as well as performing the necessary operations to implement the switching). K_{crew} indicates the number of branch energizations per time step. De-energizations of branches are usually faster, so we don't limit their number per time step. Note that we use the notation $(x)^+ = \max\{0, x\}$.

Constraint (3.19g) stipulates that nodes corresponding to cranking generators must be on, except if the cranking generator is a black start. (3.19h) imposes that a generator that has finished cranking energizes the node it connects to. (3.19i) imposes that an energized branch must have both its endpoints energized. Constraints (3.19j)-(3.19l) impose the island energization requirement: any energized bus must be connected to an energized generator that has completed cranking. This constraint is slightly different than the version used in the model of the previous chapter, in the sense that we impose the stronger requirement that a node must be connected to an energized generator that has also finished cranking to be energized. This choice was associated with an observed improved computational performance. It imposes a change in the feasible restoration sequences around the black start units during the first restoration steps. In terms of modeling, it corresponds

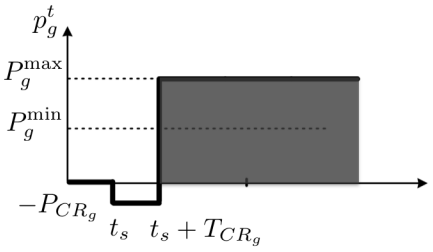

(a) Start-up curve for a non black-start unit ($u_{BS_g} = 0$) in the simplified model. After the unit starts at time t_s, it needs to crank by absorbing active power P_{CR_g} from the system for time T_{CR_g}. Following that, it can move at any point between the minimum and maximum generation, $P_g^{\min}$ and $P_g^{\max}$ respectively.

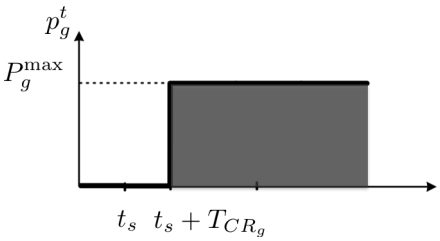

(b) Start-up curve for a black-start unit ($u_{BS_g} = 1$) in the simplified model. After the unit starts at time t_s, it needs to crank for time T_{CR_g}. However, the cranking power does not need to be provided by the system. Following that, generation can move at any non negative point below the maximum generation $P_g^{\max}$.

Figure 3.3: Generator active power curve for a black-start and a non black-start unit. The curves are jointly described by equations (3.19m)-(3.19q). The variable w_g^t corresponds to the product $u_g^t(1 - u_{BS_g})$, which is linearized.

to using the variable difference $u_g^t - u_{CR_g}^t$ in the place of u_g^t in all the IE constraints.

Constraints (3.19m)-(3.19q) define the generator model, as described in figure 3.3. Compared to the restoration model in the previous chapter, we note that we omitted the ramping constraints. This change comes from the fact that for this large scale system we are using a coarser time resolution interval (an hour). Most of the generating units that are used in the first steps of restoration are capable to ramp up or down quickly enough to render the ramping constraints redundant, which in turn allows us to use a simpler model based on step functions. We directly model the startup curves for black start and non black start units using additional binary variables instead of using the transformations of the previous sections.

Constraints (3.19p)-(3.19t) define a transportation model for the active power flow. This is in fact a major simplification made for the sake of computational tractability, since the transmission switching model used in the previous chapter is omitted. As a result, Kirchhoff's voltage law might not be respected by the solution. However, the set of constraints used ensures at least that every island that appears during the restoration process satisfies active power balance (i.e. the total island generation equals the island demand). This incorporates two important restoration considerations: First, for every generator that gets cranked, there is sufficient active power generation in the island to support its cranking power. Second, every generator that has finished cranking and needs to keep its generation above the minimum generation point $P_g^{\min}$ can find enough load in the island to do that. Finally, (3.19u) imposes an aggregate reactive power constraint (the reactive power absorbtion capability of generators, shunt reactances, and reactive load is enough to overcome the reactive power generation induced by the branch susceptances of large transmission lines).

As a conclusion to the model discussion, we should note that the aim of this optimization is not to generate a complete restoration sequence. Rather, the goal is to identify good positions for black start units in the graph, while picking black start units with suitable startup characteristics, and for that a simplified model which captures the main problem characteristics can be sufficient for a

planning tool. Generating the actual detailed restoration sequences that respect all the constraints needs a significant amount of more detail, which is hard to accomplish while also optimizing for the locations of the black start units (and is even hard if these locations are known). Of course, before an actual decision for the black starts is made, a more detailed simulation should be performed with the positions of these units fixed. We can always exclude a unit black start allocation by using a "No-Good-Cut" and resolving the problem (see chapter 4).

Model Transformation

The optimization problem as defined above, while direct and intuitive to present, employs a very large number of variables, which leads to slow computations. In this section we will use two transformations (constraint reformulations) to reduce the number of variables while mostly maintaining or even improving the quality of upper bounds. The resulting formulations have an exponential number of constraints, but by including only a small, carefully selected subset of them a priori and treating the rest as lazy constraints, we can obtain a smaller optimization problem without a significant loss in the quality of the upper bounding properties of the relaxations.

First, we can reformulate (3.19j)-(3.19l) using the observations of this chapter. Specifically, we eliminate variables f_g^t and f_{ij}^t and use the exponential in size set of Type I constraints. As shown in the previous section, the Type II constraints presented are also valid, so they can be used to further strengthen the formulation.

We will next eliminate the variables $p_g^t, p_{ij}^t, p_{SH_i}^t$ and the constraints they appear in, i.e. (3.19p)-(3.19t). To that end, we define for a given $t \in T$:

$$\hat{P}_g^{t,\max} = P_g^{\max}(u_g^t - u_{CR_g}^t) - P_g^{\min} w_g^{t-T_{CR_g}},\ g \in G \tag{3.20a}$$

$$\hat{p}_g^t = p_g^t + P_{CR_g} w_g^t - (P_{CR_g} + P_g^{\min}) w_g^{t-T_{CR_g}},\ g \in G \tag{3.20b}$$

$$\hat{P}_{SH_i}^{t,\max} = P_{D_i} u_i^t,\ i \in N \tag{3.20c}$$

$$\hat{p}_{SH_i}^t = p_{SH_i}^t - (1 - u_i^t) P_{D_i},\ i \in N \tag{3.20d}$$

$$\hat{P}_{D_i}^t = P_{D_i} u_i^t + \sum_{g \in G(i)} (P_{CR_g} w_g^t - (P_{CR_g} + P_g^{\min}) w_g^{t-T_{CR_g}}),\ i \in N \tag{3.20e}$$

Note that $\hat{P}_g^{t,\max} \geq 0$ for all feasible binary assignments, which we can see using $w_g^t = u_g^t(1 - u_{BS_g})$, equation (3.19d), and the fact that $0 \leq P_g^{\min} \leq P_g^{\max}$. Also, recall that the edge set A is a set of directed edges that correspond to the branches of the power system by arbitrarily picking a "from" and "to" direction for each branch. We also define a (directed) edge set $\tilde{A}$ based on the edge set A which contains both the arcs (ji) and (ij) for every arc $(ij) \in A$. That way, every flow p_{ij}^t satisfying (3.19r) in A can be decomposed into two non negative flows in $\tilde{A}$ with $\hat{p}_{ij}^t = \max(0, p_{ij}^t)$ and $\hat{p}_{ji}^t = \max(0, -p_{ij}^t)$ (and conversely we can obtain a flow for A by setting $p_{ij}^t = \hat{p}_{ij}^t - \hat{p}_{ji}^t$.

Using the above definitions, equations (3.19p)-(3.19t) are equivalently expressed:

$$0 \leq \hat{p}^t_g \leq \hat{P}^{t,\max}_g,\ g \in G \tag{3.21a}$$

$$0 \leq \hat{p}^t_{ij} \leq \bar{S}_{ij} u^t_{ij},\ 0 \leq \hat{p}^t_{ji} \leq \bar{S}_{ij} u^t_{ij},\ (ij) \in \tilde{A} \tag{3.21b}$$

$$0 \leq \hat{p}^t_{SH_i} \leq \hat{P}^{t,\max}_{SH_i},\ i \in N \tag{3.21c}$$

$$\sum_{j:(ji)\in\tilde{A}} \hat{p}^t_{ji} - \sum_{j:(ij)\in\tilde{A}} \hat{p}^t_{ij} + \sum_{g\in G(i)} \hat{p}^t_g + \hat{p}^t_{SH_i} = \hat{P}^t_{D_i},\ i \in N \tag{3.21d}$$

Note the variables $p^t_g, p^t_{ij}, p^t_{SH_i}$ are uniquely defined by the variables $\hat{p}^t_g, \hat{p}^t_{ij}, \hat{p}^t_{SH_i}$ and vice versa based on the transformations given above. The system (3.21) is feasible for $\hat{p}^t_g, \hat{p}^t_{ij}, \hat{p}^t_{SH_i}$ if and only if the following system of equations is feasible. For all $S \subseteq N$:

$$\sum_{i\in S} \hat{P}^t_{D_i} + \sum_{(ij)\in\delta(S)} \bar{S}_{ij} u^t_{ij} \geq 0 \tag{3.22a}$$

$$\sum_{i\in S} \hat{P}^{t,\max}_{SH_i} + \sum_{g\in G(S)} \hat{P}^{t,\max}_g + \sum_{(ij)\in\delta(S)} \bar{S}_{ij} u^t_{ij} \geq \sum_{i\in S} \hat{P}^t_{D_i} \tag{3.22b}$$

where we denote with $\delta(S)$ the edges in A with exactly one endpoint in S. The equivalence is straightforward application of Hoffman's Circulation Theorem or the maximum flow - minimum cut theorem. We give a proof for reasons of completeness.

Proposition 11. *System* (3.21) *has a solution with respect to* $\{\hat{p}^t_g\}_{g\in G}$, $\{\hat{p}^t_{ij}\}_{ij\in A}$, $\{\hat{p}^t_{SH_i}\}_{i\in N}$ *if and only if system* (3.22) *is satisfied.*

Proof. ($\Longrightarrow$) Assume (3.21) has a solution with respect to $\{\hat{p}^t_g\}_{g\in G}$, $\{\hat{p}^t_{ij}\}_{ij\in A}$, $\{\hat{p}_{SH_i}\}_{i\in N}$. Given a set $S \subseteq N$, by summing equations (3.21d) for $i \in S$, we obtain:

$$\sum_{(ji)\in\tilde{A}: j\in N\setminus S, i\in S} \hat{p}^t_{ji} + \sum_{g\in G(S)} \hat{p}^t_g + \sum_{i\in S} \hat{p}^t_{SH_i} = \sum_{i\in S} \hat{P}^t_{D_i} + \sum_{(ij)\in\tilde{A}: i\in S, j\in N\setminus S} \hat{p}^t_{ij}$$

Due to (3.21a)-(3.21c), the left hand side of the above equation is non negative and the right hand side is less than or equal to $\sum_{i\in S} \hat{P}^t_{D_i} + \sum_{(ij)\in\delta(S)} \bar{S}_{ij} u^t_{ij}$. This yields equation (3.22a). Furthermore, again due to (3.21a)-(3.21c), the right hand side of the above equation is greater than or equal to $\sum_{i\in S} \hat{P}^t_{D_i}$ and the left hand side is less than or equal to $\sum_{i\in S} \hat{P}^{t,\max}_{SH_i} + \sum_{g\in G(S)} \hat{P}^{t,\max}_g + \sum_{(ij)\in\delta(S)} \bar{S}_{ij} u^t_{ij}$. This yields equation (3.22b).

($\Longleftarrow$) In order to show the reverse implication, we construct the graph of figure 3.4. The node set consists of the power system nodes N, a source node n_s, a sink node n_t, and a node corresponding to generators n_G. We define $N_{\text{pos}} = \{i \in N : \hat{P}^t_{D_i} > 0\}$ and $N_{\text{neg}} = \{i \in N : \hat{P}^t_{D_i} < 0\}$. Note that due to (3.22a) for $S = N$, we have that $\sum_{i\in N} \hat{P}^t_{D_i} \geq 0$.

We add the following directed capacitated edges:

1. From n_s to n_G, with capacity $\sum_{i\in N} \hat{P}^t_{D_i}$.

2. From n_s to $i \in N_{\text{neg}}$, with capacity $-\hat{P}^t_{D_i}$.

3. From $j \in N_{\text{pos}}$ to n_t, with capacity $\hat{P}^t_{D_j}$.

4. From $i \in N$ to $j \in N$ if $(ij) \in \tilde{A}$, with capacity $\bar{S}_{ij} u^t_{ij}$

5. From n_G to $i \in N$ with capacity $P^{t,\max}_{SH_i} + \sum_{g \in G(i)} \hat{P}^{t,\max}_g$.

We will now show that, if (3.22) holds, the minimum $n_s - n_t$ cut in this graph is exactly equal to $\sum_{i \in N_{\text{pos}}} \hat{P}^t_{D_i}$. In order to show that, we show that every cut is greater than or equal to $\sum_{i \in N_{\text{pos}}} \hat{P}^t_{D_i}$. Since the cut $S = \{n_s, n_G, N\}$, $T = \{n_t\}$ has exactly that capacity, it is a minimum cut.

Indeed, we have two cases: If node n_G belongs to T, the capacity of the cut is:

$$\sum_{i \in N} \hat{P}^t_{D_i} + \sum_{ij \in \delta(S)} \bar{S}_{ij} u^t_{ij} + \sum_{i \in N_{\text{neg}} \cap T} (-\hat{P}^t_{D_i}) + \sum_{i \in N_{\text{pos}} \cap S} \hat{P}^t_{D_i},$$

which is greater than or equal to $\sum_{i \in N_{\text{pos}}} \hat{P}^t_{D_i}$ due to (3.22a) applied to set S. If node n_G belongs to S, the capacity of the cut is:

$$\sum_{i \in T} P^{t,\max}_{SH_i} + \sum_{g \in G(T)} \hat{P}^{t,\max}_g + \sum_{ij \in \delta(T)} \bar{S}_{ij} u^t_{ij} + \sum_{i \in N_{\text{neg}} \cap T} (-\hat{P}^t_{D_i}) + \sum_{i \in N_{\text{pos}} \cap S} \hat{P}^t_{D_i},$$

which is greater than or equal to $\sum_{i \in N_{\text{pos}}} \hat{P}^t_{D_i}$ due to (3.22b) applied to set T.

Since the minimum cut exactly equals $\sum_{i \in N_{\text{pos}}} \hat{P}^t_{D_i}$, there exists a corresponding maximum flow of the same value on the graph. Since the flows from $i \in N_{\text{pos}}$ to n_t are non negative and upper bounded by $\hat{P}^t_{D_i}$, and the total flow into n_t has to equal $\sum_{i \in N_{\text{pos}}} \hat{P}^t_{D_i}$, we have that each flow from $i \in N_{\text{pos}}$ to n_t exactly equals $\hat{P}^t_{D_i}$. Using a similar argument, since $\sum_{i \in N_{\text{pos}}} \hat{P}^t_{D_i} = \sum_{i \in N} \hat{P}^t_{D_i} + \sum_{i \in N_{\text{neg}}} (-\hat{P}^t_{D_i})$, the flow from n_s to $i \in N_{\text{neg}}$ is equal to $(-\hat{P}^t_{D_i})$ and the flow from n_s to n_G is equal to $\sum_{i \in N} \hat{P}^t_{D_i}$. The remaining flows on the graph yield feasible values for $\hat{p}^t_g$, $\hat{p}^t_{ij}$, and $\hat{p}^t_{SH_i}$ in the system (3.21). Specifically, the flow on $(ij) \in \tilde{A}$ corresponds to $\hat{p}^t_{ij}$ and the flow on the edge from n_G to i corresponds to $\sum_{g \in G(i)} \hat{p}^t_g + \hat{p}^t_{SH_i}$. The flow balance equation for node $i \in N$ yields (3.21d). □

The constraint set (3.22) can be separated efficiently using minimum cut on the graph in figure 3.4 of the last proof. This separation can be used in a Benders-like scheme and is faster in general than solving the linear program (3.21). To be more precise, given a point $\{\hat{P}^t_{D_i}\}_{i \in N}$, $\{P^{t,\max}_{SH_i}\}_{i \in N}$, $\{u^t_{ij}\}_{(ij) \in E}$, $\{\hat{P}^{t,\max}_g\}_{g \in G}$:

1. If $\sum_{i \in N} \hat{P}^t_{D_i} < 0$, add cut (3.22a) for $S = N$.

2. If $\sum_{i \in N} \hat{P}^t_{D_i} \geq 0$, create the graph of figure 3.4:

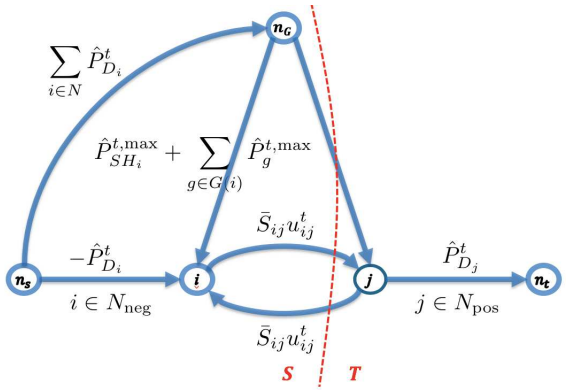

Figure 3.4: Graph used to separate constraints (3.22).

- If the minimum $n_s - n_t$ cut is less than $\sum_{i \in N_{\text{pos}}} \hat{P}^t_{D_i}$ and n_G belongs to the sink set T, add cut (3.22a) for the set T.
- If the minimum $n_s - n_t$ cut is less than $\sum_{i \in N_{\text{pos}}} \hat{P}^t_{D_i}$ and n_G belongs to the source set S, add cut (3.22b) for the source set S.
- If the minimum $n_s - n_t$ cut is equal to $\sum_{i \in N_{\text{pos}}} \hat{P}^t_{D_i}$, all the constraints (3.22) are satisfied.

The other advantage of having an explicit form for the reformulation (as opposed to only a cut generation scheme) is that we can add some of the constraints a priori, if we believe that they are going to be effective in deriving good bounds. In fact, we will exploit that in the computations of the Texas system. Note finally that the new variables $\hat{P}^{t,\max}_g$, $\hat{P}^{t,\max}_{SH_i}$, $\hat{P}^t_{D_i}$ are never introduced in the optimization - constraints (3.22) are simplified to only contain the original binary variables before these get added to the optimization.

Customized Heuristic for Lower Bounds

A customized heuristic is used to obtain lower bounds (feasible solutions) to the problem. The heuristic used is the same step-wise greedy heuristic that was described in the previous chapter to obtain feasible solutions - gradually fixing binary variables up to a given time step and then solving the LP relaxation of the problem corresponding to the future time steps, and subsequently repeating for the next time step. There are two enhancements: First, since even the LP relaxation is hard to solve for large systems and for the full horizon, a smaller look-ahead time was considered in the heuristic subproblems instead (typically up to 10 time steps). Second, when using a small enough look-ahead (of $2 - 5$ time steps), we can obtain near optimal solutions for that restricted mixed integer program instead of the LP relaxation, which we can also use in the greedy step-wise heuristic.

3.10 Experimental Results

All optimization problems in this section were formulated using Gurobi with Python. Each simulation was executed at a single node of the Lawrence Livermore National Laboratory quartz server (2 $\times$ Intel Xeon E5-2695, 36 cores, 128 GB RAM), running Red Hat Enterprise. The simulations employ instances of the ICI and BSA problem, in which the IE constraint appears. We experiment with the impact that reformulating the IE constraint has on these instances. We perform two types of simulations. First, we want to evaluate the bound quality improvement due to the difference in the strength of the formulations, for the two applications of interest. Second, we want to compare how the difference in the formulation of the problem impacts the computational times in practice. The second part is important, since formulation strength is not the only factor that influences the computational time - including all constraints from a large formulation can often be too time consuming.

As far as the quality of bound is concerned, we compare four possible implementations and solve the relaxation of the root node in each case:

(i) Formulation F_1.

(ii) Formulation F_3 (Type I cuts), which is equivalent to formulation F_2.

(iii) Formulation F_1 with Type II cuts.

(iv) Formulation F_3 (Type I cuts) with Type II cuts.

For the separation of the Type I constraints we use an implementation of the push-relabel algorithm for the maximum flow in the python-igraph package [35]. For the separation of the Type II constraints, we implement a cutting plane algorithm for submodular minimization based on minimizing the Lovasz extension [10, 145], using linear programming. The separation is not exact, due to the numerical tolerances used. Specifically, we stopped adding constraints when the maximum violation found was less than 0.001. In some cases, this process did not terminate within the 20000s time limit imposed. In these cases the final objective was reported - in fact in all of these cases at least the first 5 significant digits of the objective value did not change in the last iteration. These termination criteria are not necessarily good indicators of obtaining an accurate optimal objective for the root node relaxation, which is why the values reported should be treated as upper bounds for the BSA problem and lower bounds for the ICI problem of the actual root node relaxation objective.

For the second part of simulations, we will solve for points over the same feasible region in $\mathbb{Z}^b$, implemented using the following alternatives for imposing the IE constraints:

(A) Formulation F_1.

(B) Formulation F_2.

ICI Root	F1 [%]	F3 (Type I) [%]	F1 & Type II [%]	F3 & Type II [%]	Best Bound
IEEE-118 $K = 4$	27.36	11.75	18.87	11.75	3.68
Polish $K = 3$	0.89	0.44	0.44	0.44	17.77
Polish $K = 4$	4.61	1.34	3.79	1.34	27.39
Polish $K = 5$	6.24	0.81	4.07	0.81	44.91

Table 3.1: Optimal ICI root node relaxation for the IEEE-118 and Polish systems, splitting the system into K islands, employing the different formulations. The last column corresponds to the best bound found by the complete branch and cut tree, when the problem was solved to 1% optimality. Columns 2-5 show the difference of the root node lower bound of the respective formulation from the best lower bound found in column 5, as a percentage of the best bound.

(C) Formulation based on F_3 (Type I cuts). For this implementation, we a priori included in the constraint body passed to the solver the Type I constraints with $|S| \in \{1, |N|\}$. We use integer callbacks to lazily add the remaining Type I constraints, only if they are violated for an integer feasible point found by the solver. Since these points are integer, separation of Type I cuts can be done simply through a graph traversal (we can find islands that violate the IE constraints in linear time). Note that since we do not use nodal callbacks in the branch and bound tree, we lose part of the strength of formulation F_3. However, in our computational experiments, this compromise resulted in faster solution times.

(D) Formulation based on F_3 enhanced with Type II cuts. For this implementation, we a priori included in the constraint body passed to the solver the Type I and Type II constraints with $|S| \in \{1, |N|\}$. We use integer callbacks to lazily add the remaining Type I constraints, only if they are violated for an integer feasible solution. For the islands that are identified to violate the constraint, we also add the Type II cuts.

Unless specified otherwise, for these simulations a 2000s time limit was set to the solver and a 1% optimality gap termination was considered (i.e. a solution guaranteed to be within 1% of the optimal is denoted as optimal) for all simulations. Some instances caused the B&B tree to run out of memory due to the size of the problem. For these instances (indicated with *), we present results using settings that limit the solver's memory use by restricting the number of threads to 4 and using the file system as temporary storage.

Optimal Intentional Controlled Islanding

The most common practice behind ICI is that the generators of the grid can be divided into groups of coherent generators, based on their relative angle response to a disturbance. By isolating unstable generators or grouping together only generators that are coherent to each other, a cascaded outage may be avoided. In [81], an optimal ICI model was devised to propose switching actions.

Optimal ICI	Gap [%]	Upper Bound	Lower Bound	Time [s]
IEEE-118	$K = 4$			
(A)	Optimal	3.684	3.684	0.11
(C)	Optimal	3.684	3.684	0.64
(D)	Optimal	3.684	3.684	0.66
(R)	Optimal	3.684	3.684	1.5
Polish	$K = 3$			
(A)	Optimal	17.771	17.612	3
(C)	Optimal	17.771	17.771	12
(D)	Optimal	17.771	17.771	10
(R)	Optimal	17.771	17.771	41
	$K = 4$			
(A)	Optimal	27.390	27.181	19
(C)	Optimal	27.425	27.248	21
(D)	Optimal	27.422	27.156	13
(R)	Optimal	27.390	27.390	293
	$K = 5$			
(A)	Optimal	44.944	44.774	34
(C)	Optimal	44.951	44.774	16
(D)	Optimal	44.951	44.774	15
(R)	Optimal	44.916	44.901	1312

Table 3.2: Optimal ICI for the IEEE-118 and Polish systems, splitting the system into K islands (Presolve on).

The goal was to create a partition of the grid into islands of coherent generators with minimal power-flow disruption.

The formulation provided in [81], which we denote with F_4, utilizes a mixed integer program to identify the optimal islanding. The authors of [81] deal with the intractability of formulation F_4 by constructing a heuristic based on LP relaxations. In this chapter, we provide an equivalent optimization problem to F_4, that makes use of the IE constraint formulations F_1, F_2 and F_3; see Appendix 3.A for the formulation we employ.

In order to perform a computational comparison between the different formulations of the problem, we considered two test systems: the IEEE-118 bus system (118 buses, 186 branches, 54 generators) and an instance of the Polish system (3374 buses, 4161 branches, 596 generators). Due to the size of the resulting model and the memory limitations, formulation F_2 was impractical and was not implemented.

The results for the lower bounds to the ICI problem using the different formulations are presented in Table 3.1. Note that after the introduction of all Type I and Type II constraints, the bound obtained is very close to the best bound found from the solution of the problem using branch and

Optimal ICI	Gap [%]	Upper Bound	Lower Bound	Time [s]
IEEE-118	$K = 4$			
(A)	Optimal	3.684	3.684	0.16
(C)	Optimal	3.684	3.684	0.49
(D)	Optimal	3.684	3.684	0.55
(R)	Optimal	3.684	3.684	0.94
Polish	$K = 3$			
(A)	Optimal	17.771	17.612	5
(C)	Optimal	17.771	17.771	19
(D)	Optimal	17.771	17.771	12
(R)	Optimal	17.771	17.771	509
	$K = 4$			
(A)	Optimal	27.390	27.390	12
(C)	Optimal	27.390	27.390	53
(D)	Optimal	27.425	27.248	26
(R)	Optimal	27.390	27.390	3098
	$K = 5$			
(A)	Optimal	44.915	44.915	13
(C)	Optimal	44.915	44.655	68
(D)	Optimal	45.073	44.689	30
(R)	1.46	44.915	44.258	20000

Table 3.3: Optimal ICI for the IEEE-118 and Polish systems, splitting the system into K islands (Presolve off).

cut (with 1% optimality guarantee) in most instances. Also note that the additional benefit from Type II constraints is not visible in the bound after all Type I constraints are introduced.

The computational results for solving the problem to near optimality are presented in Table 3.2. In addition to the implementations discussed in the introduction of this section, we denote with (R) the implementation of F_4. Due to a significant difference in performance, we also provide the same computations with the solver presolve turned off in table 3.3 (and using a longer time limit of 20000s). This would not be a choice in a practical setting, but it allows to preserve the formulations at the start of branch and cut and offers a more accurate picture of the comparison between formulations without the solver preprocessing and strengthening. The IEEE-118 system solves relatively quickly for all three formulations considered. For the Polish system, we observe that (R) seems to be at least one order of magnitude slower than F_1. Implementation (C) performs slightly worse than (A) (with, in fact, more than half the simulation time spent in separating the violated constraints). Implementation (D) behaves similarly to (C), with a slightly faster computational time, possibly due to the additional presence of the Type II cuts. In this case formulation F_1 has the best performance.

BSA Root	F_1 [%]	F_3 (Type I) [%]	F_1 & Type II [%]	F_3 & Type II [%]	Best Bound
IEEE-39	21.75	15.59	15.35	15.35	2199.15
IEEE-118	6.57	1.89	1.41	1.23	5051.41
Illinois-200	8.45	3.37	2.43	2.43	6480.59
WECC-225	4.13**	1.48	1.47	1.47	16598.51
IEEE-300	16.19	6.47	4.85	4.81	12684.21
South Carolina-500	16.99	4.19	1.07	0.95	13778.61

Table 3.4: Optimal BSA root node relaxations for synthetic test systems, employing the different formulations. The last column corresponds to the best bound found by the branch and cut tree in the results of table 3.5. Columns 2-5 are percentages above the best upper bound found from branch and bound (column 6). The $**$ indicate suboptimal termination due to numerical errors in Gurobi.

Optimal Black Start Allocation

We performed simulations using the model described on section 3.9 for a number of test cases, obtained from the Matpower database [159]. Reasonable initializations were used for the restoration parameters. All the parameters used can be found online at [108].

The results for the quality of the root node relaxation are given in table 3.4. One first observation is that there is a significant improvement in the quality of the lower bound between using the single commodity flow formulation F_1 and the formulation with all Type I and II cuts (column F_3 & Type II). A second observation is that the best bound obtained (last column) in most cases is actually fairly close to the bound obtained by including all Type I and Type II cuts. Finally, the Type II cuts seems to only make a noticeable difference in the strength of the lower bound compared to simply using just Type I cuts only in the larger test systems (IEEE-300 and South Carolina-500).

For the simulations to near optimality, we implement the configurations discussed in the introduction of this section, i.e. implementations (A)-(D). In all of these implementations, the constraints (3.19p)-(3.19t) are used to impose the active power requirement. We additionally consider the following implementation:

(E) Type I and II constraints are used to impose the IE constraint in the place of (3.19j)-(3.19l). Specifically, Type I and II constraints for $|S| \in \{1, |N|\}$ are added a priori. We use integer callbacks to lazily add the remaining Type I constraints, only if they are violated for an integer feasible point. For the islands that are identified to violate the constraint, we also add the Type II cuts. The system (3.22) is used to impose the active power constraints. The constraints (3.22a) and (3.22b) for $|S| \in \{1, |N|\}$ are added a priori, and the remaining constraints are imposed through an integer callback.

The first observation is that implementation (B), which uses formulation F_2 is unable to com-

Optimal BSA	Gap [%]	Upper Bound	Lower Bound	Time [s]
IEEE-39				
(A)	Optimal	2221.04	2199.15	2.6
(B)	Optimal	2210.59	2199.15	10
(C)	Optimal	2199.15	2199.15	3.9
(D)	Optimal	2199.15	2199.15	3.2
(E)	Optimal	2206.75	2199.15	1.7
IEEE-118				
(A)	Optimal	5066.87	5018.69	50
(B)	24.9	5101.76	4084.56	2000
(C)	Optimal	5062.64	5018.16	47
(D)	Optimal	5051.41	5019.56	55
(E)	Optimal	5053.76	5018.56	120
Illinois-200				
(A)	Optimal	6480.59	6460.99	147
(B)	–	6517.80	0	2000
(C)	Optimal	6494.89	6460.99	53
(D)	Optimal	6510.60	6446.90	42
(E)	Optimal	6494.54	6460.79	44
WECC-225				
(A)	Optimal	16598.51	16574.62	96
(B)*	–	16696.60	0	2000
(C)	Optimal	16604.51	16444.93	58
(D)	Optimal	16610.33	16516.27	71
(E)	Optimal	16610.56	16510.42	53
IEEE-300				
(A)	8.69	12916.52	11883.79	2000
(B)*	–	16989.79	0	2000
(C)	3.98	12807.97	12317.66	2000
(D)	2.02	12773.35	12520.20	2000
(E)	1.18	12684.21	12536.08	2000
South Carolina-500				
(A)	156.47	13987.39	5453.70	2000
(B)*	–	19009.15	0	2000
(C)	8.55	14262.80	13138.36	2000
(D)	4.35	13778.61	13203.37	2000
(E)	5.22	13782.59	13098.70	2000

Table 3.5: Optimal BSA results for synthetic test systems.

BSA Implementation	UB after root	Time after root [s]	UB at time limit	LB at time limit	Gap at time limit
(A)	178217	3519	178217	164112	8.59%
(C)	175326	2429	173725	164112	5.85%
(D)	171850	5667	171479	164112	4.49%
(E)	171805	669	170775	164112	4.06%

Table 3.6: Simulations in Gurobi for the different implementations for the Texas system BSA. The second column corresponds to the best upper bound found after solving the root node relaxation. Note that Gurobi presolve is on. The third column corresponds to the time for solving the root node relaxation. The last three columns give the final upper bound, lower bound, and gap at the time limit of 20000s.

pete with the other implementations due to its size. In fact, for the larger systems (IEEE-300 and South Carolina-500), not even the root node relaxation can be solved within the 2000s time limit. A second observation is that all the other implementations seem to be able to solve the four smaller power systems fairly easily. Additionally, we observe that Formulation F_1 is outperformed by the cut-based formulations for imposing the IE constraint - it is slightly slower in the Illinois-200 system, and significantly outperformed in the IEEE-300 and South Carolina-500 systems. Type II cuts, employed in (D) and (E), seem to help for the largest two systems in obtaining a better bound within the time limit. Finally, for the same systems, the use of the active power cuts (3.22a) and (3.22b) help the solver to achieve a gap better by approximately 1 percentage unit.

Solving an Industrial Size Test Case for BSA

The synthetic Texas system consists of 2 000 buses, 3 206 branches, 544 generators. This instance is the largest one considered in this paper, and in order to solve it we use additional techniques to the ones described in the previous subsections. It also represents the extent of the size of models we can handle at this point using our BSA model. We devote this subsection to a more detailed description of the solution approach for this system. The system data (buses, branches, generators) and the power flow characteristics were obtained from the data sets of Texas A&M University [13]. We performed reasonable or random initialization of the restoration related parameters, as described in the next paragraph.

We used a time horizon of 40 time steps, with one time step corresponding to an hour. The trade-off coefficient in the objective was set to $\lambda_G = 1$ (note that the mean p.u. value of $P_g^{\max}$ over $g \in G$ is 1.84) and $\alpha_L = 1.2$. The parameter K_{crew} was set to 120 branch energizations per hour.

The resulting optimization problem has 1 830 671 constraints, 779 178 variables, of which 505 114 are continuous and 274 064 are binary, and a total of 4 977 963 nonzero elements in the constraint matrix.

Directly passing this problem to Gurobi does not yield a feasible solution within an 20000s time limit for (3.19). Using the heuristic strategy described in subsection 3.9, we were able to obtain a

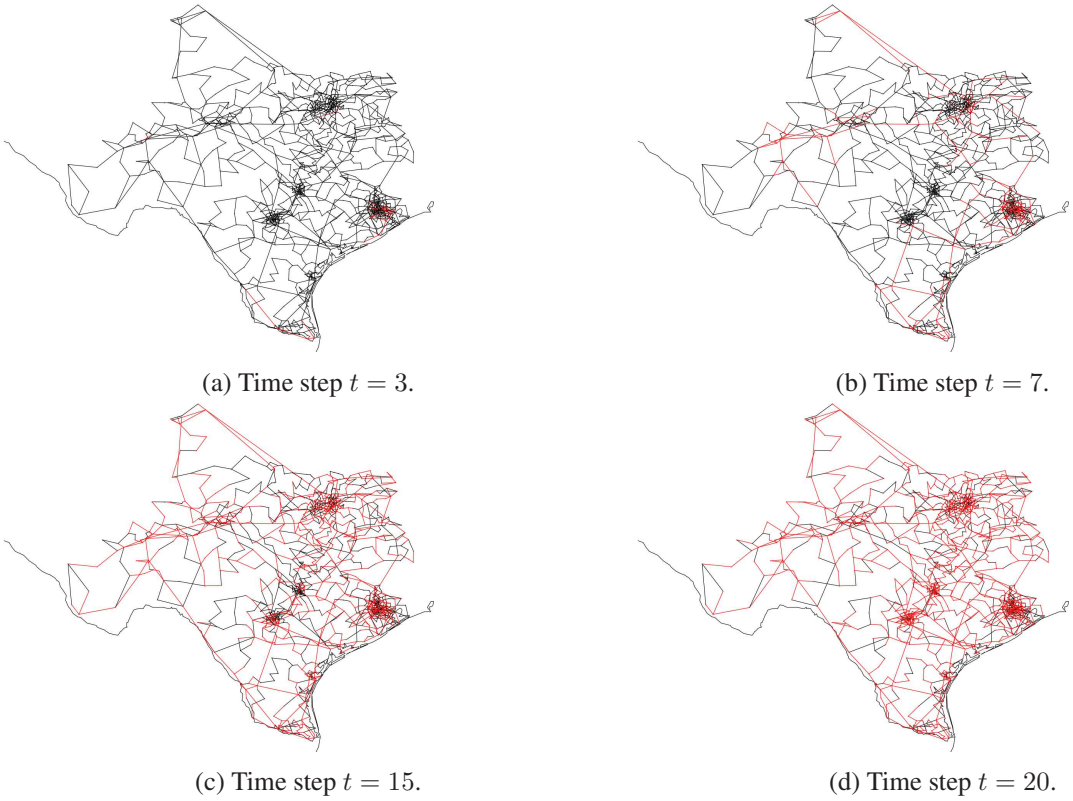

(a) Time step $t = 3$.

(b) Time step $t = 7$.

(c) Time step $t = 15$.

(d) Time step $t = 20$.

Figure 3.5: Visualization of four snapshots from the Texas system restoration in the 4.06% optimal solution found. The energized part of the system is indicated with red and the de-energized with black. A system aggregation is used before plotting for better visualization. A total of 9 black starts were assigned.

feasible solution with objective 164113. The next goal is to obtain an upper bound guarantee for this solution and - if possible - a better solution.

Gurobi Optimizer version 9.0.2 was used to solve the problem with the Python interface (Gurobipy). For all simulations the "Method" parameter in Gurobi was set to 3. The "Heuristics" parameter was increased to 0.3 (i.e. 30% of the time is spent on heuristics to improve the lower bound solution and potentially the upper bound by triggering integer callbacks and adding cuts). Due to an observed better computational performance, we set the number of threads to 8 and we introduced constraint (3.19f) as a lazy constraint, by simultaneously adding a-priori the weaker constraint $\sum_{(ij)\in A}(u_{ij}^{t} - u_{ij}^{t-1}) \leq K_{\text{crew}}$. For (C), (D), and (E), since callbacks are used, we set the Gurobi parameter "LazyConstraints" to 1 and "PreCrush" to 1. The remaining parameters were kept at their default values.

Simulation results are shown on table 3.6. First, we note that unfortunately none of the implementations could yield an improvement to the MIP start found by our specialized heuristic and used as a start start point by the MIP solver. The implementation that achieves the best optimality guarantee within the time limit is (E).

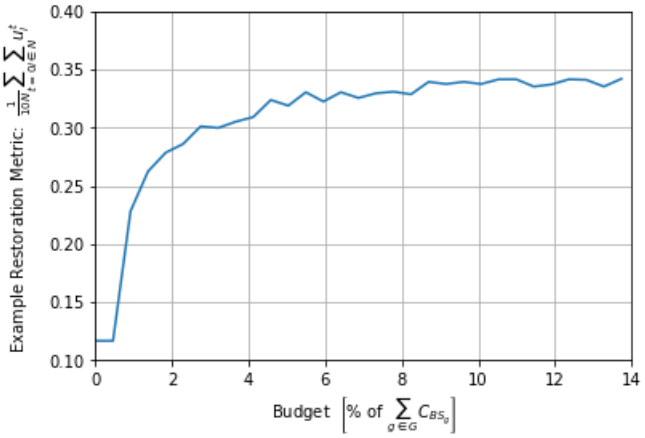

Figure 3.6: Plot of an example metric as a function of the budget allocated to enhance the black start capability of the simplified WECC system.

We should note that, in the case of the formulations with exponentially many constraints, these constraints are added through integer callbacks (and not at fractional points), so the linear programming relaxation does not actually reflect the full strength of the formulation. Hence, the constraints that are reflected in the root node relaxation solution are mainly the ones that are added a priori. Of course, since presolve is activated and may behave differently for each implementation and solver heuristics might trigger the addition of a few additional constraints through the callbacks, the upper bound value and time presented on table 3.6 serves only as a checkpoint of the progress of the solver. We should also note that, without presolve, (D) would provide at least as good a bound as (E) after the root node, since it includes the complete formulation for power flows.

Finally, a visualization of the solution (for which a 4.06% optimality guarantee was obtained by the best performing (E) implementation) is shown in figure 3.5. The black start generators assigned are (generator indices): 34, 173, 185, 398, 460, 480, 487, 488, 505. It should be, of course, reiterated that due to the random initialization of the restoration generator profiles in the simulation, this assignment may not correspond to a realistic allocation.

Black Start Capability Upgrade Example

In this section, we provide one potential use of the model we presented for black start planning. We will use the WECC-225 system as an example. We assume there is already one black start unit in the system, namely generator 81. The system operator considers potential upgrades in the black start capability of the system. The operator may be interested in different metrics - these could be the objective of the optimization problem used for BSA, or something related that is captured in the model. In our example, we assume one metric of interest is the average of the buses restored over the first 10 time steps, namely $\sum_{t=0}^{9}\sum_{i\in N} u_i^t$. Following that, we can construct a plot of the metric as a function of the allocated budget for black start upgrades - i.e. the optimization model

is solved for different values of the parameter B (the unit already allocated is excluded from the budget constraint and set to a black start). The outcome is shown in figure 3.6.

Based on that plot, we can see that by investing 2.74% of the total investment cost to convert all units to BS ($\sum_{g \in G} C_{BS_g}$), we can get a 157% estimated improvement on the metric of interest. This corresponds to allocating a total of 4 new black start units. Also, based on the plot we notice that, for this particular metric, there seems to be not much additional improvement above investing approximately 4% of $\sum_{g \in G} C_{BS_g}$. We should of course notice that the realization of this improvement after allocating the black start units suggested by the model needs to be verified with more detailed models and simulations of the restoration process. However, this test case illustrates how the model can serve as the first step of a planning tool to enhance the restoration capability of the power system.

3.11 Conclusions

One main takeaway of this chapter is that, while it might be easy to formulate a power systems problem as a MILP, choosing the right way to formulate the problem can make a significant difference in the solution times. Among others, some issues to consider when selecting the right formulation are the tightness of the formulation (i.e. how tight is the linear programming relaxation around the integer hull) and the size of the formulation (number of constraints and variables). There is usually a trade-off between the size and the tightness of the formulation, that can be resolved by numerical experimentation for each problem. Also, even if a problem is intractable in practice with one formulation, a reformulation could yield an acceptable computational performance.

For the ICI problem, even though F_4 and F_1 are reformulations for the same problem and are both employing single-commodity flow to enforce connectivity, their computational performance was very different, since F_1 is more compact than F_4 (fewer variables and constraints). The problem formulated using F_4 solved orders of magnitude slower compared to F_1. The size of F_2 made it completely intractable. Finally, the exponential size of F_3 (that forced the implementations (C) and (D) to employ lazy constraints added through callbacks) made the computational performance of the formulation slightly worse that the weaker F_1.

The situation for the optimal BSA problem was different. Formulation F_2 was still impractical, due to its size. However, implementations (C) and (D) that utilized Type I and Type II cuts outperformed F_1, even though they employ an exponential number of constraints. The reasons for that are twofold: Firstly, (C) and (D) used strong cuts. Secondly, the Type I & II constraints, other than those for $|S| \in \{1, |N|\}$, are rarely violated in incumbents of the BSA problem, so candidates found by the solver heuristics don't often trigger the callback. The intuition on why this is the case is that for the restoration problem we expect that the direction of the problem is such that branches get energized (rather than de-energized). If branches are mostly getting energized around energized generators, the situation where islands without an energized generator will show up are actually rare, so lazily generating the cuts for F_3 is faster than including the entire formulation F_1 in the optimization solver.

One choice that made a significant difference in the performance of the simulations was including a subset of the constraints a priori, instead of waiting for them to be generated by the callback. These constraints were the Type I and II constraints for $|S| \in \{1, |N|\}$. Note that these constraints were shown to be facet defining for the integer hull under simplifying assumptions and are relatively small in size. If the constraints are not included a priori, there is in fact no guarantee that the separation algorithm will choose to include them at a later point and the performance will be hindered. We recommend adding these constraints in the formulation whenever the IE requirement is valid, regardless of the way it is imposed (i.e., explicitly using one of the formulations of this paper, or implicitly as a result of other sets of constraints).

We should finally note that how much a particular reformulation will influence the performance of the problem highly depends on the modeling of the rest of the problem. For the models we used in this section, we were able to observe a significant computational benefit by employing the reformulations described. Also, all the reformulations used are applicable to any model with the IE constraint substructure. However, the performance improvements are not guaranteed for all the problems that exhibit this substructure. In particular, based on limited simulation experiments, when we used the black start allocation objective of chapter 2 or incorporated the more detailed linearized version of flows presented, we did not get such significant performance improvement.

Appendix

3.A Optimal Islanding Formulation

The optimal ICI problem we use in the text is formulated in [81], based on a previous work by the same authors in [82]. We denote this formulation F_4 and we describe it first in this appendix. The goal is to find a minimum cost partitioning of the grid to islands given a partitioning of the generators. More specifically, the generators are divided into $|K|$ subsets of coherent generators $G_h, h \in K$, i.e. of generators that will be in the same island after the reconfiguration of the grid and in different islands from the generators of the other subsets. There is a cost d_{ij} associated with switching off branch $(ij) \in E$ and a minimum size requirement M of every bus set in the partition. The set of nodes N is assumed to be $\{1, 2, \ldots, |N|\}$.

Denote with $\tilde{A}$ the directed set of edges that contains two edges, (ij) and (ji) for every undirected edge $e \in E$ with endpoints i and j (we will also slightly abuse notation and use both d_{ij} and d_{ji}, with $d_{ij} = d_{ji}$). Let $i \in N$ denote a bus of the system, $(ij) \in \tilde{A}$ a branch, and $g \in G$ a generator. We denote the node that generator g is connected by $n(g)$. Let the binary variables x_i^h/w_{ij}^h denote (if equal to 1) that node i/branch (ij) belongs to partition $h \in K$. Let the binary variable z_{ij} denote that branch (ij) is switched on (i.e. it belongs to some partition). Let the variables f_{ij}^h denote network flows that will ensure the connectivity of partition $h \in K$. The binary variable v_i^h becomes 1 for the lowest index node in partition h. The binary variable y_i^h is 0 for all nodes before the lowest index node in partition h, and 1 otherwise. The binary variables y_i^h, v_i^h, w_{ij}^h, z_{ij} can actually be relaxed in $[0, 1]$.

$$\text{minimize} \quad \sum_{(ij)\in\tilde{A}} \frac{1}{2}(1 - z_{ij})d_{ij}$$

subject to

$$x^h_{n(g)} = 1, g \in G_h, h \in K \tag{3.23a}$$

$$w^h_{ij} \leq x^h_i, w^h_{ij} \leq x^h_j,\ (ij) \in \tilde{A}, h \in K \tag{3.23b}$$

$$z_{ij} = z_{ji}\ (ij) \in \tilde{A} \tag{3.23c}$$

$$z_{ij} = \sum_{h \in K} w^h_{ij},\ (ij) \in \tilde{A} \tag{3.23d}$$

$$\sum_{h \in K} x^h_i = 1,\ i \in N \tag{3.23e}$$

$$\sum_{i \in N} x^h_i \geq M,\ h \in K \tag{3.23f}$$

$$\sum_{i=1}^{j} \frac{x^h_i}{|N|} \leq y^h_j \leq \sum_{i=1}^{j} x^h_i,\ j \in N, h \in K \tag{3.23g}$$

$$y^h_j \geq x^h_j,\ j \in N, h \in K \tag{3.23h}$$

$$v^h_j = y^h_j - y^h_{j-1},\ j \in N \setminus \{1\}, h \in K \tag{3.23i}$$

$$v^h_1 = y^h_1,\ h \in K \tag{3.23j}$$

$$\sum_{j \in N} v^h_j = 1,\ h \in K \tag{3.23k}$$

$$v^h_j \sum_{i \in N} x^h_i + \sum_{ij:(ij) \in \tilde{A}} f^h_{ij} - \sum_{i:(ji) \in \tilde{A}} f^h_{ji} = x^h_j,\ j \in N, h \in K \tag{3.23l}$$

$$0 \leq f^h_{ij} \leq |N| z_{ij}\ , (ij) \in \tilde{A}, h \in K \tag{3.23m}$$

The objective function minimizes the cost of switched off lines. Constraint (3.23a) ensures that nodes with a coherent generator of group h will be assigned to partition h. Constraint (3.23b) forces nodes i and j to belong to the same partition as the edge (ij). Constraint (3.23c) ensures that both directed edges have the same status (on or off). Constraint (3.23d) defines the variables z_{ij} as the variable indicating if (ij) belongs to some partition. Constraint (3.23e) imposes that each node must belong to a partition. Constraint (3.23f) forces a lower bound to the size of every partition. Constraints (3.23g) and (3.23h) force y^h_j to be zero before the first node (in terms of index) belonging to partition h and 1 elsewhere. Constraints (3.23i) and (3.23j) define the variables indicating the lowest index node in the partition. Constraint (3.23k) stipulates that every partition has exactly one minimum index node. Constraint (3.23l) enforces that every node that belongs to partition h, i.e. has $x^h_i = 1$, acts as a source of 1 unit of network flow. $\sum_{i \in N} x^h_i$ units on network flow are generated at the lowest index node of the partition. Note this constraint has a nonlinear term (product), which are linearized using McCormick envelopes. Finally, constraint (3.23m) forces that a line that is not energized can not bear any flow.

Note that a single-commodity flow formulation approach is essentially used in the above model. Network flow can be generated from the node of least index within every partition and equals exactly the number of nodes. In our single commodity flow formulation for the same problem,

we instead make use of the fact that the generators in each coherent group are forced to belong to the corresponding partition, so one of them can be used as the source of the network flow. Note that we also don't duplicate the edges, since we allow bidirectional flows in our formulation. We proceed to describe our formulation.

Let $i \in N$ denote a bus of the system, $(ij) \in E$ a branch, and $g \in G$ a generator. Also, for each set G_h, denote one of the generators (assumed to be the isochronous one, even though the specific choice is not important) with $G_h^{(0)} \in G_h$. We denote the node that generator g is connected by $n(g)$. Let the binary variables u_i^h/u_{ij}^h/u_g^h denote (if equal to 1) that node i/branch (ij)/generator g belongs to partition $h \in K$. Let the binary variable z_{ij} denote that branch (ij) is switched on (i.e. it belongs to some partition). Let the variables f_{ij}^h, f_g^h denote the network flows that will ensure the connectivity of partition $h \in K$. Finally, there is a cost d_{ij} associated with switching off branch (ij) and a minimum size requirement M of every bus set in the partition.

$$\text{minimize} \quad \sum_{(ij)\in E} d_{ij}(1 - z_{ij})$$

subject to

$$z_{ij} = \sum_{h\in K} u_{ij}^h, (ij) \in E \tag{3.24a}$$

$$\sum_{h\in K} u_i^h = 1, i \in N \tag{3.24b}$$

$$\sum_{i\in N} u_i^h \geq M, h \in K \tag{3.24c}$$

$$u_{ij}^h \leq u_i^h, u_{ij}^h \leq u_j^h, (ij) \in E, h \in K \tag{3.24d}$$

$$u_g^h \leq u_i^h, g \in G(i) \tag{3.24e}$$

$$0 \leq f_g^h \leq u_g^h, \ g \in G, \ h \in K, \tag{3.24f}$$

$$-u_{ij}^h \leq f_{ij}^h \leq u_{ij}^h, \ (ij) \in E, \ h \in K, \tag{3.24g}$$

$$\sum_{j:(ji)\in E} f_{ji}^h - \sum_{j:(ij)\in E} f_{ij}^h + \sum_{g\in G(i)} f_g^h = \frac{1}{|N|} u_i^h, \quad i \in N, \ h \in K \tag{3.24h}$$

$$u_g^h = \begin{cases} 1, & \text{if } g = G_h^{(0)} \\ 0, & \text{otherwise} \end{cases}, h \in K \tag{3.24i}$$

$$u_{n(g)}^h = 1, \ g \in G_h, h \in K \tag{3.24j}$$

The objective of the problem minimizes the weighted cost of switching off edges. Constraint (3.24a) imposes that a bus is switched on if it belongs in one of the partitions. Constraint (3.24b) ensures that each bus is assigned to exactly one partition, constraint (3.24c) ensures that each partition has at least M buses, constraints (3.24d) require that if a branch belongs to a partition, both its endpoints belong to it, constraint (3.24e) ensures that if a generator belongs to partition h,

the node it is connected to will belong to the same partition. Constraints (3.24f)-(3.24h), together with (3.24d) and (3.24e), are the IE constraints of formulation F_1 imposed for every partition h. These constraints can be equivalently substituted with the constraints of F_2 or F_3, as we have shown in this chapter. Finally, (3.24i) allows only the generator $G_h^{(0)}$ to generate the network flow that ensures the connectivity of each partition h and (3.24j) forces each node of the coherent generators to belong to the corresponding partition.

One last note is that, even though the second formulation has a strictly better performance than the first one, it is not necessarily the strongest or most compact formulation one can devise for this particular problem. After all, one underlying structure of this application is the graph partitioning problem and an extensive body of MIP literature is devoted to reformulations, strengthening, and dedicated branching schemes. For example, one further modification could be to set $f_g^h = \frac{1}{|N|}\sum_{i\in N} u_i^h$ for $g = G_h^{(0)}$ and 0 otherwise. The formulation above, however, is sufficient to illustrate a significant difference in computational performance for the instances considered and utilizes the substructure that this section focused on.

Chapter 4

A Stochastic Program for Black Start Allocation

4.1 Abstract

This chapter extends the ideas of the black start allocation model developed previously in one important fashion: accommodating for stochasticity in the possible power outages. More specifically, the case of a complete blackout, as examined in the previous chapters, is only one of the possible outage scenarios. Partial outages of the power system are also (if not more) likely. In such cases, one or more islands of the power system have survived the blackout, so the restoration of the system can depend not only on the black start units, but also on these energized islands. In addition, the outage might leave parts of the power system inoperable, such as lines or branches that have suffered irreparable damage and can not be used in the restoration process. We extend our model for black start allocation to incorporate these considerations when deciding on an allocation.

We formulate a two-stage stochastic program that optimizes the allocation of BS resources over a number of outage scenarios. We use a scenario decomposition algorithm to solve the resulting optimization problem to near-optimality on a high performance computing environment. The main idea behind the use of this algorithm is that the characteristics of the generators pertinent to the black start capability remain the same across all scenarios, so a good candidate black start unit for one scenario is very likely to perform well if chosen as a black start in many other scenarios. We conduct numerical experiments using the proposed model and decomposition method on the IEEE-39 test system. To ensure this chapter is self contained, some of the modeling choices made in our previous treatment of the black start allocation problem are repeated, with slight modifications to accommodate for the additional scenario-dependent considerations.

Nomenclature

Sets

E Set of branches (ordered pair of buses).

G Set of generators.

$G(i)$ Set of generators connected to bus $i \in N$.

N Set of buses.

S Set of scenarios.

T Set of consecutive integer time instances, starting from 1.

Variables

$p_{SH_i}^{t,s}$ Active power load shed at bus $i \in N$, time $t \in T$ and scenario $s \in S$.

$q_{\text{sys}}^{t,s}$ System-wide reactive power capability at time $t \in T$ for scenario $s \in S$.

$\delta_i^{t,s}$ Voltage phase of bus $i \in N$ at time $t \in T$ for scenario $s \in S$.

$f_g^{t,s}$ Network flow for energizing paths from generator $g \in G$ at time $t \in T$ for scenario $s \in S$.

$f_{ij}^{t,s}$ Network flow for energizing paths for branch $(ij) \in E$ at time $t \in T$ for scenario $s \in S$.

$p_g^{t,s}$ Active power generation of generator $g \in G$ at time $t \in T \cup \{0\}$ for scenario $s \in S$.

$p_{ij}^{t,s}$ Active power flow of branch $(ij) \in E$ at time $t \in T$ for scenario $s \in S$.

$u_g^{t,s}$ Binary variable indicating generator $g \in G$ energized at time $t \in T$ for scenario $s \in S$.

$u_i^{t,s}$ Binary variable indicating node $i \in N$ energized at time $t \in T$ for scenario $s \in S$.

u_{BS_g} Binary variable indicating generator $g \in G$ is BS generator.

$u_{ij}^{t,s}$ Binary variable indicating branch $(ij) \in E$ energized at time $t \in T$ for scenario $s \in S$.

Parameters

$\cos(\phi_{D_i})$ Power factor of load at node $i \in N$.

ϵ Decomposition algorithm termination gap.

λ Trade-off coefficient for reactive capability.

μ Trade-off coefficient for inertia.

$\overline{S}_{ij}$ Maximum flow limit for branch $(ij) \in E$.

π_s Weight assigned to scenario $s \in S$.

$\underline{\delta}, \overline{\delta}$ Lower and upper bounds for voltage phases.

$\underline{Q}_g$ Minimum reactive power generation from generator $g \in G$.

$\underline{Q}_{SH_i}$ Shunt reactor for bus $i \in N$.

$\underline{V}, \overline{V}$ Lower and upper bounds for voltage magnitude.

B Total budget for BS generator installations.

b_{ij} Susceptance for branch $(ij) \in E$.

$B_{SH_{ij}}$ Shunt susceptance of branch $(ij) \in E$.

C_g Operational cost of generator $g \in G$.

C_{BS_g} Cost of turning $g \in G$ to a BS generator.

C_i Cost of load shed in node $i \in N$ after the blackout.

J_g Inertia of generator $g \in G$.

K_{R_g} Ramp rate of generator $g \in G$.

$P_g^{\max}$ Maximum active power generation from generator $g \in G$.

P_{CR_g} Cranking power required to be provided to generator $g \in G$ to initiate its start-up.

P_{D_i} Available load at bus $i \in N$.

T_{CR_g} Time between generator $g \in G$ being energized until it can increase its active power from zero.

$u_g^{0,s}$ Binary parameter indicating state of generator $g \in G$ at time $t \in T$ for scenario $s \in S$.

$u_g^{\text{avail},s}$ Binary parameter indicating the availability of generator $g \in G$ for scenario $s \in S$.

$u_i^{0,s}$ Binary parameter indicating state of node $i \in N$ at time $t \in T$ for scenario $s \in S$.

$u_i^{\text{avail},s}$ Binary parameter indicating the availability of node $i \in N$ for scenario $s \in S$.

$u_{ij}^{\text{avail},s}$ Binary parameter indicating the availability of branch $(ij) \in E$ for scenario $s \in S$.

4.2 Introduction

Despite ongoing efforts to increase the reliability of power systems, natural events, human or equipment faults, attacks or other possible causes can still result in large-scale outages [95]. Power System Restoration (PSR), i.e. restoring the grid to normal operation after an outage, is considered a primary objective within the scope of achieving grid resiliency. One of the main challenges is that most of the generators are unable to start without receiving an initial amount of power (cranking power, corresponding to ancillary equipment and initial energy needs) from the power systemfor a certain amount of time (cranking time). The restoration process relies, then, on selected units (called black start units) that have the capability to start on their own. This capability can be achieved through technical upgrades, such as installing a small diesel generator that can provide the initial cranking power to the unit. System operators are often responsible for compensating these units for the black start (BS) service availability, as well as for regular testing of the technical requirements.

For most systems, detailed procedures exist and regular training of the personnel is in place to ensure a quick and efficient response to a possible blackout. These procedures are specific to each power system and they describe the order in which to energize branches and crank generators, aiming to that critical loads will be energized as soon as possible and that the grid will be restored in a secure way. Critical loads include the auxiliary equipment of nuclear power plants, critical natural gas infrastructure, critical communication equipment, or command and control facilities [118]. The restoration process plan is usually devised for the case of a complete blackout but, with the same priorities in mind, other plans can be constructed for cases of partial blackouts.

A number of approaches have been suggested in literature to construct a restoration plan given the location of the BS units. In [71, 90], the authors develop a tool that suggests the next step in a restoration sequence. In [74, 134] the authors consider instead a mixed integer program (MIP) where binary decision variables correspond to energization steps. A different modeling approach including reactive power considerations is adopted in [22], aiming to motivate the use of microgrids for PSR. A mixed integer non-linear program is formulated in [27] and feasible solutions are found using ant colony optimization. The sectionalization problem is solved in [146] using binary decision diagrams. Including wind power in restoration is discussed in [61]. Literature reviews of relevant approaches are provided in [23, 157].

The effectiveness of a restoration plan highly depends on the choice of the black start units in the grid. Some units are inherently more suitable for the role of black start compared to others. For example, pumped-storage hydro-power plants are ideal to act as black starts, due to the negligible amount of cranking power and cranking time they require and their high ramping capabilities. On the other hand, some units may be better placed within the power grid, i.e. closer to the critical loads. The problem of allocating black start capabilities has also been discussed in the litera-

ture. General guidelines to heuristically select black start units are available [75, 118, 125, 133]. In [121, 122], a minimum procurement cost BS allocation problem is formulated. In [115], the BS allocation problem is formulated including an increased detail of the resulting restoration process and solved to near optimality through a heuristic that proposes candidate feasible restoration sequences. All of the aforementioned studies examine the case of a total blackout for the BS allocation problem.

Solving the BS allocation problem based on the scenario of a total blackout, while useful, is not necessarily representative of reality. We rarely expect a complete system outage, rather smaller outages that leave a number of stable islands with functional generators, from where restoration actions can start as well. Also, some parts of the grid may be more prone to outages than others, due to abnormal weather conditions, unpredictable demand or even the local grid configuration. Furthermore, after an outage, we can not expect that all system components will be in their pre-outage condition. Some generators, lines or buses may have suffered faults or permanent damage, which will make them unavailable for the purposes of restoration.

In this work we seek to address the aforementioned challenges by proposing a stochastic program for BS allocation. A number of scenarios is considered, that corresponds to possible partial system outages, as well as possible unavailability of some lines, generators or buses. The black start allocation is optimized over the scenarios (first stage variables), while a different restoration sequence for each scenario is calculated (second stage variables). The resulting MIP can become very large as the number of scenarios increases. In order to achieve tractability, we observe that, since the critical loads and the characteristics of the generators are the same for all scenarios, the allocation found by considering a scenario in isolation could perform well for the other scenarios. A scenario decomposition technique devised to exploit this observation [4, 124] is employed to solve the stochastic program. The computational performance of the decomposition technique is illustrated using the IEEE-39 test power system.

The remainder of this chapter is organized as follows. Section 4.3 presents the problem formulation, section 4.4 describes the decomposition algorithm, section 4.5 the simulation results and section 4.6 concludes the chapter. The work of this chapter was published in [109].

4.3 Optimization Model

In this section we describe the optimization model employed for the BS allocation problem. A two-stage stochastic program describes decisions that happen before uncertainty is revealed, i.e. first stage decisions, and after uncertainty realized, i.e. second stage decisions. For our problem, the first stage decision is the allocation of the black start capabilities to units. This decision is the same for all the scenarios considered, since we make this decision before the occurrence of any outage. Each scenario corresponds to possible partial or total outages of the power grid, as well as the possible unavailability of grid components (lines, generators or buses). Finally, the second stage decisions are the restoration steps that need to be implemented given the scenario that has occurred and based on the BS allocation of the first stage.

First Stage

A binary variable u_{BS_g} is associated with the allocation of each unit $g \in G$ as a BS generator (a value of 1 indicates that a unit is allocated). Units can be excluded from being allocated by explicitly setting the variable equal to 0 in the optimization problem. Furthermore, a unit that is already a black start can have its corresponding binary variable preset to 1 (and this variable can be excluded from the budget constraint). The allocation of a unit translates, for our model, to the installation of a diesel generator that will provide the initial cranking power needed by the unit to start.

Budget Constraint

Allocating a black start unit is associated with a number of costs [73]. These may include compensation to the utility owner for the service, costs for technical upgrades and costs to regularly test and maintain the equipment. The cost highly depends on the type of the unit and the commitment approach for black starts that the operator adopts. For our model, we assume that all the costs are reduced to a lump sum payment C_{BS_g} for unit $g \in G$. Therefore, the following budget constraint is imposed at the first stage. Note that, there might be a black start allocation that achieves a feasible (worse) restoration plan and uses up a smaller installation budget, but in this work we do not address this trade-off.

$$\sum_{g \in G} C_{BS_g} u_{BS_g} \leq B \ . \tag{4.1}$$

Second Stage

While the first stage variables (black start allocation variables) are the same for all scenarios, the second stage variables are optimized for every scenario independently, i.e. they are chosen given a known uncertainty realization, which is why there exists a copy of these variables for every scenario (i.e. they are all indexed by scenario $s \in S$). The scenarios of the model represent different outage cases and possible unavailability of components. Second stage variables are the decisions to be made in order to restore normal operation of the system for each scenario, for a finite time horizon T. Among these, there are binary variables that correspond to the energization of buses $u_i^{t,s}$, lines $u_{ij}^{t,s}$ and generators $u_g^{t,s}$, which become 1 at the time step $t \in T$ if the component is energized.

Scenarios

After the blackout, the operator needs to identify the surviving parts of the grid. These are usually stable islands with generation supporting them. The identification process will also determine which components of the grid are inoperable after the outage (due to a severe fault or malfunction), which cannot be used during the restoration process. In our model, the binary parameters $u_g^{0,s}$ and $u_i^{0,s}$ determine the initially energized grid for scenario $s \in S$ (1 if energized). The parameters

$u_i^{\text{avail},s}$, $u_{ij}^{\text{avail},s}$ and $u_g^{\text{avail},s}$ are set to 0 if the corresponding bus, line or generator is unavailable in scenario $s \in S$. Note that in this model, unavailability is constant across all time steps for each scenario. However, a straightforward extension would be to index the parameter by time in order to indicate that a component is available after some reparation/replacement time. This modification also allows to model switches that require manual operation (i.e. they can not be operated using remote control systems, but instead manned units need to be dispatched on-site to operate them), which need a certain amount of time before operation becomes possible. Finally, the scenario generation process for our purposes is synthetic because the computations employ artificially constructed IEEE test systems. In a real setup, however, the scenarios can be constructed by system experts or historical outage data, based on the individual characteristics of a power system.

Node Active Power Balance

The node balancing constraint at every time instant is:

$$\begin{aligned}\sum_{g\in G(i)} \left(p_g^{t,s} + P_{CR_g}(u_g^{\text{avail},s} u_{BS_g} - u_g^{t,s})\right) + \sum_{j:(ji)\in E} p_{ji}^{t,s} \\ - \sum_{j:(ij)\in E} p_{ij}^{t,s} = P_{D_i} - p_{SH_i}^{t,s}, \forall i \in N, \forall t \in T, \forall s \in S.\end{aligned} \tag{4.2}$$

Constraint (4.2) stipulates the active power conservation at node $i \in N$ for every time instant $t \in T$. Note the following: if a generator is chosen to be BS ($u_{BS_g} = 1$), then its cranking power is provided for (by an external source), so it can be immediately energized ($u_g^{1,s} = 1$). On the other hand, if we want a non-BS generator $g \in G$ to get energized, the constraint above introduces a negative term $-P_{CR_g}$, so the cranking power needs to be provided for either by a different generator in the same node or by incoming power flows. In the initial phases of the restoration, this constraint will ensure that only the generators that are assigned to be BS or are already connected to an energized island can be energized.

Usually, when a load is picked up after an extended outage, the demand is greater than before the outage. This phenomenon is referred to as cold load pickup. Some of the factors that affect the magnitude and duration of cold load are outage duration, type of load, time of day and load level. One reason for this phenomenon is that, while some loads are usually diverse and cycle, after the re-energization they tend to all draw current at the same time for several minutes [55]. Despite the uncertainty in the load when closing the switches, the operators usually have the ability to pick load in small enough chunks. Even more, load is used as a tool to alleviate overvoltages and increase the system stability (by allowing more generation to be committed as well). For these reasons, load behaves more like a decision variable for restoration purposes. Therefore, in our model, a continuous load shed variable is employed, that satisfies:

$$\begin{aligned}(1 - u_i^{t,s}) P_{D_i} \leq p_{SH_i}^{t,s} \leq P_{D_i}, \\ \forall i \in N, \forall t \in T, \forall s \in S.\end{aligned} \tag{4.3}$$

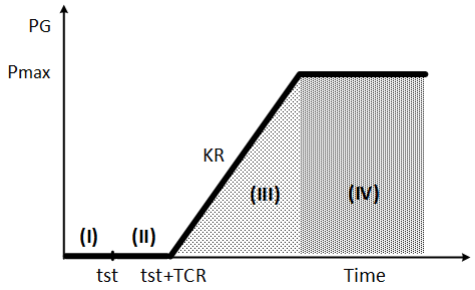

(a) Generator power output. A generator that gets energized at time t_{st} needs to be cranked for T_{CR} periods before it can inject power to the grid. $T_{CR}+1$ periods after energized, the generator can ramp up its active power production with a maximum rate of K_R, until its maximum generation limit P_{max} is reached.

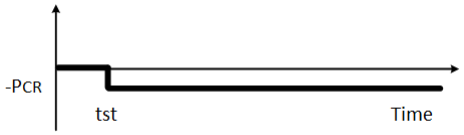

(b) Cranking power of generator unit. As soon as the generator is energized ($u_g^{t,s} = 1$), it needs to absorb power P_{CR}. This power is either provided by other generators (if the unit does not have BS capability), or by a dedicated diesel BS unit or battery (if the unit has BS capabilities).

Figure 4.1: Typical generator curve. The parameters T_{CR}, P_{CR}, T_{CR}, P_{max} vary depending on the type of generator.

Reactive Power

Reactive power capability is important in maintaining the voltages of the power system within security limits. For this model, we introduce a system-wide reactive power capability variable $q_{\text{syst}}^{t,s}$.

$$\sum_{i\in N}\sum_{g\in G(i)} \underline{Q}_g u_g^{\max\{0,t-T_{CR_g}-1\},s} + \sum_{(ij)\in E} B_{SH_{ij}} u_{ij}^{t,s} + \sum_{i\in N} Q_{SHi} u_i^{t,s} - \sum_{i\in N} (P_{D_i} - p_{SH_i}^{t,s}) \tan(\phi_{D_i}) = q_{\text{syst}}^{t,s}, \quad \forall t \in T, \forall s \in S. \tag{4.4}$$

A line injects reactive power $\frac{1}{2} B_{SH_{ij}} V^2 u_{ij}^t$ at each of the buses it connects to, if energized, where the bus voltage V is assumed close to 1.0pu for this constraint, in order to allow for a linear formulation. The reactive power can be absorbed by either generators that have been energized at least $T_{CR_g} + 1$ time units in advance, by reactive compensation connected to the bus Q_{SH_i}, or by loads with lagging power factor ($\tan(\phi_{D_i}) > 0$). The load is assumed picked up at a constant power factor, as in [31] and [22]. The modeling of the system-wide reactive power follows the ideas in [74]. This assumption may not hold during the startup of many loads, it is however more restrictive than assuming that the load reactive power can be controlled independently of its active power.

Generator Model

A typical generator startup model is assumed, following similar assumptions as in [115, 134]. Figure 4.1 depicts these assumptions. The binary variable $u_g^{s,t}$ is associated with the energization

status of generator $g \in G$. This variable is exogenously defined based on the availability of active power or BS unit assignment in constraint (4.2). The cranking power requirement corresponds to figure 4.1b. The equations that describe figure 4.1a are:

$$0 \leq p_g^{\tau,s} \leq P_g^{\max} u_g^{t,s}, \forall g \in G,$$
$$\forall \tau \in \{t, t+1, \ldots, t+T_{CR_g}+1\}, \forall t \in T \cup \{0\}, \forall s \in S, \tag{4.5a}$$
$$p_g^{t,s} - p_g^{t-1,s} \leq K_{R_g}, \forall g \in G, \forall t \in T, \forall s \in S, \tag{4.5b}$$
$$p_g^{t-1,s} - p_g^{t,s} \leq K_{R_g}, \forall g \in G, \forall t \in T, \forall s \in S. \tag{4.5c}$$

Constraint (4.5a) makes sure that the active power cannot be positive for at least T_{CR_g} units of time after the generator is energized, both for BS and for non BS generators. Also, the maximum active power limit is imposed at all time instances that the generator has positive active power production. The ramping rate capability is imposed through constraints (4.5b) and (4.5c).

Line Switching

A constraint that a line can have nonzero flow only if it has been switched on by the restoration process needs to be imposed. For that purpose, the transmission switching modeling with the dc approximation is utilized [66]. The constraints that impose this requirement are:

$$-\overline{S}_{ij} u_{ij}^{s,t} \leq p_{ij}^{t,s} \leq u_{ij}^{t,s} \overline{S}_{ij}, \forall (ij) \in E, \forall t \in T, \forall s \in S, \tag{4.6a}$$
$$\underline{\delta} \leq \delta_i^{t,s} \leq \overline{\delta}, \forall i \in N, \forall t \in T, \forall s \in S. \tag{4.6b}$$

Constraint (4.6a) is linearized using the big-M reformulation:

$$b_{ij}(\delta_i^{t,s} - \delta_j^{t,s}) - p_{ij}^{t,s} + (1 - u_{ij}^{t,s}) M_{ij} \geq 0,$$
$$\forall (ij) \in E, \forall t \in T, \forall s \in S, \tag{4.7a}$$
$$b_{ij}(\delta_i^{t,s} - \delta_j^{t,s}) - p_{ij}^{t,s} - (1 - u_{ij}^{t,s}) M_{ij} \leq 0,$$
$$\forall (ij) \in E, \forall t \in T, \forall s \in S, \tag{4.7b}$$

where $M_{ij} \geq |b_{ij}|(\overline{\delta} - \underline{\delta})$. Let us note here that the dc approximation of the power flow equations together with the aggregate reactive power constraint are not an accurate representation of the system. However, for the purposes of the BS allocation problem, this simplified approach that still retains the main characteristics of a complete model is adopted in order to achieve tractability.An increased accuracy can be obtained (especially for the cases where the optimization problem is aiming to identify a restoration sequence) by using the ac power flow equations or dedicated ac approximations of the power flow equations, such as the one in [8].

Consistency of Energized Grid

A series of constraints that ensure the consistency of the grid are imposed. By consistency, we mean that any island of the grid needs to have at least one energized generator to support it.

Equivalently, we need to ensure that for any energized component of the grid (line or bus), there exists a path of energized lines that lead to a node with an energized generator. One compact way to impose that is the following set of constraints, that make use of network flow variables:

$$0 \leq f_g^{t,s} \leq u_g^{t,s}, \forall g \in G, \forall t \in T, \forall s \in S, \tag{4.8a}$$

$$-u_{ij}^{t,s} \leq f_{ij}^{t,s} \leq u_{ij}^{t,s}, \forall (ij) \in E, \forall t \in T, \forall s \in S, \tag{4.8b}$$

$$\sum_{j:(ji)\in E} f_{ji}^{t,s} - \sum_{j:(ij)\in E} f_{ij}^{t,s} + \sum_{g\in G(i)} f_g^{t,s} = \frac{1}{|N|} u_i^{t,s}, \quad \forall i \in N, \forall t \in T, \forall s \in S. \tag{4.8c}$$

Constraints (4.8a), (4.8b) and (4.8c) impose a feasibility problem given fixed values of $u_g^{t,s}$, $u_{ij}^{t,s}$ and $u_i^{t,s}$ for the flows $f_{ij}^{t,s}$ and $f_i^{t,s}$. A node can be energized ($u_i^{t,s} = 1$) if there is a feasible flow from one or more of the generators with $u_g^{t,s} = 1$, flowing only through branches with $u_{ij}^{t,s} = 1$, such that the load of that node $\frac{1}{|N|} u_i^{t,s}$ can be satisfied. Otherwise, the state of that node has to be $u_i^{t,s} = 0$. We also impose the following constraints:

$$u_{ij}^{t,s} \leq u_i^{t,s}, u_{ij}^{t,s} \leq u_j^{t,s}, \forall (ij) \in E, \forall t \in T, \forall s \in S, \tag{4.9}$$

i.e. a branch cannot be energized unless both of the nodes connected to it are energized. Also, if any generator connected to a node is energized, then the node is considered energized:

$$u_g^{t,s} \leq u_i^{t,s}, \forall i \in N, \forall g \in G(i), \forall t \in T, \forall s \in S. \tag{4.10}$$

We include a time staging constraint which imposes that a line can only be energized at time t if one of its nodes was energized at time $t-1$.

$$u_{ij}^{t,s} \leq u_i^{t-1,s} + u_j^{t-1,s}, \forall (ij) \in E, \forall t \in T, \forall s \in S. \tag{4.11}$$

Finally, we assume that buses and generators, once energized, must remain energized until the end of the horizon:

$$u_g^{t,s} \geq u_g^{t-1,s}, \forall g \in G, \forall t \in T, \forall s \in S, \tag{4.12a}$$

$$u_i^{t,s} \geq u_i^{t-1,s}, \forall i \in N, \forall t \in T, \forall s \in S. \tag{4.12b}$$

Component Unavailability

We model the possible unavailability of components in a scenario using the parameters $u_g^{\text{avail},s}$ for generators, $u_i^{\text{avail},s}$ for nodes, and $u_{ij}^{\text{avail},s}$ for lines, which are equal to 1 if the corresponding component is available and 0 otherwise. The following constraints are added to the formulation to ensure that an unavailable component will not be used or energized throughout the restoration process:

$$u_g^{t,s} \leq u_g^{\text{avail},s}, \forall g \in G, \forall t \in T, \forall s \in S, \tag{4.13a}$$

$$u_i^{t,s} \leq u_i^{\text{avail},s}, \forall i \in N, \forall t \in T, \forall s \in S, \tag{4.13b}$$

$$u_{ij}^{t,s} \leq u_{ij}^{\text{avail},s}, \forall i \in N, \forall t \in T, \forall s \in S. \tag{4.13c}$$

Objective Function

The objective of the problem highly depends on the specific power system we are interested in. A generic form of objective, that is also used in this work, can be stated as follows:

$$\begin{aligned}\text{minimize} \quad & \sum_{s\in S}\pi_s\Big(\sum_{t\in T}\sum_{i\in N}C_i^t p_{SH_i}^{t,s} \\ & + \lambda\sum_{t\in T}q_{\text{sys}}^{t,s} - \mu\sum_{t\in T}\sum_{g\in G}u_g^{t,s}J_g\Big)\end{aligned}$$

The objective penalizes: (i) the load shed (depending on how critical the load that is being shed is at various time instances after the blackout), (ii) the reactive power capacity (a negative reactive power capacity ensures that the reactive power injected by the high voltage transmission lines during the low load operating points of restoration can be absorbed), and (iii) the additive inverse of the total inertia of the system (higher inertia leads to higher system stability).

4.4 Scenario Decomposition Approach

The size of the stochastic program grows linearly with the number of scenarios, since a copy of the second stage variables is added for every scenario, along with the corresponding constraints. Even though there are techniques to reduce the number of scenarios [67] or carefully select them, the number of scenarios necessary for the needs of a problem can be large, especially when the underlying uncertainty is characterized by low-probability high-impact events (such as component unavailability). For this reason, special purpose algorithms have been developed to decompose the problem by scenario. These algorithms aim to solve smaller optimization problems corresponding to one or more scenarios (which may be easier to solve) and then combine the information to approach the solution of the complete stochastic program. In this section, we describe the decomposition algorithm of [4, 124] in the context of our problem.

Let $\boldsymbol{u}_{BS} \in \mathbb{B}^{|G|}$ be the vector of the first stage BS allocation, and $\boldsymbol{y}_s$ be a vector that contains all the second stage variables for scenario $s \in S$. Let X be the feasibility set imposed by the constraints involving only first stage variables:

$$X = \left\{ \boldsymbol{u}_{BS} \in \mathbb{B}^{|G|} : \sum_{g\in G} C_{BS_g} u_{BS_g} \leq B \right\}. \tag{4.15}$$

Let $Y_s(\boldsymbol{u}_{BS})$ be the set to which $\boldsymbol{y}_s$ must belong, enforced by the rest of the constraints (including the integrality of the energization variables), for scenario $s \in S$, if the first stage variables are fixed at a value of $\boldsymbol{u}_{BS}$:

$$Y_s(\boldsymbol{u}_{BS}) = \{\boldsymbol{y}_s : (4.2) - (5), (7) - (13)\}, \forall s \in S. \tag{4.16}$$

Finally, define the functions f_s, for $s \in S$, that return the optimal value of the second stage optimization problem for scenario s given the BS allocation $\boldsymbol{u}_{BS}$:

Initialization Phase
$k \leftarrow 0, UB \leftarrow \infty, LB \leftarrow -\infty, W \leftarrow \emptyset$
Main Body
repeat
$k \leftarrow k + 1$
Lower Bounding Phase
Solve scenario subproblems:
for $s \in S$ **do**
$\boldsymbol{u}^k_{BS,s} \in \underset{\boldsymbol{u}_{BS} \in X \setminus W}{\operatorname{argmin}} f_s(\boldsymbol{u}_{BS})$
end for
Update Lower Bound:
LB $\leftarrow \sum_{s \in S} \pi_s f_s(\boldsymbol{u}^k_{BS,s})$
Upper Bounding Phase
for $s \in S$ **do**
Check termination criterion:
if $\frac{\text{UB}-\text{LB}}{\text{UB}} \leq \epsilon$ **then** Break
end if
Evaluate scenario solutions:
$\text{UB}_s \leftarrow \sum_{i \in S} \pi_i f_i(\boldsymbol{u}^k_{BS,s})$
Update Upper Bound:
UB $\leftarrow \min\{\text{UB}, \text{UB}_s\}$
end for
Cut Phase
Exclude points already tested:
for $s \in S$ **do**
$W \leftarrow W \cup \{\boldsymbol{u}^k_{BS,s}\}$
end for
until $\frac{\text{UB}-\text{LB}}{\text{UB}} \leq \epsilon$

Figure 4.1: Decomposition scheme from [4] applied to the BS Allocation Problem. The Lower Bounding Phase involves solving smaller optimization problems than the original, since the scenario is fixed, whereas the Upper Bounding Phase involves smaller problems since both the first stage and the scenario are fixed (just evaluations of the function f_s).

$$\begin{aligned} f_s(\boldsymbol{u}_{BS}) = \underset{\boldsymbol{y}_s \in Y_s(\boldsymbol{u}_{BS})}{\text{minimize}} \quad & \sum_{t \in T} \sum_{i \in N} C^t_i p^{t,s}_{SH_i} \\ & + lambda \sum_{t \in T} q^{t,s}_{\text{sys}} \quad -\mu \sum_{t \in T} \sum_{g \in G} u^{t,s}_g J_g \end{aligned} \tag{4.17}$$

Based on these definitions, the stochastic BS allocation problem can be rewritten as:

$$\text{minimize} \quad \sum_{s \in S} \pi_s f_s(\boldsymbol{u}_{BS}) \tag{4.18}$$

The main body of the algorithm is divided into three phases, the Lower Bounding Phase, the Upper Bounding Phase and the Cut Phase. In the Lower Bounding Phase, we fix every scenario

$s \in S$ and solve for the optimal first stage decision given that scenario, over a space $X \setminus W$. This yields $|S|$ scenario specific solutions for the first stage variables $\boldsymbol{u}_{BS}$ at iteration t. In the first iteration, the set W is empty, so we are essentially solving $|S|$ scenario subproblems without any interaction, i.e. we are solving the initial problem after relaxing the non-anticipativaty constraints. Since we are solving a relaxation, at least for the first iteration, we are guaranteed to get a lower bound on the optimal solution to (4.18). For the next iterations, we get lower bounds for (4.18) solved over the restricted space of first stage variables $X \setminus W$.

In the Upper Bounding Phase of the algorithm, the $|S|$ scenario specific solutions for the first stage variables found during the previous phase are tested into the full problem. If feasible, each one of them yields an upper bound to (4.18). That way, we can possibly update the upper bound and the first stage solution that yields it.

Finally, in the Cut Phase, we add the points $\{\boldsymbol{u}^k_{BS,s}\}_{s\in S}$ in the set W. Our objective function value has already been calculated for all of these points during the previous phase, so we can exclude them from any further consideration. This is achieved by adding a global cut in the optimization problems solved in the first phase, for every point in W. The following "No-Good-Cut" is employed to cut off the point $\boldsymbol{u}^k_{BS,s}$:

$$\boldsymbol{u}^T_{BS}(\mathbf{1} - \boldsymbol{u}^k_{BS,s}) + (\mathbf{1} - \boldsymbol{u}_{BS})^T \boldsymbol{u}^k_{BS,s} \geq 1. \tag{4.19}$$

The algorithm will terminate once the desired optimality guarantee ϵ is achieved. Due to the construction of the algorithm, it is guaranteed to terminate in a finite number of steps (since there are only a finite number of binary points in the space of the first stage variables and each step eliminates at least one). Of course, for suitable problems, the algorithm is expected to terminate much earlier in practice. A setup where this would occur is when the solutions obtained by solving for individual scenarios are close to each other. If the first stage solution for a scenario in the first phase of the algorithm yields a reasonable allocation for other scenarios as well, that implies that a tight upper bound will be obtained in the second phase of the algorithm. Even more, if the individual scenario first stage solutions are only slightly different from each other, by eliminating them from future consideration in the next iteration of the algorithm, we may end up with individual scenario solutions that are the same for all scenarios. The black start allocation problem is a suitable candidate, since the main driving forces of the allocation of BS units are the location of the critical loads and the characteristics of each generator (a small cranking time and high ramping rate usually make for an ideal BS unit), all of which are the same across scenarios. The differentiation caused by the scenario specific initial stable islands and component unavailability might lead to slightly different allocations for the individual scenarios, which can be eliminated using the "No-Good-Cuts".

4.5 Experimental Results

All the computations are performed using the Cab cluster of the Lawrence Livermore National Laboratory. Each node of the Cab cluster has two Intel Xeon E5-2670 processors at 2.6GHz and 32GB of RAM memory. We formulate the mathematical programs using Mosel 4.0.4 and use

```
for g ∈ G, s ∈ S do
    if Random() > p_G then
        u_g^{0,s} = 1
        NODERECURSION(N(g), s)
    else
        u_g^{0,s} = 0
    end if
end for

function NODERECURSION (n ∈ N, s ∈ S)
    if u_n^{0,s} = 1 then
        return
    else if Random() > p_N then
        return
    else
        for i ∈ Neigbor(n) do
            NODERECURSION(i, s)
        end for
    end if
end function
```

Figure 4.1: Code that generates the initial islands for every scenario in a way that each island contains (at least) one energized (isochronous) generator. Note that $\mathrm{N}(g)$ is the node to which generator $g \in G$ is connected, Neighbor(i) is the set of neighboring nodes to node $i \in N$ and Random is a (different for every call) uniformly distributed random variable in $[0, 1]$. As far as the component unavailability is concerned, every initially de-energized component in a scenario was considered unavailable for the whole process with probability 0.001.

Xpress 8.5.0 for solving them [62]. The decomposition algorithm was parallelized in 6 nodes with 2 jobs per node (i.e. solving up to 12 mathematical programs in parallel) and 8 threads per job (i.e. setting Xpress to use 8 threads for traversing the branch-and-bound tree). A simple recursive function in Python, described in figure 4.1, was used to generate the synthetic scenarios. We use Matlab to manage and visualize the results.

Simulation of the IEEE-39 Bus System

In order to illustrate the effectiveness of the proposed model, a small test case is initially considered. The IEEE-39 bus system consists of 39 buses, 10 generators and 34 branches [11]. The parameters used can be found in [115]. The parameters for generator 10 are purposefully chosen in a way that favors turning it into a BS unit (i.e. small cranking power of 1MW and a small cranking time of 10 minutes). The length of the time horizon is set to $T = 40$ time units, with a 5 minutes time step, whereas 20 equally probable scenarios are used in the stochastic program. Some of the scenarios are depicted in figure 4.2. The problem has 596541 constraints and 229010 variables, of which 76010 are binary. Without the decomposition algorithm, Xpress is unable to even find a feasible point after 10 hours of execution in a node of the Cab cluster utilizing 16 threads (and default settings).

Number of scenarios	20
Variables per scenario	11450
Constraints per scenario	29437
Binaries per Scenario	3202
Lower Bounding Phase Mean Time [s]	292
Upper Bounding Phase Mean Time [s]	118
Mean Time for solution evaluation [s]	126
Total Algorithm Time [s]	6700

Table 4.1: Computational performance of the decomposition algorithm. Note that not all solution evaluations need to happen at the second stage, since some of the solutions found by the subproblems of the Lower Bounding Phase are repeated and the evaluations in the Upper Bounding Phase for the repeated points happen only once.

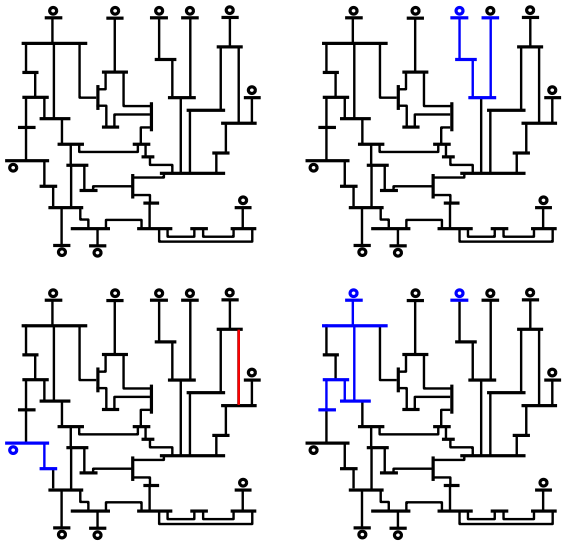

Figure 4.2: A few of the different scenarios considered in the simulations. Components in black indicate de-energized parts of the system, components in blue indicate the initial stable islands and components in red indicate unavailability. Initial line variables are not employed in our model, but we assume that initially a line between two energized nodes is energized. The top left scenario is the case of a total blackout. The top right and bottom left scenarios have one initial energized island each, but the bottom left scenario has one line that is unavailable for the whole restoration process. The bottom right scenario has two initial islands, each one with a functional generator.

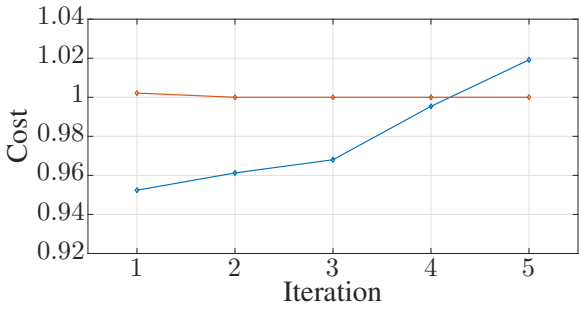

Figure 4.3: Convergence behavior of the decomposition algorithm in figure 4.1, for the IEEE-39 bus system. The UB (red line) is decreasing and the LB (blue line) increasing. Note that, since during the LB evaluation feasible solutions are chopped off by the No-Good-Cuts, the LB is not necessarily a lower bound of the stochastic problem. However, when LB becomes higher than the running UB, we have a guarantee that a near optimal solution (within the precision that the upper bounding phase subproblems are solved) is found (corresponding to the current UB).

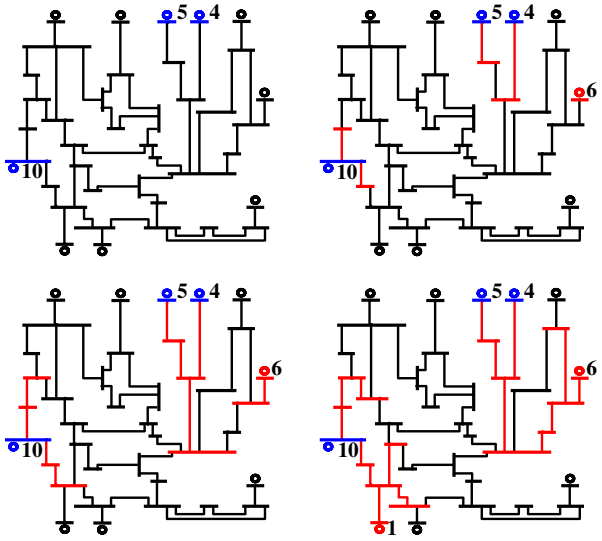

Figure 4.4: Initial restoration steps for the IEEE-39 bus system in a scenario where generators 4, 5 and 10 are initially energized (pictured in blue in the upper left figure). Generator 6 is a BS unit, so it can start at time step 1. Generator 10 is also a BS unit, but it was not influenced by the blackout, so it did not have to restart. The restoration steps (around the initial stable islands and the BS unit) can be seen in red.

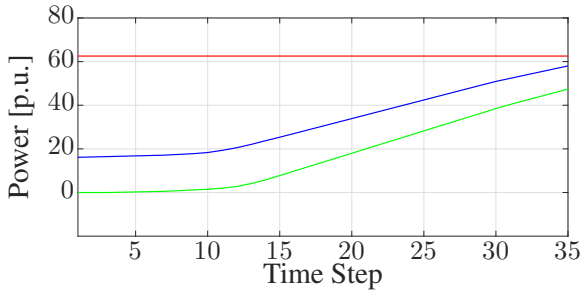

Figure 4.5: Plot of total system load (red line) with the total generation for the scenario of total blackout (green line) and a scenario with two initially energized generators (blue line) for the 39 bus system. Note that in the case of a total blackout, the generation power starts from zero and ramps up, while in the other scenario the total generation starts from a positive value, since not all of the grid is out of service.

The convergence behavior of the algorithm can be seen in figure 4.3. A computational study of the scenario decomposition algorithm is presented in Table 4.1. The algorithm terminates after 5 iterations. The solution yields the allocation of two black start units, at generators 6 and 10. The initial restoration steps are depicted in figure 4.4. The total generation and total load for two scenarios are shown in figure 4.5.

4.6 Conclusions

We presented a model for the problem of optimal BS allocation for power system restoration in the form of a two-stage stochastic program. The model also captures the basic characteristics of the restoration process. Different scenarios corresponding to different initial states of the grid failure and different component availability for the restoration process are considered and a scenario decomposition algorithm is tested. Simulations verify the effectiveness of the proposed approach for a test system.

Chapter 5

An Algorithm for Large-Scale Power System Islanding

5.1 Abstract

Intentional Controlled Islanding (ICI) is an online measure employed to prevent cascaded system outage after a disturbance in the power system. By switching off select lines, the system operator can create smaller, easier to control islands. An algorithm for ICI should be fast to implement in real time, as well as capable of integrating islanding requirements such as coherency of the generators in an island and minimum disruption of the power balance caused by the switching of lines.

In chapter 3, we referred to the problem of optimal islanding in the context of a Mixed Integer Programming (MIP) formulation. In that chapter, we assumed the generator coherency sets are known in advance. In this chapter, we provide more details on how these coherency sets (generator partitioning) can be determined. Additionally, since the optimal islanding is essentially a large scale graph partitioning problem, the computational performance of MIP algorithms tends to be fairly slow for the needs of an online decision system that has to act within seconds to prevent a cascaded failure of the system. In this chapter, we instead approximate the solution to a common ICI formulation by utilizing a known combinatorial approximation scheme of the normalized cut. This approach is easily implementable and numerically robust, exhibits high computational efficiency and allows for a natural integration of islanding requirements (such as generator minimum load and inflexible lines) into the problem solution. Experimental results on systems with up to 3000 buses verify the effectiveness of our approach.

5.2 Introduction

Mitigating the impacts of an extended outage is among the main characteristics of a resilient grid. Intentional Controlled Islanding (ICI) is a well studied technique employed to prevent widespread blackout after a large scale grid disturbance. The idea is that, by disconnecting branches of the power system, the operator can create small islands that are stable or easily controllable. That way, a cascaded outage can be avoided. Since time is of the essence after a power disturbance, any algorithm employed for intentional islanding needs to be robust and executable in real time, while also resulting in an effective islanding scheme.

A common objective for the islanding is to split the power grid into islands that only contain coherent generators. Coherent generators are generators whose phase angle difference does not change much after a disturbance, i.e. generators that swing together. The goal is to eliminate interarea oscillations, which are a common cause of blackouts. More specifically, interarea oscillations occur when two incoherent generators (or groups of generators) swing against each other after a disturbance, at frequencies of 1Hz or less, leading to large power variations in the tie-line [102]. If the system also suffers from insufficient oscillation damping, this power variation can lead to an extended blackout. Hence, by disconnecting these two groups of generators from each other, the operator may prevent a cascaded outage.

The idea that generator coherency with respect to the slowest modes (which are the ones responsible for interarea oscillations) can be used for determining an islanding scheme appeared in some of the seminal works in the field [28, 155]. Generator coherency with respect to the slowest modes has been associated with weak coupling between the state variables of the generators belonging to incoherent sets [29, 80]. This gives rise to a generator islanding scheme based on minimizing the coupling between generators in different islands. In [41], bipartitioning of the generators into two coherent groups is formulated as a normalized cut problem [129] and approximated through solving a generalized eigenvector problem and a clustering problem based on the second eigenvector. Similar approaches are used in [42, 48, 79].

Following the generator grouping, the specific set of lines to switch off in order to create islands that contain the corresponding generator groups needs to be defined. To that end, the set of lines is commonly chosen to minimize the total power imbalance (i.e absolute value of algebraic sum of power flows of the switched lines) or the power flow disruption (i.e. sum of absolute values of the power flows of the switched lines). This can be achieved through variations of constrained spectral clustering [41, 48], through mixed integer programing [81], or through graph cuts [155]. Often, grid simplification and aggregation steps are required to ensure computational efficiency [152].

While the aforementioned schemes are the most dominant in literature, there are also many approaches that utilize different techniques and include further islanding considerations. Among them, a submodular optimization problem is formulated in [92], an efficient multilevel graph partitioning algorithm is used in [86], and multiple mixed integer programming models have been proposed [58, 137, 138, 158].

In this work, a normalized cut problem that combines generator coherency and minimum power flow disruption is formulated. The formulation can allow for the integration of further islanding constraints, such as inflexible lines, minimum generator limits, or forcing components of the

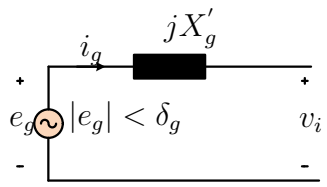

Figure 5.1: Classical transient generator model. The internal generator node, of voltage e_g, is connected to the terminal (power system) node $i \in N$, of voltage v_i, through a transient reactance $X_g^{'}$. The transient internal voltage e_g is calculated based on the steady state operation using the transient reactance. Following that, the magnitude $|e_g|$ is assumed constant and the angle δ_g is initialized based on the steady state value $\hat{\delta}_g$ and then follows the dynamics of the differential equations (5.5).

system to belong to the same island. An adaptation of the approximation algorithm proposed in [68, 70] is employed. The resulting scheme runs at the complexity of a minimum cut, which is generally faster and more numerically robust than eigenvector computations. The efficiency of the approach allows it to run fast even for large scale systems, obviating the need for grid simplification. The performance in terms of the two objectives of the islanding problem (coherency and power flow disruption) is better or comparable to the spectral clustering approach performance.

The rest of this chapter is organized as follows: section 5.3 presents the background to setup the problem, section 5.4I presents the problem formulation and the algorithm employed, section 5.5 shows experimental results, and section 5.6 draws conclusions. This work has been published in [112].

5.3 Controlled Islanding Objectives

In this section we review the necessary background for the problem formulation, i.e. the logic behind the two main objectives considered in this work (generator coherency and minimal power flow disruption).

Generator Coherency

We briefly describe a typical model for small signal system analysis to motivate the discussion on coherent generator sets. The analysis examines two instances of the system: the pre-disturbance system and the post-disturbance system. The pre-disturbance system is assumed in steady state. Its state is calculated through the power flow equations and is used for initializing the transient phenomena. After the disturbance, the transient dynamics are captured through the second order differential equations of the generators (swing equations), as well as the power flow equations.

The generators are represented using a classical model, as shown in figure 5.1. Each generator g in the set of generators G is modeled through an internal node with complex transient voltage e_g, that is connected to the power system bus (terminal generator node) through a transient reactance

$X_g^{'}$. The magnitudes $|e_g|$ of internal voltages e_g are constant throughout the transient phenomenon, based on the assumption of constant flux linkage in the machine. The phase angles δ_g of the internal voltages, on the contrary, are the state variables of our system. The coupling between the phase angle responses from different generators will eventually be the criterion used for grouping generators in coherent sets.

A number of approaches can be used for load modeling [100], but a typical one for stability studies is to represent the load as a constant impedance. For a given node, if the pre-disturbance load active and reactive power P_D, Q_D and the load bus voltage V_D are known, the impedance is calculated by:

$$Y_D = \frac{P_D - jQ_D}{|V_D|^2} \tag{5.1}$$

and is assumed constant in the post-disturbance system.

We can now form a generalized $(|G|+|N|) \times (|G|+|N|)$ admittance matrix $\boldsymbol{Y}$, that considers the buses (set N) as well as the internal generator nodes (therefore takes into account the load impedances, the generator transient reactances, and the rest of the system). The following equality holds:

$$\begin{bmatrix} \boldsymbol{i}_G \\ \boldsymbol{i}_N \end{bmatrix} = \boldsymbol{Y} \begin{bmatrix} \boldsymbol{e}_G \\ \boldsymbol{v}_N \end{bmatrix} = \begin{bmatrix} \boldsymbol{Y}_{GG} & \boldsymbol{Y}_{GN} \\ \boldsymbol{Y}_{NG} & \boldsymbol{Y}_{NN} \end{bmatrix} \begin{bmatrix} \boldsymbol{e}_G \\ \boldsymbol{v}_N \end{bmatrix} \tag{5.2}$$

where $\boldsymbol{e}_G$, $\boldsymbol{i}_G$ are the $|G|$-dimensional complex vectors of voltage and current injections in the internal generator nodes and $\boldsymbol{v}_N$, $\boldsymbol{i}_N$ the $|N|$-dimensional vectors of voltage and current injections in the buses of the power system. Note that, due to the fact that loads are modeled through constant impedances (included in the matrix $\boldsymbol{Y}$) and generators are modeled through additional nodes connected to the buses through constant reactances, the current injections for all the buses of the power system are zero $\boldsymbol{i}_N = \boldsymbol{0}$. Following that, by using Kron reduction [46], we eliminate the variables $\boldsymbol{v}_N$ and obtain the $|G| \times |G|$ effective admittance matrix $\boldsymbol{Y}^{'} = \boldsymbol{Y}_{GG} - \boldsymbol{Y}_{GN}\boldsymbol{Y}_{NN}^{+}\boldsymbol{Y}_{NG}$ (where $\boldsymbol{Y}_{NN}^{+}$ the Moore-Penrose inverse), which satisfies $\boldsymbol{i}_G = \boldsymbol{Y}^{'}\boldsymbol{e}_G$. The imaginary part of this matrix is usually dominating the real part in terms of order of magnitude, so a common assumption is to neglect it and consider: $\boldsymbol{Y}^{'} \approx -j\boldsymbol{B}^{'}$, where the effective transient susceptance matrix $\boldsymbol{B}^{'}$ is assumed real symmetric with its off diagonal entries non negative.

Restricting ourselves to the reduced network that only contains the internal generator nodes, notice that for $g, g' \in G$, the nodes g and g' are connected through a branch of reactance $1/\boldsymbol{B}_{gg'}^{'}$, therefore the active power transfer from g to g' is:

$$P_{gg'} = |e_g||e_{g'}|\boldsymbol{B}_{gg'}^{'} \sin\left(\delta_g - \delta_{g'}\right) \tag{5.3}$$

and the total active power that a generator g sends to the grid is equal to

$$P_g^e = \sum_{g' \in G, g' \neq g} P_{gg'} \tag{5.4}$$

If for a generator g this power is not equal to the mechanical input of the generator, P_g^m, the imbalance will cause a change in the internal voltage phase angle according to the swing equation for that generator (with inertia constant H_g, angular frequency ω_0, damping neglected):

$$\frac{2H_g}{\omega_0}\ddot{\delta}_g = P_g^m - P_g^e \tag{5.5}$$

Substituting (5.3) and (5.4) into (5.5), we get a set of $|G|$ second order equations for the $|G|$ dimensional vector of internal generator angles $\boldsymbol{\delta}$ (state variables). By linearizing the system around the pre-disturbance operating point $\hat{\boldsymbol{\delta}}$ we obtain:

$$\boldsymbol{M}\ddot{\boldsymbol{\delta}} = \boldsymbol{K}\boldsymbol{\delta} \tag{5.6}$$

where the g, g' entry of the $|G| \times |G|$ matrix $\boldsymbol{K}$ for $g \neq g'$ equals:

$$\begin{aligned} \boldsymbol{K}_{gg'} &= -\frac{\partial P_{gg'}}{\partial \delta_{g'}}\Big|_{\substack{\delta_g=\hat{\delta}_g \\ \delta_{g'}=\hat{\delta}_{g'}}} \\ &= |e_g||e_{g'}|\boldsymbol{B}'_{gg'}\cos\left(\hat{\delta}_g - \hat{\delta}_{g'}\right) \end{aligned} \tag{5.7}$$

and for $g = g'$ equals $\boldsymbol{K}_{gg} = -\sum_{g''\in G, g''\neq g} \boldsymbol{K}_{gg''}$. The $|G| \times |G|$ matrix $\boldsymbol{M}$ is diagonal with $\boldsymbol{M}_{gg} = \frac{2H_g}{\omega_0}$ for all $g \in G$. Note for the linearization that the internal voltage magnitudes $|e_g|$ are constants (equal to their pre-disturbance value) and so is the mechanical input of each generator P_g^m (equal to the electrical output of the generator before the disturbance, where the system was at steady state).

Two generators are characterized as "coherent" if their internal voltage angle difference (which is a function of time) does not change much after a disturbance. Therefore, coherent generators swing together and can be aggregated in transient system simulations. While there are many formal definitions of coherency, one that has particularly nice structural properties characterizes two generators as coherent with respect to a subset of the modes of the system of differential equations (5.6), if none of these modes are observable from the voltage angle difference. In [80], coherency with respect to the slowest modes is related to small values of a scalar quantity ζ that depends on the off-diagonal entries of the matrix $\boldsymbol{K}$. More specifically, for the case of partitioning the generator set G into two sets of coherent generators V_G and $\bar{V}_G = G \setminus V_G$, we have:

$$\zeta(V_G) = \frac{\sum_{(gg')\in\delta(V_G)} \boldsymbol{K}_{gg'}}{\sum_{g\in V_G} \boldsymbol{M}_{gg}} + \frac{\sum_{(gg')\in\delta(V_G)} \boldsymbol{K}_{gg'}}{\sum_{g\in \bar{V}_G} \boldsymbol{M}_{gg}} \tag{5.8}$$

where $\delta(\cdot)$ is the undirected cutset of a set and its complement, i.e. $\delta(V_G)$ contains all pairs (g, g') with one generator in V_G and one in $\bar{V}_G$.

It has been verified that splitting the post-disturbance grid based on groups of coherent generators leads to stable islands and prevents fault propagation [149, 153]. Furthermore, an objective similar to (5.8) has been recognized as a normalized graph cut [129] for the bipartition of the generator set in [41]. Since solving the minimum normalized graph cut problem is NP-hard, a spectral clustering approximation algorithm based on a generalized eigenvalue problem was obtained in [41]. Partitioning of the grid into more than two islands can be accomplished, if necessary, by repeating the same procedure for the resulting islands.

Minimal Power Flow Disruption

A common objective when identifying a set of lines to switch off in order to isolate coherent generator groups is that of minimal power imbalance. If the set of buses N is partitioned into the sets S and $\bar{S} = N \setminus S$, the power imbalance is calculated by:

$$\sum_{(i,j)\in\delta(S)} |P_{ij}| \tag{5.9}$$

where P_{ij} the active power on the transmission lines between buses i and j (algebraic sum for the case of multiple lines or flow directions). The idea behind this penalty is that we seek to remove lines in a way that causes minimum change from the pre-disturbance power flows within the resulting islands. The advantages and disadvantages of using this objective have been extensively examined in literature [41].

5.4 A Combinatorial Algorithm for Optimal Islanding

Problem Formulation

We formulate an optimal islanding problem that incorporates both generator coherency and power imbalance with a trade-off, i.e. the problem of interest is:

$$\underset{S\subseteq N}{\text{minimize}} \quad \frac{\sum_{(ij)\in\delta(S)} \boldsymbol{W}_{ij}}{\sum_{i\in S} \boldsymbol{Q}_{ii}} + \frac{\sum_{(ij)\in\delta(S)} \boldsymbol{W}_{ij}}{\sum_{i\in\bar{S}} \boldsymbol{Q}_{ii}} \tag{5.10}$$

In the equation above, the weights are defined for nodes $i, j \in N$, $i \neq j$:

$$\boldsymbol{W}_{ij} = \sum_{(g,g')\in(G(i)\times G(j))} \boldsymbol{K}_{gg'} \; + \; \lambda \, |P_{ij}| \, \mathbb{I}_E\{(ij)\} \tag{5.11}$$

where $G(i)$ denotes the set of generators connected to node i, λ a trade-off coefficient (which is the only tuning parameter of the optimization problem), and $\mathbb{I}_E$ is the indicator function of the set of undirected branches E. Note that the weight W_{ij} can be nonzero only if both buses i and j have a connected generator or if there is a branch in the power system connecting i and j. The balancing weights for a node $i \in N$ are given below (zero if $G(i) = \emptyset$).

$$\boldsymbol{Q}_{ii} = \sum_{g\in G(i)} \boldsymbol{M}_{gg} \tag{5.12}$$

The output of the optimization problem (5.10) is an optimal partitioning of the nodes S. All the lines in the cutset $\delta(S)$ will be switched off to create (at least) two islands. If further partitioning of the grid is required, the optimization can be formulated for each of the remaining islands. Note that lines that are inflexible (cannot be remotely switched off) can be assigned a large weight $\boldsymbol{W}_{ij}$, which will ensure that they will not belong to the cutset.

Another critical concern for stable islands is that a generator operates in a more stable fashion if its generation exceeds a minimum, which means that one or more load nodes should belong to the same island as this generator. We can easily force the generator to belong to the same island as a load node by assigning large weights to the edges in one or more paths between them. These paths and load nodes can be efficiently found by graph search algorithms (such as Breadth First Search) around the generators.

The alternative, two step approach to formulate the problem, common in literature, would be to pick the partition of the generators in the first step and in the second step the optimal set of lines to switch off to minimize power flow disruption in a way that respects the generator grouping. The techniques described in what follows can be used in this two-step setting as well. However, the same result can be simulated using the single step optimization problem (5.10) by picking a small trade-off coefficient for the power flow disruption: The optimal generator grouping will be selected based only on generator coherency (dominant terms), and then (since there can be multiple ways to select lines to switch off and achieve the same generator grouping), the solution among them that minimizes power imbalance will be chosen.

Theoretical Justification for the Algorithm

The problem in (5.10) can be recognized as a normalized cut problem on a graph with $|N|$ nodes and at most $|G| + |E|$ edges. Since the problem is NP-hard in general, we use an algorithm from [70] to solve a relaxation of the problem. This algorithm has been used, among others, in neuroscience [131] and nuclear material identification [154]. In this section, we adapt some results from [70] to our problem and illustrate the main idea behind the algorithm. First, define the problem:

$$\underset{S\subseteq N, b\in\mathbb{R}_+}{\text{minimize}} \quad \frac{(1+b)^2 \sum_{(ij)\in\delta(S)} \boldsymbol{W}_{ij}}{\sum_{i\in S} \boldsymbol{Q}_{ii} + b^2 \sum_{i\in\bar{S}} \boldsymbol{Q}_{ii}} \tag{5.13a}$$

$$\text{subject to} \quad G(S) \neq \emptyset, G(\bar{S}) \neq \emptyset \tag{5.13b}$$

$$b = \frac{\sum_{i\in S} \boldsymbol{Q}_{ii}}{\sum_{i\in\bar{S}} \boldsymbol{Q}_{ii}} \tag{5.13c}$$

where $G(S), G(\bar{S})$ the set of generators connected to nodes of S and to the complement of S respectively. The problem (5.13) is equivalent to (5.10). To see that, first note that in (5.10) neither of $G(S)$, $G(\bar{S})$ can be empty for a finite objective value. The equivalence of the objectives can be seen by substituting $b = \frac{\sum_{i\in S} \boldsymbol{Q}_{ii}}{\sum_{i\in\bar{S}} \boldsymbol{Q}_{ii}}$ into the objective of (5.13). The algorithm developed in [70] solves (5.13) with constraint (5.13c) relaxed. For the different values of the parameter β, define the following problem:

$$P(\beta) = \underset{S\subseteq N: G(S), G(\bar{S})\neq\emptyset}{\text{minimize}} \sum_{(ij)\in\delta(S)} \boldsymbol{W}_{ij} \; + \; \beta \sum_{i\in S} \boldsymbol{Q}_{ii} \tag{5.14}$$

Claim 1: Any optimal solution (partition S, $\bar{S}$) of problem (5.13) with constraint (5.13c) relaxed is an optimal solution to problem $P(\beta)$, for some value of the parameter β. The proof of the claim is provided in the Appendix.

Based on the previous claim, instead of solving the relaxation of (5.13), we will solve problem (5.14) for all values of the parameter β. To that end, first note that (5.14) only allows partitions in which both sets S and $\bar{S}$ must contain at least one generator. For two generators $g, g' \in G$, with $g \neq g'$, let $P^{gg'}(\beta)$ denote the optimization problem $P(\beta)$ with the additional constraint that $n(g) \in S$, $n(g') \in \bar{S}$, where $n(g) \in N$ denotes the node to which generator g is connected. Then, the problem $P(\beta)$ can be solved as:

$$P(\beta) = \underset{g,g' \in G, g \neq g'}{\text{minimize}} \; P^{gg'}(\beta) \tag{5.15}$$

Therefore, by solving at most $O(|G|^2)$ problems of the type $P^{gg'}(\beta)$, we can solve $P(\beta)$. However, in order to reduce the real time computational burden, we will instead heuristically pick two generators g, g' and force them to belong to different sets. The generators g and g' can be picked based on a heuristic, such as weakest coupling $\boldsymbol{K}_{gg'}$, or empirical knowledge of the particular power system. Even though this approach yields a worse objective, it is reasonable for cases in which we may want to force separation between two generators.

Finally, for a given pair g, g', the problem $P^{gg'}(\beta)$ can be solved efficiently using the graphs of figure 5.1. To see that, note first that the capacity of an $s-t$ cut in the graph for $\beta \geq 0$ is exactly the objective from (5.14). The big-M capacity arcs from s to $n(g)$ and from $n(g')$ to t ensure that $n(g) \in S$ and $n(g') \in T$. Therefore, the minimum-cut problem on the graph solves $P^{gg'}(\beta)$. For $\beta < 0$, the capacity of the cut is $\sum_{(ij)\in\delta(S)} \boldsymbol{W}_{ij} + (-\beta) \sum_{i\in T} \boldsymbol{Q}_{ii} = \sum_{(ij)\in\delta(S)} \boldsymbol{W}_{ij} + \beta \sum_{i\in T} \boldsymbol{Q}_{ii} - \beta \sum_{i\in N} \boldsymbol{Q}_{ii}$, which again solves $P^{gg'}(\beta)$ since the last term in the summation is a constant. In both problems, the parameter $|\beta|$ appears on strictly increasing functions of capacities only from the source/only to the sink. This ensures we can solve for all values of β efficiently at the complexity of a maximum flow problem (parametric cut) [69]. By the same theory, we know there will be at most $|N|$ different partitions generated from the parametric cut solution, for all the parameters β. Therefore, we can efficiently calculate the objective of interest for all of them and pick the best.

The Algorithm

Based on the analysis and theoretical justification presented in the previous sections, the proposed algorithm for optimal islanding following an extended grid disturbance is presented a stepwise fashion below.

Step 1: Identify the surviving power system, the operational generators, buses and edges. Based on the last known pre-disturbance measurements and the analysis presented in subsection 5.3, calculate the matrices $\boldsymbol{K}_{gg'}$, $\boldsymbol{M}_{gg}$ for the surviving generators. Note that if these calculations are periodically performed online for the power system in steady state, the matrices for the surviving system can be updated more efficiently (but we will not focus on that aspect in this work). Calculate the weights $\boldsymbol{W}_{ij}$ and $\boldsymbol{Q}_{ii}$ based on equations (5.11) and (5.12) and any other requirements

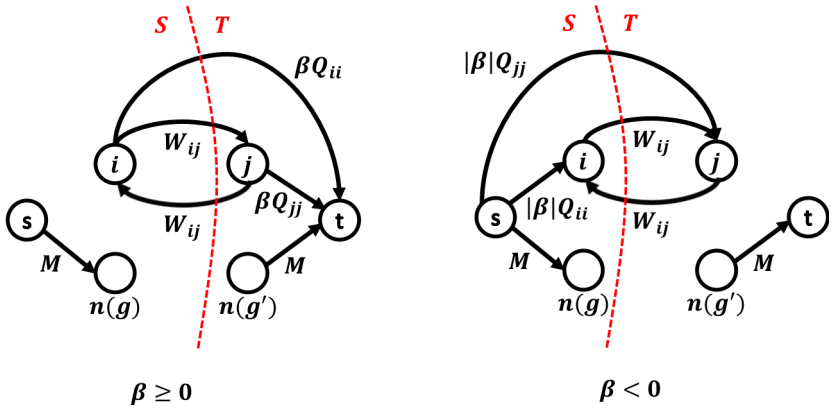

Figure 5.1: Directed graphs to solve $P^{gg'}(\beta)$ for the different values of β, following the construction in [70]. The graph has all the nodes in N, plus two dummy (source and sink) nodes s,t. The partition is S, $T = \bar{S}$. The weights $\boldsymbol{W}_{ij}, \boldsymbol{Q}_{ii}$ refer to the objective of (5.14). M is a large number. For every pair i, j with non zero weight $\boldsymbol{W}_{ij}$, two directed edges are added. For every generator node i (i.e. $G(i) \neq \emptyset$), one directed edge of weight $\beta \boldsymbol{Q}_{ii}$ is added.

that we want to impose on the system (such as inflexible lines or minimum load requirements, as described in subsection 5.4).

Step 2: Formulate the graphs from figure 5.1 and solve the parametric minimum cut problem on both of them. The output of the algorithm for each graph will be at most $|N|$ different partitions of N, each one corresponding to a value of β [69]. Calculate the objective value of (5.10) for each one of them and pick the partition with the best objective. On a technical note, the calculation of the objective for each partition can be done in $O(|N|)$ by using the optimal parametric cut objective that yielded this partition. Note that if an implementation of the parametric cut is not available, one can simply pick some values of β instead and solve the problem only for them, as a heuristic.

Step 3: Repeat the process from Step 2 for each of the partition sets to further split the grid into smaller islands.

5.5 Experimental Results

We simulated the algorithm on the IEEE-9, IEEE-39, IEEE-300 and Polish test systems. The results are reported below. More specifically, the graph structure (nodes, edges, generators and the underlying connections) were used. Lines between two nodes with multiplicity higher than one were merged and their power flows were added. Based on [100], we assumed that the transient reactance of the generators is $X_g^{'} = \max\{0.1, 92.8(P_g^{\max})^{-1.3}\}$, where $X_g^{'}$ is expressed in p.u. with respect to the system basis $S_{\text{base}} = 100$MVA and $P_g^{\max}$ is the nominal power of generator g is MW. We also assumed that $H_g = 0.04 P_g^{\max}$, where H_g is in p.u. with respect to the system basis. Matpower [160] was used to calculate the pre-disturbance ac power flow.

The algorithm from [41], which is conceptually close to our approach and uses a well established partitioning technique based on spectral clustering, was also simulated. We implemented

Alg.	Node Partition $(\|S\|, \|\bar{S}\|)$	Generator Partition $(\|V_G\|, \|\bar{V}_G\|)$	Power Disruption MW	ζ	Time [s]
	IEEE-9				
ICI^1	(2,7)	(1,2)	71.7	68.44	0.055
ICI^2	(1,8)	(1,2)	163.0	67.82	0.081
	IEEE-39				
ICI^1	(3,36)	(1,9)	85.4	57.97	0.068
ICI^2	(8,31)	(5,5)	4611.8	31.94	0.462
	IEEE-300				
ICI^1	(4,296)	(1,68)	140.1	2.33	0.067
ICI^2	(83,217)	(1,68)	33434.5	2.33	2.030
	3375-bus Polish system				
ICI^1	(52,3322)	(1,440)	554.5	582.13	0.960
ICI^2	(478,2896)	(1,440)	81495.5	9918.4	277

Table 5.1: Optimal bipartition based on the algorithm of this chapter (ICI^1) and the algorithm from [41] (ICI^2) for IEEE test cases and the Polish system. The metrics compared are the quantity ζ from (5.8), the power flow disruption, and the algorithm execution time.

the two algorithms in Matlab. For our implementation, since the Matlab graph environment does not support parametric maximum flow, we simply solved problem (5.14) for 20 values of β evenly spaced between -1 to 1 and the solution with the best objective was chosen. The trade-off was set to $\lambda = 1$, however the optimal solution in the instances solved was often not sensitive to changes in the value of λ, which is an indication that both objectives are solved to optimality. We focus on bipartitions in the results. Multiple applications of the algorithm can break the system into smaller islands if necessary.

Table 5.1 shows the main computational results. Note that, both the power disruption values and the normalized generator cut ζ values are comparable or lower for our approach. The time of execution is also significantly better using the proposed approach. Compared to the spectral clustering approximation, our approach tends to lead to smaller islands, but it turns out that these solutions still have better objectives. If the problem changes, by introducing further islanding constraints, larger islands can be obtained. An example of introducing islanding constraints is shown in figure 5.1.

5.6 Conclusions

In this chapter, we examined an efficient approach for controlled islanding based on a combinatorial approximation of the normalized cut. The algorithm allows integration of further requirements through the use of large arc weights, a practice that will not influence the computational efficiency due to the strongly polynomial nature of the algorithms for minimum cut. Experimental results showed that the computations are fast even for large systems, hence no grid simplification

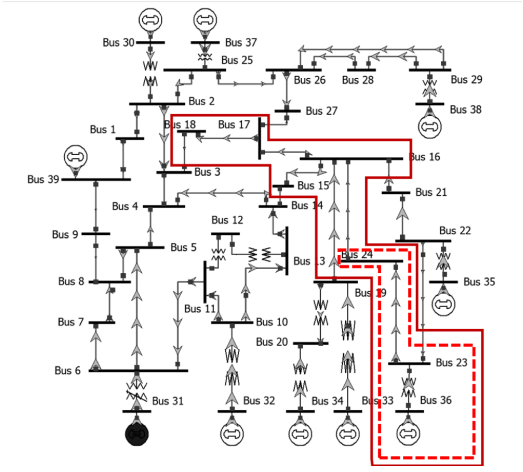

Figure 5.1: The optimal bipartition for the IEEE-39 bus system is shown with red dashed line. The purple solid line indicates the partitioning when the generator in bus 36 is required to be connected to load in node 16. This is imposed by using large weights for the path leading to the bus, in this case for branches $(36, 23), (23, 24), (24, 16)$.

is required. Future research directions include an efficient implementation of the parametric minimum cut procedure, an algorithmic description and implementation of the generator-load mapping for every island, possible generalizations to multicut partitioning, and additional simulations to verify the effectiveness of the approach.

Appendix

5.A Proof of Claim 1

The proof is based on ideas in [68]. Let S^*, b^* be an optimal solution to (5.13) with constraint (5.13c) relaxed and let the value of the objective be z^*, i.e.:

$$z^* = \frac{(1+b^*)^2 \sum_{(ij)\in\delta(S^*)} \boldsymbol{W}_{ij}}{\sum_{i\in S^*} \boldsymbol{Q}_{ii} + (b^*)^2 \sum_{i\in\bar{S}^*} \boldsymbol{Q}_{ii}} \tag{5.16}$$

We will show that S^* is an optimal solution to the optimization problem $P(\hat{\beta})$, as defined in (5.14), with $\hat{\beta} = z^* \frac{b^*-1}{b^*+1}$. By the optimality of S^*, b^*, we have that for any $S \subseteq N : G(S), G(\bar{S}) \neq \emptyset$:

$$\frac{(1+b^*)^2 \sum_{(ij)\in\delta(S)} \boldsymbol{W}_{ij}}{\sum_{i\in S} \boldsymbol{Q}_{ii} + (b^*)^2 \sum_{i\in\bar{S}} \boldsymbol{Q}_{ii}} \geq z^* \tag{5.17}$$

which can be equivalently written, after a few algebraic manipulations and substituting $\sum_{i\in\bar{S}} \boldsymbol{Q}_{ii}$ $= \sum_{i\in N} \boldsymbol{Q}_{ii} - \sum_{i\in S} \boldsymbol{Q}_{ii}$, as follows:

$$\sum_{(ij)\in\delta(S)} \boldsymbol{W}_{ij} + z^* \frac{b^*-1}{b^*+1} \sum_{i\in S} \boldsymbol{Q}_{ii} \geq z^* b^* \sum_{i\in N} \boldsymbol{Q}_{ii}, \quad \forall\, S \subseteq N : G(S), G(\bar{S}) \neq \emptyset \tag{5.18}$$

Note that the left hand side is the objective of $P(\hat{\beta})$, the right hand side is a constant, and the inequality holds for all feasible S in $P(\hat{\beta})$. Now, for the particular choice $S = S^*$, we can see from (5.16) that (5.18) holds with equality. Therefore, S^* is an optimal solution for $P(\hat{\beta})$ and the proof is complete.

Chapter 6

The Hidden Cost of Priority Dispatch for Wind Power

6.1 Abstract

Renewable generation, such as wind power, is commonly considered a must-take resource in power systems. The goal of this chapter is to illustrate that, given the technical capabilities of current wind turbines, this approach could lead to major economic inefficiency as wind integration levels in power systems increase. We initially provide intuition for cases in which the optimal operating point involves shedding renewable generation, even though no cost is associated with it in the optimization objective, illustrated in small power systems. We then explore the expected benefit from dispatching wind resources at a lower level than their available output in a Stochastic Unit Commitment (SUC) framework. The modeling and evaluation approach adopted are described. A decomposition technique that utilizes global cuts and Lagrangian penalties to achieve convergence is used to solve the resulting large scale mixed integer optimization problem, in a high performance computing environment. A reduced California system is examined as a test case.

6.2 Introduction

The worldwide drive towards a cleaner and sustainable electricity generation mix has lead to increased renewable integration goals for the coming years. California, for example, is on track for achieving its 2020 goal of 33% of energy needs satisfied by renewable resources and now aims for 50% by 2030 [1]. Renewable resources have been traditionally treated - and are still treated by many system operators - as must-take resources (negative load), i.e. they are fully integrated in the electricity network regardless of their level or variability. Renewable curtailments only occur in cases where operational feasibility is at risk. The increased renewable integration, however, gradually brings about new operating conditions, such as steeper power ramps, overgeneration and decreased frequency response capabilities. Conventional generation by itself is unable or extremely costly to deal with these new conditions and a paradigm shift is necessary, in which renewable generation is called upon to contribute to ancillary services and grid flexibility by systematically dispatching at levels defined by operational and cost considerations. The need for such policies is already becoming apparent in regions with increased renewable integration; the California Independent System Operator (CAISO) curtailed about 1% of the total potential renewable generation during the first quarter of 2017, with solar curtailment reaching up to 30% at specific times, while it has already adopted market based curtailment mechanisms [2]. In Europe, on the other hand, directive 2009/28/EC is currently in force and stipulates by law that "Member States shall ensure that when dispatching electricity generating installations, transmission system operators shall give priority to generating installations using renewable energy sources in so far as the secure operation of the national electricity system permits and based on transparent and non-discriminatory criteria" [49]. As of November 2016, however, there is an initiative to review the directive and an active debate of whether to include renewable curtailments; in fact, the latest version of the proposal (February 2017) to revise the legislation does not include prioritizing renewable generation.

We focus on mobilizing the flexibility of wind dispatch. Current wind generators and power plants have advanced controls [110] that allow them to operate practically at any point below their (maximum) available output [98, 99, 111]. However, their available output itself depends on the weather conditions, i.e. the availability of wind. Consequently, they are considered semi-dispatchable (in contrast to conventional resources for which complete control over the output point is possible). These technical capabilities, however, enable us to consider the optimization of the wind generation setpoint, instead of integrating all of the available wind generation into the system. The benefits from curtailing wind production have been examined from various perspectives. In [53] and [14], NREL provides a series of cases of wind curtailment in systems in the US or abroad. In [88] and [94] CAISO uses the software PLEXOS to simulate a rolling unit commitment problem in the presence of wind curtailment for high wind penetration. In [130] it is shown that allowing for renewable curtailment enables significant reduction of the required system storage size, in [17] the benefits are motivated mainly through solving a Security Constrained Optimal Power Flow (SCOPF) problem, in [101] through a market coupling and a nodal pricing model of part of the European system, in [39, 47] through a Security Constraint Unit Commitment (SCUC) Problem and in [143] a dynamic interaction of wind curtailment with storage is examined when the ramping rates of power plants are considered. An overview of the motivation behind wind curtailment is

given in [60], whereas in [76] wind curtailment is employed for active network management. A flexible wind dispatch margin for the joint energy and reserves market and offline policies to obtain it are examined in [65] and [64].

We decided to motivate flexible wind dispatch in the context of the Stochastic Unit Commitment (SUC) problem instead. The Unit Commitment problem is a widely studied mixed integer program [20,36,51] that determines the set of generators, among all the available ones, that will be committed to satisfy the load during the following day. The two stage Stochastic Unit Commitment problem (SUC) formulates the same decision in the presence of uncertainty (renewable generation, faults, load), captured by a finite set of possible realizations (scenarios) [19,37,104,135,140]. While wind curtailment is a usual assumption when formulating the SUC problem, in this work we explicitly focus on calculating the expected benefit from optimizing the wind output setpoint versus an approach that treats wind as a priority resource. A similar approach appears in [77], where coordination with storage is considered to illustrate the benefits from dispatchable wind. The size of the optimization problem scales linearly with the number of scenarios and for that purpose a large amount of research has been devoted to decomposition techniques to iteratively approximate the solution of the problem. Among these, in [26], the Progressive Hedging (PH) algorithm is adapted to successfully solve the SUC problem. In [78] a cutting plane algorithmic approach is used. In [106] a parallel implementation of Lagrangian relaxation in a high performance computing environment is employed. In [7] an asynchronous parallelized algorithm based on stochastic subgradient is utilized to efficiently solve the problem.

In this chapter, we provide a complete framework to understand and evaluate the expected benefit from flexible wind dispatch in a SUC setting, while also introducing innovations in the implementation of the various components of the model. To begin with, since wind generation is not associated with any fuel costs in the objective, it is not self evident why we could be better off curtailing it and using costly conventional generation in its place. For this reason, we present small motivating examples to offer intuition regarding the most common setups where such benefit may occur: operation during oversupply, ramping requirements, technical minima of generators and congestion. We then proceed to describe the complete evaluation framework, by introducing its basic components: the Uncertainty and Optimization Modules.

The Uncertainty Module is responsible for generating sample scenarios that capture the underlying uncertainty for renewables and system faults. It is based on existing wind speed modeling techniques, which we extend by using a non parametric modeling methodology for the aggregate power curve, i.e. the mapping of wind speed to wind generation, utlizing local polynomial regression [30]. The Optimization module, on the other hand, is responsible for solving the SUC problem given a set of scenarios. It specializes an algorithm presented in [4] for general two stage stochastic programs with binary first stage variables. The intuition behind the algorithm is that, if the different scenarios of a stochastic program are similar, then it is possible that a good (first stage) solution to the full problem will come from solving the significantly smaller subproblems that only look at scenarios in isolation. By solving the scenarios in isolation in the first phase of the algorithm, we obtain lower bounds to the SUC optimal objective. Then, by testing the various first stage solutions we got from the individual scenario subproblems to the full problem, we get feasible solutions to the full problem (upper bounds) in the second phase of the algorithm. We

proceed to eliminate these solutions from consideration in the next iterations, when we resolve the individual scenario subproblems. The algorithm is executed until the desired optimality guarantee is obtained.

In the experimental results of [4, 124], the algorithm is tested without implementing dual updates (just employing cuts to eliminate solutions already tested). Even though SUC satisfies the technical requirements of the algorithm, the cuts employed fail to efficiently reduce the gap for the SUC problem on their own. To remedy that, we combine the use of cuts with Lagrangian penalties in the objective of the individual scenario subproblem to convey information from other scenarios, so as to obtain scenario specific solutions that perform well in the full problem. The exact penalties we use are the same as the Progressive Hedging Lower Bounds [56], in a way that the lower bounding property of the first phase of the algorithm is preserved, and lead to a projected subgradient descent optimization scheme at every iteration (an update that lies within the general framework of the algorithm in [4]). One advantage of the algorithm from [4] is that termination of the algorithm with any desired optimality gap is (at least in theory) guaranteed, in contrast to a simple subgradient optimization scheme for the dual where the achievable accuracy is limited by the duality gap between the primal and dual problems at best.

We test our framework on a reduced model of the Western Electricity Coordinating Council (WECC) system from 2010 [156], consisting of 130 thermal generators, 225 nodes and 371 lines for three wind penetration scenarios (low, medium and high). After the SUC problem is solved, we utilize its optimal solutions to compare the cost of policies that treat wind as a must-take resource versus ones that allow flexible wind dispatch. Regarding the value of wind flexibility, our results indicate negligible cost benefit in the low and medium integration case, but a 15% cost improvement in the high integration case, supporting the argument that flexible wind dispatch should be directly integrated in the operation of the power market.

The chapter is structured as follows: In section 5.3, the motivating examples are provided, in section 5.4, the general modeling is described, in section 5.5 experimental results are shown, and in section 5.6 we conclude and discuss policy implications of the work. This work has been published in [113].

6.3 Motivating Examples

In order to motivate the discussion and provide some intuition on the cost benefits from allowing wind generation to deviate from the available wind power output, four stylized examples are examined. These examples try to illustrate that, even though wind generation is not associated with any cost in the objective, it can still be beneficial to spill wind resources for a cost efficient allocation of conventional generation. Figure 6.1 outlines the parameters for these examples.

Technical Minima

In example 1, if the 40MW of wind power are treated as a must-take resource, the total residual load that needs to be satisfied by conventional generation would be 20MW. Due to the technical

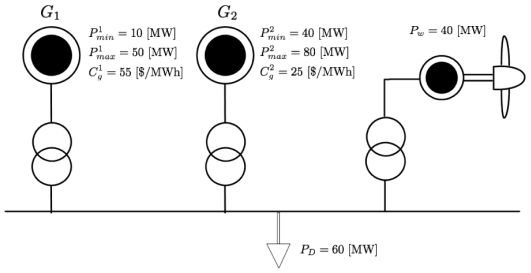

(a) Example 1. The generator specifications in this case are minimum and maximum generation limits ($P_{\min}$, $P_{\max}$) and marginal costs C_g. The available (maximum) wind power generation is P_w and the load is P_D.

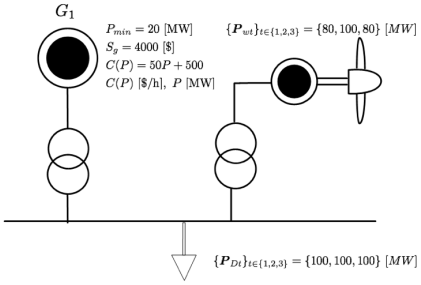

(b) Example 2. The generator specifications are the minimum generation limit ($P_{\min}$), the startup cost S_g and the operating cost $C(P)$ as a function of the generation level P. The available (maximum) wind power generation P_{wt} and load P_{Dt} are given for three consecutive time periods, $t = 1, 2, 3$. G_1 is assumed turned off at the beginning.

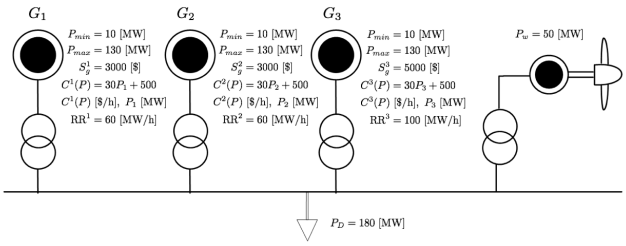

(c) Example 3. The generator specifications are minimum and maximum generation limits ($P_{\min}$, $P_{\max}$), the startup cost S_g, the operating cost $C(P)$ as a function of the generation level P and the ramping rate RR. The available (maximum) wind power generation is P_w and the load is P_D. The generators are initially assumed turned off and we are only interested in the first time period.

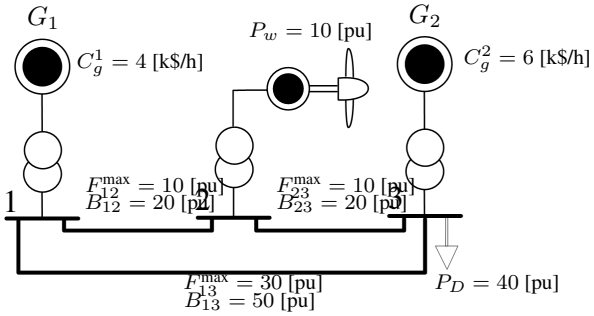

(d) Example 4. The system consists of three buses and three branches with susceptances B and capacities $F^{\max}$ as provided in the figure. The generator specifications are the marginal costs C_g, the maximum available wind production is P_w and the load is P_D.

Figure 6.1: Small examples to illustrate potential benefits of wind power spilling.

minimum 40MW of generator G_2, we need to use the expensive G_1, resulting in a 1100 \$/h cost of operation. If instead the output of the wind generator is adjusted at 20MW, G_1 can be used and the cost drops to 1000 \$/h.

Startup Costs

In example 2, if wind power is a must-take resource, it can fully satisfy demand for time period 2. A residual load of 20MW should be satisfied by conventional generation in periods 1 and 3. That, however, means that generator G_1 must restart at period 3 and the startup costs are incurred twice, leading to a total cost of 11000\$ for the three periods. If, instead, 20MW of wind are spilled during the second time period, G_1 can stay on and the total cost is now 8500\$. Note that this intuition could be extended for more time periods or for instances with more conventional generators.

Ramping Constraints

In example 3, the goal is to satisfy $N-1$ security. More specifically, if any of the generators fail, we should be able to recover the lost generation within the next time unit (an hour is used here, but a smaller time resolution could be considered). Generators G_1 and G_2 are identical and have a lower startup cost than generator G_3, however their ramping rates are limited to 60MW/h, whereas G_3 has a ramping rate of 100MW/h. In the case where no wind spill is allowed, utilizing only the cheap generators does not yield a feasible solution, since assuming they share the residual load of 130MW by generating 65MW each, the ramping capabilities of G_1 are not sufficient in case G_2 fails (in case they share the load unevenly, the same problem arises if the highest generating unit fails). So the costly generator G_3 needs to be utilized, leading to a total cost of $\$12900$. Now, if instead we dispatch the wind unit at 40MW, by spilling 10MW of wind power, we can satisfy the residual load of 140MW by evenly sharing between G_1 and G_2, i.e. 70MW each. In case G_2 suffers a fault, we can cover 60MW of its generation by G_1 and the remaining 10MW we can obtain by ramping up the wind generation to its available output. For that, we exploit the fact that wind turbine controls allow for very fast ramping. The second dispatch amounts to a lower cost of $\$11200$.

Congestion

Finally, in example 4, a DC optimal power flow problem is solved to illustrate how allowing for flexible wind dispatch may lead to a more economical allocation by alleviating congestion. In the case where the 10pu of wind power are treated as a must-take resource, in the optimum they all pass through branch $2-3$ to satisfy the load of bus 3, binding the phase angle difference between buses 2 and 3 as well. That means the flow of branch $2-3$ is at its capacity, so the flow on the line $1-2$ must be zero. Because of that, the phase of bus 1 has to equal that of bus 2 and that constrains the flow on line $1-3$ to 25pu. We observe that both line $1-2$ and line $1-3$ are not utilized close to their full capacity, whereas line $2-3$ is congested. Also, 5pu of the load is satisfied by the

expensive generator G_2, leading to a total cost of \$130000/h. If we instead dispatch wind at 8pu, we can satisfy the load without using the expensive generator, by generating 32pu with G_1 and the remaining 8pu through wind, leading to a lower total cost of \$128000/h. The flows are in this case $P_{12} = 2$pu, $P_{23} = 10$pu and $P_{13} = 30$pu, which also corresponds to a better utilization of the line capacities.

6.4 Model Outline

The examples of the previous section constitute favorable scenarios in which introducing flexible wind dispatch allows for a lower cost of operation, due to technical minima of conventional generation, efficient scheduling, ramping requirements or congestion. In order to make an argument for a more general case, however, we need to consider a large set of scenarios, generated based on a model of the underlying uncertainty of an actual system. For that purpose, the procedure depicted in figure 6.1 is adopted. The developed model comprises of two basic components, the Uncertainty Module and the the Optimization Module. The Uncertainty Module tries to capture the underlying uncertainty of the system, which in our case is assumed to come from wind generation and line or generator faults. The module is trained based on a data set and then used to generate scenarios whenever these are necessary. The Optimization Module, on the other hand, takes as input a set of scenarios and solves a stochastic unit commitment problem, providing in its output a commitment schedule of the slow generators for the next day. The Optimization Module can be treated as a black box that a system operator uses to make the day ahead scheduling based on a set of available scenarios. Furthermore, it has two settings; in the first setting the optimization treats wind generation as a must-take resource, whereas in the second setting wind generation is allowed to dispatch at lower levels.

Based on these modules, the testing process is the following: Initially, the Uncertainty Module generates a set of scenarios. These scenarios are treated as the uncertainty information the system operator utilizes to make the scheduling decision. Based on this information, the Optimization Module makes one scheduling decision for each of two cases: the one in which wind is a must-take resource, and the one that it is not. In the final step, we wish to evaluate the difference between the costs associated with each case. To that end, we generate a new set of scenarios from the Uncertainty Module, representing possible actual realizations of the uncertainty the next day, and compare the expected costs of each of the two cases (Test Optimal Commitment Block).

Uncertainty Module

The underlying uncertainty of the problem considered consists of three main components: the wind model, the power curve model and the reliability model. The purpose of the wind model is to generate synthetic wind speed time series with hourly resolution, representative of the wind sites under consideration. Subsequently, the power curve model takes as input the wind speed time series and outputs a wind power generation series for every wind site. Finally, the reliability model is a discrete (Bernoulli) distribution from where faults of lines and generators are drawn, as

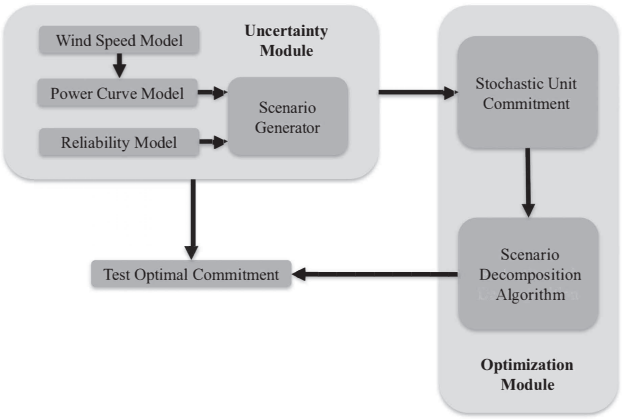

Figure 6.1: General model outline. The Uncertainty Module generates scenarios to be used as input for the Optimization Module, which defines an optimal commitment. It also generates a new set of scenarios to test this optimal commitment.

in [104]. Note the uncertainty model could be extended in a straightforward way to include load uncertainty as well, but in this work we do not consider it. This simplification is not unreasonable since the variability of load around its forecasted value is not as high as the variability of wind generation.

Wind Speed Model

This section describes the creation of a model that captures the characteristics of wind speed from multiple wind sites. The approach follows most basic steps from [83], which builds upon [103] and [96]. The input data used to train the model are wind speed measurements ξ_{gk}^{train}, where $g \in G_W$ indicates the different wind sites and $k \in \{1, 2, ... T_{\text{train}}\}$ indicates the T_{train} hourly measurements that are available at every wind location. The goal is to train a model based on these measurements and then use it to generate artificial wind series. The output of the process is a wind time series $\xi_{gts}^{\text{sample}}$ with $g \in G_W$ (for the various wind sites), $t \in T$ (for the desired time steps of the SUC problem), and $s \in S$ (different scenarios/samples used to capture the stochastic nature of the problem). The steps employed are divided in two phases; in the first one (Learning Phase) the model is trained using the time series data, whereas in the second one (Time Series Generation Phase) randomly generated wind time series to be used in a Monte Carlo simulation are created based on the model.

Learning Phase The learning phase aims to (approximately) transform the measurement data from the various locations to a set of independent Gaussian time series, whose characteristics will be captured using basic Auto-Regressive Moving Average (ARMA) models [15]. The following steps are employed.

*S*tep 1: Since the data wind time series is not necessarily stationary, we initially remove diurnal and seasonal effects to get a new (approximately) stationary time series $\tilde{\xi}_{gk}^{\text{train}}$.

$$\tilde{\xi}_{gk}^{\text{train}} = \frac{\xi_{gk}^{\text{train}} - \mu_{gmd}}{\sigma_{gmd}}\,, \tag{6.1}$$

where μ_{gmd} and σ_{gmd} are the mean and standard deviation respectively of the time series created by the samples ξ_{gk}^{train} that correspond to epoch m and hour of day $d \in \{1, 2, ... 24\}$ for wind site $g \in G_W$.

*S*tep 2: The stationary time series samples of the previous step do not necessarily follow a Gaussian distribution. Through a bijective mapping that employs the estimated non parametric Cumulative Distribution Function (CDF) $\hat{F}_g$ of the time series from Step 1 in site $g \in G_W$ and the inverse standard normal CDF Φ, the random samples $\tilde{\xi}_{gk}^{\text{train}}$ are mapped to samples $\hat{\xi}_{gk}^{\text{train}}$ drawn from the standard normal distribution, according to:

$$\hat{\xi}_{gk}^{\text{train}} = \Phi^{-1}(\hat{F}_g(\tilde{\xi}_{gk}^{\text{train}})) \tag{6.2}$$

*S*tep 3: The data $\hat{\xi}_{gk}^{\text{train}}$ are now assumed Gaussian stationary time series, but the time series between the different locations can still be correlated. For that reason, based on the ideas discussed in [83], the diagonalization of the symmetric $|G_W| \times |G_W|$ matrix $\boldsymbol{\Sigma}$, where $\boldsymbol{\Sigma}_{ij} = \sigma_{ij}^2$ are the sample covariances between the time series in two different locations i and j

$$\sigma_{ij}^2 = \frac{1}{T_{\text{train}}} \sum_{k=1}^{T_{\text{train}}} \hat{\xi}_{ik}^{\text{train}} \hat{\xi}_{jk}^{\text{train}}\,, \tag{6.3}$$

is employed $\boldsymbol{\Sigma} = \boldsymbol{U}\boldsymbol{D}\boldsymbol{U}^T$, where $\boldsymbol{D}$ diagonal and $\boldsymbol{U}$ orthogonal. The linear transformation induced by the matrix $\boldsymbol{U}^T$ will map the $|G_W|$ correlated Gaussian time series for every location to Γ uncorrelated ones (in our case $|G_W| = \Gamma$, however in the case of a large number of wind sites we may choose to only keep the $\Gamma < |G_W|$ most important eigenvalues and corresponding eigenvectors). Let $\{\hat{\boldsymbol{\Xi}}\}_{gk} = \hat{\xi}_{gk}^{\text{train}}$ be the matrix whose rows correspond to the correlated time series, then the rows of $\{\boldsymbol{\Omega}\}_{\gamma k} = \omega_{\gamma k}^{\text{train}}$, for $\gamma \in \{1, \ldots, \Gamma\}$ and $k \in \{1, \ldots, T_{\text{train}}\}$.

$$\boldsymbol{\Omega} = \boldsymbol{U}^T \hat{\boldsymbol{\Xi}} \tag{6.4}$$

will comprise of Γ time series that will be assumed independent.

*S*tep 4: For any fixed γ, the time series $\omega_{\gamma k}^{\text{train}}$ is modeled using a univariate ARMA(p,q) model, utilizing the Box–Jenkins method [15].

Time Series Generation Phase At this point the model for wind speed time series has been trained. The goal of the Time Series Generation Phase is to generate scenarios of synthetic wind time series $\xi_{gts}^{\text{sample}}$ based on this model. Each scenario $s \in S$ consists of T_H time samples $t \in T$ for every wind site $g \in G_W$. The following procedure is employed:

*S*tep 1: The first step of the process is to generate Γ time series $\omega_{\gamma ts}^{\text{sample}}$ for every scenario $s \in S$, based on the ARMA model of Step 4 of the Learning Phase.

*S*tep 2: The inverse transformation of (6.4), for every scenario $s \in S$, yields a time series $\hat{\xi}_{gts}^{\text{sample}}$ with $t \in T$, corresponding to each wind location $g \in G_W$.

*S*tep 3: The inverse transformation of (6.2) then yields a time series $\tilde{\xi}_{gts}^{\text{sample}}$ for every scenario and every wind site.

*S*tep 4: Finally based on the epoch and the time of day we want to simulate, the diurnal and seasonal effects are added back in, using the inverse of (6.1), to yield the final wind speed time series $\xi_{gts}^{\text{sample}}$ with $t \in T$, $s \in S$ and $g \in G_W$.

Power Curve Model

For every site of wind generation an aggregate power curve that will provide an estimate of the wind power generation given the wind speed needs to be constructed. For that purpose, wind data and the corresponding wind power generations are used to train a power curve model. The power generation data points come from an aggregation of multiple wind turbines in each site, with potentially different individual power curves and characteristics. Therefore, the use of the standard parametric power curve model of a single wind turbine to describe the wind speed and power relationship [93] would not be a satisfactory approximation and a data driven non-parametric fit is more suitable. The model should also be able to capture the nonlinear behavior of the power curves, that is dependent on the wind speed operating point. For the aforementioned reasons, a local polynomial regression scheme is proposed.

More specifically, for every fixed $g \in G_W$ the wind speed and wind power measurement data $\left(\xi_{gk}^{\text{train}}, P_{gk}^{\text{train}}\right)$, $k \in \{1, \ldots, T_{\text{train}}\}$ are sorted (based on the lexicographical ordering) in L_g wind speed intervals $[a_{gi}, b_{gi}]$, where $i \in \{1, 2, ...L_g\}$, with approximately equal number of measurements, represented by a central wind speed point c_{gi}.We locally approximate the power curve mapping for this site with a polynomial of degree p, i.e. $m_{gi}(x) \approx \beta_{gi0} + \beta_{gi1}(x - c_{gi}) + \beta_{gi2}(x - c_{gi})^2 + ... + \beta_{gip}(x - c_{gi})^p$. The coefficients $\beta_{gi0}, \ldots, \beta_{gip}$ are trained for each interval based on a weighted least squares problem, where the weights are kernel functions of the distance of a point from the center of its interval. After an initial fit is obtained, the procedure in [30] is adopted to ensure the fit is robust to outliers.

Following that process, we feed the wind speed samples $\xi_{gts}^{\text{sample}}$, obtained by the wind speed model, to the trained power curve model, to obtain available wind power samples P_{Wgts}, for $g \in G_W$, $t \in T$, $s \in S$:

$$P_{Wgts} = \sum_{i=1}^{L_g} m_{gi}(\xi_{gts}^{\text{sample}}) \mathbb{I}_{[a_{gi}, b_{gi}]}(\xi_{gts}^{\text{sample}}) \tag{6.5}$$

Optimization Module

Stochastic Unit Commitment

The generating units available to the system operator are divided into slow and fast, based on how long prior to operation a commitment decision for that unit has to be made. The output of the SUC problem is the commitment of slow generating units. The challenge is that the commitment decision for slow units has to be made a day before operation, when the underlying uncertainty is still unknown, i.e. the commitment decisions (binary variables) for these units have to be the same across all scenarios (first stage variables). On the other hand, the other variables of the problem, such as the commitment of fast generating units and the generation levels, are allowed to vary depending on which scenario of nature was realized (the decision for them is made with knowledge of the uncertainty), hence their value can be different for every scenario (second stage variables).

Our formulation is that of [104], adapted to explicitly model the flexibility of wind resources. The same methodology could be applied to determine the value of other types of renewable resources, such as solar, but the focus here is wind generation, so the model is built around that. The objective of the SUC problem is minimizing the expected, over the different scenarios, operational costs (startup, minimum load and fuel costs), as well as the highly penalized load shed variables. Wind generation is not associated with any fuel costs in the objective. The only modification of our formulation, compared to the one in [104], is that wind will be treated as a must-take resource when an additional parameter i_{allin} is set to 1. This is imposed through the (additional) constraints:

$$p_{gts} + p_{WS_{gts}} = P_{Wgts}, \forall g \in G_w, \forall t \in T, \forall s \in S, \tag{6.6a}$$

$$p_{WS_{gts}} \geq 0, \forall g \in G_w, \forall t \in T, \forall s \in S, \tag{6.6b}$$

$$p_{WS_{gts}} \leq (1 - i_{\text{allin}}) P_{Wgts}, \forall g \in G_w, \forall t \in T, \forall s \in S, \tag{6.6c}$$

where the wind spill $p_{WS_{gts}}$ is set to zero if $i_{\text{allin}} = 1$ (forcing the wind generation p_{gts} to equal the available generation P_{Wgts}), or optimized to a value between zero and the maximum available wind production P_{Wgts}, if $i_{\text{allin}} = 0$. Note, however, that the policy adopted by the operators when prioritizing wind generation is that they may still impose curtailments of wind generation, if the system feasibility is compromised. This corresponds to introducing constraint (6.6c) with a big-M penalty in the objective instead (which will lead to positive wind spill only in case enforcing (6.6c) as a hard constraint would cause infeasibility). The impact of the penalty is in that case subtracted from the objective cost reported, since the big-M has no physical meaning for the problem costs.

Note that the UC modeling standard in industry has slightly evolved from the model used in this work, so as to be able to cope with large scale systems. More specifically, tighter formulations of some constraints (such as ramping constraints [36]) are utilized, a modified set of variables has been offering improved computational performance by handling efficiently generator technical minima [97], whereas the shift factor formulation enhanced with lazy constraint evaluation has been noted to offer greater computational benefits (since the operators know which constraints are usually tight and need to be introduced) [142]. However, the qualitative and computational ideas conveyed in this work do not depend on the exact formulation.

Initialization Phase
$t \leftarrow 0, UB \leftarrow \infty, LB \leftarrow -\infty$, $w_s^t \leftarrow 0, \forall s \in S, W \leftarrow \emptyset$
Main Body
repeat
$t \leftarrow t + 1$,
Lower Bounding and Lagrangian Update Phase
Solve scenario subproblems:
for $s \in S$ **do**
$\boldsymbol{x}_s^t \in \underset{\boldsymbol{x} \in X \setminus W}{\operatorname{argmin}} \{ f_s(\boldsymbol{x}) + \boldsymbol{x}^T \boldsymbol{w}_s^{t-1} \}$
end for
Update Lower Bound:
LB $\leftarrow \sum_{s \in S} \pi_s f_s(\boldsymbol{x}_s^t)$
Update objective weights:
for $s \in S$ **do**
$\hat{\boldsymbol{x}}^t \leftarrow \sum_{s \in S} \pi_s \boldsymbol{x}_s^t$
$\boldsymbol{w}_s^t \leftarrow \boldsymbol{w}_s^{t-1} + \rho_t \left(\boldsymbol{x}_s^t - \hat{\boldsymbol{x}}^t \right)$
end for
Upper Bounding and Cut Phase
Evaluate scenario solutions for Upper Bounds:
for $s \in S$ **do**
$\text{UB}_s \leftarrow \sum_{i \in S} \pi_i f_i(\boldsymbol{x}_s^t)$
end for
Update Upper Bound:
UB $\leftarrow \min\{\text{UB}, \{\text{UB}_s\}_{s \in S}\}$
Exclude points tested:
for $s \in S$ **do**
$W \leftarrow W \cup \{\boldsymbol{x}_s^t\}$
end for
until $\frac{\text{UB} - \text{LB}}{\text{UB}} \leq$ eps

Figure 6.2: Decomposition scheme proposed in [4], adapted to solve the SUC problem. The Lower Bounding Phase involves solving smaller optimization problems than the original, since the scenario is fixed, whereas the Upper Bounding Phase involves smaller problems since the first stage and the scenario are fixed. As discussed in subsection 6.4, not both phases are necessarily executed at every iteration.

Scenario Decomposition Algorithm

Let f_s, for $s \in S$, be the set of (well defined) functions that, given the first stage variables, yield the optimal cost for the second stage. That is, each evaluation of $f_s(\boldsymbol{x})$ accounts for solving an optimization problem for scenario $s \in S$ and for first stage variable $\boldsymbol{x}$. Then, the SUC can be reformulated:

$$\text{minimize} \quad \sum_{s \in S} \pi_s f_s(\boldsymbol{x}) \tag{6.7}$$

The main body of the algorithm is divided into two phases, the Lower Bounding and Lagrangian Update Phase and the Upper Bounding Phase and Cut Phase. In the Lower Bounding Phase, we fix

every scenario $s \in S$ and solve for the optimal first stage decision given that scenario, over a space $X \setminus W$. This yields $|S|$ scenario specific solutions for the first stage variables $\boldsymbol{x}_s^t$ at iteration t. In the first iteration, the set W is empty and the penalty coefficients $\boldsymbol{w}_s^t$ are zero, so we are essentially solving $|S|$ scenario subproblems without any interaction, i.e. we are solving the initial problem after relaxing the non anticipativaty constraints. Since we are solving a relaxation, at least for the first iteration, we are guaranteed to get a lower bound on the optimal solution to (6.7). For the next iterations, it is still straightforward [56] to show we get lower bounds for (6.7) solved in the restrained space of first stage variables $X \setminus W$.

Following that, the objective value penalties w_s for every scenario $s \in S$ are updated. These penalties aim to drive the scenario solutions together. Intuitively this is achieved in the following way: say that $\boldsymbol{x}$ is just an one dimensional x and for some iteration t we have that the mean of the scenario specific solutions is $\hat{x}^t$. If for some scenario $s \in S$, the scenario specific solution x_s^t is away from the mean of the scenarios $\hat{x}^t$ (say $x_s^t = 0$ and $\hat{x}^t = 0.9$), we would like to penalize this deviation in the objective of the scenario subproblem the next time we iterate, at time $t+1$. So, at iteration $t+1$ a term $(x_s^t - \hat{x}^t)x$ will appear in the objective of scenario s, so that the new solution x of the scenario will be driven towards the mean of the scenarios (in the arithmetic example, the penalty in the objective would be $(0 - 0.9)x = -0.9x$ which will drive x to be 1 in the minimization, i.e. closer to the mean of the scenarios at the previous iteration).

In the Upper Bounding Phase of the algorithm, the $|S|$ scenario specific solutions for the first stage variables found during the previous phase are tested into the full problem. If feasible, each one of them yields an upper bound to (6.7). That way, we can possibly update the upper bound and the first stage solution that yields it. We then add the points $\{\boldsymbol{x}_s^t\}_{s \in S}$ in the set W. Our objective function value has already been calculated for all of these points, so we can exclude them from further consideration, except for the one that has yielded the best upper bound so far. That is, the execution of the Lower Bounding Phase for the next iteration should only consider points not in W. In practice, this is achieved by adding a global cut in the optimization problems solved in the first phase, for every point in W so as to cut off this particular point. More specifically, a "No-Good-Cut" is employed, i.e. a constraint of the form $\boldsymbol{x}^T(\mathbf{1} - \boldsymbol{x}_s^t) + (\mathbf{1} - \boldsymbol{x})^T \boldsymbol{x}_s^t \geq 1$, in order to cut off the point $\boldsymbol{x}_s^t$. The algorithm iterates until the Lower Bound (LB) and Upper Bound (UB) come close enough to satisfy the desired optimality guarantee (eps).

To get some technical intuition for the algorithm, let us note that the Lower Bounding phase is essentially a step in a projected subgradient ascend scheme for the dual of (6.7) in the reduced space $X \setminus W$, if the non-anticipativaty constraints are dualized. For a suitable choice of ρ_t as a function of time, repeated evaluations of that phase would converge to the dual optimum. However, the dual optimum could be quite smaller than the primal optimum, due to the existence of a non zero duality gap, so we may never reach our desired optimality guarantee. This is where the existence of the second phase of the algorithm becomes important: by expanding the set W, the duality gap between the primal in the space $X \setminus W$ and its dual becomes smaller and, due to the finiteness of X, we are guaranteed to eventually reach any predefined optimality guarantee threshold. In practice, the objective penalties of the first phase are more useful at the beginning of the algorithm, since they lead the scenario specific solutions towards the same point $\boldsymbol{x}$, while the global cuts are more useful after the first iterations, to reduce the optimality gap by cutting out points when the

Type	**U**nits	**C**apacity [MW]
Nuclear	2	4499
Gas	101	21781
Coal / Oil	3 /1	199 / 121
Dual Fuel	23	4679
Import	5	9931
Biomass	3	502
Geothermal	2	1073
Hydro	6	8613
Wind Low / Medium / High	5	1414 / 2121 / 2828

Table 6.1: Generator mix for the test system from [103, 106].

Wind Integration Level	Cost with/without load shed [$M]		Wind Integration [%]	
	Must Take	Wind Spill	Must Take	Wind Spill
Low	8.23/8.23	8.23/8.23	13.2	13.0
Medium	6.98/6.98	6.95/6.95	19.8	18.9
High	16.09/7.27	6.11/6.11	26.3	23.4

Table 6.2: SUC solution evaluated on the test set: Mean cost of operation (without accounting for load shed) and wind penetration (percentage of mean, over the scenarios, wind energy over mean total generated energy).

scenario solutions are similar to each other and the Lagrangian penalties do not offer significant improvements any more. So , the first phase of the algorithm is executed multiple times until a convergence indication is obtained. Following that, the second phase is executed and this process is repeated a few times.

6.5 Experimental Results

We consider a reduced model of the Western Electricity Coordinating Council (WECC) system [156] with 225 buses, 371 lines and 130 conventional generators. The same model is used in [103] and [106]. A typical winter weekday is simulated for three different integration cases: high, medium and low. High integration corresponds to 26% wind energy penetration, the medium integration corresponds to 19% penetration and the low integration to 13%. The average load is 28056MW, with a minimum of 21438MW and a maximum of 32300MW. The capacity of thermal generation is 31281MW and the total generating capacity, not including wind resources, is 51402MW. The cost of load shedding is assumed $5000/MW-h and twice this value is assigned to the big-M relaxation of (6.6c). The generation mix is shown in Table 6.1.

The uncertainty model is trained based on data taken from [104]. These correspond to yearly

Wind Integration Level	Wind Spill [%]		Load Shed [%]	
	Must Take	Wind Spill	Must Take	Wind Spill
Low	0	1.06	0	0
Medium	0	4.48	0	0
High	0.3	11.1	0.26	0

Table 6.3: SUC solution evaluated on the test set: Percentage of mean (over scenarios) wind spill over mean available generation and percentage of mean loadshed over the total load.

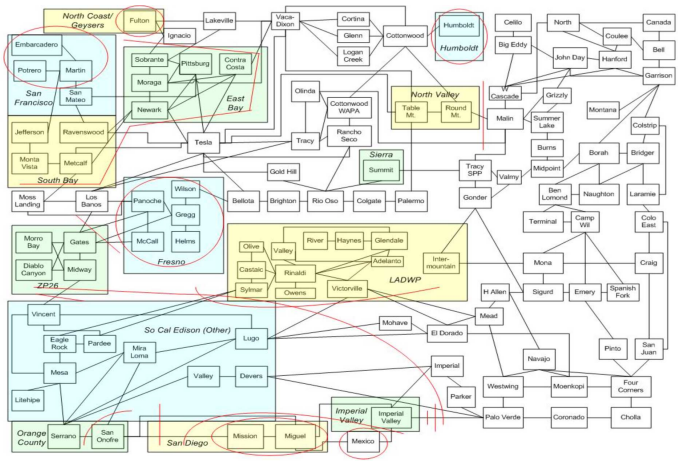

Figure 6.1: Map of the reduced 225 bus WECC system [156].

time series of wind speeds and wind power generations with hourly resolution for five aggregate wind sites. The initial source was 2006 wind production data from the National Renewable Energy Laboratory database. A discrete distribution is assumed for the reliability model, as in [103]. More specifically, a probability of generator failure of 1% and a probability of transmission line failure of 0.1% is assumed, independently.

All the computations are performed on the Cab cluster of the Lawrence Livermore National Laboratory. For the computations, Mosel 4.0.4 was used with Xpress [62]. Each excecution was parallelized in 10 nodes of the Cab cluster by utilizing the dedicated features of Mosel [32], allowing 4 threads per job and 4 jobs per node. The typical values used for ρ_t for the decomposition algorithm were $\rho_t \in [0.001, 0.01]$, where the objective costs were normalized in \$M. A 2% optimality guarantee was set as a stopping criterion for the algorithm.

A total of 160 scenarios was generated and used as an input to the SUC problem. These scenarios represent the model available to the operator in the day ahead, based on which the optimization problem that defines the first stage variables is solved. A new set of 160 scenarios is generated, representing the actual realization of the uncertainty the day ahead. We explore two alternative

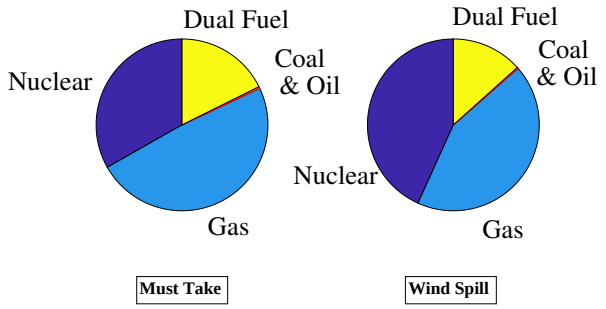

Figure 6.2: Breakdown of total energy generation from conventional sources for the two policies examined in the high integration case. Note that the increased flexibility introduced by the wind allows for a higher utilization of the cheap generation from nuclear power plants.

policies; one that allows for wind spill and one that assumes wind is a must-take resource, for the three integration cases. The evaluation of the two policies, each one yielding a different first stage solution, is based on how they perform with the unseen scenarios.

The typical computational performance of the algorithm was as follows. The Lower Bounding phase would be executed until the LB would not improve more than 0.05% for two iterations. Note that, since the dual function is non-differentiable, there is no guarantee that the subgradient will yield a descent direction, so this stopping criterion is merely a heuristic. Typically, the lower bounding phase would terminate within at most 10-15 iterations. After that, the upper bounding phase would start by evaluating the function for the points that correspond to the best LB obtained. This process would be repeated typically $2-3$ times to obtain the desired optimality guarantee. It is important to note that, while the algorithm offers guaranteed convergence to any required precision (as oposed to subgradient optimization schemes), it has a significant disadvantage for applications that prioritize speed instead of accuracy. The Lower Bounding phase essentially has to solve multiple subgradient optimization problems and the Upper Bounding phase needs to evaluate the objective for $|S|$ points (which can be decomposed to solving $|S|^2$ smaller mixed integer programs). The typical execution time was in the order of $1-2$ hours, which is above the state-of-the art times reported in literature [7].

Tables 6.2 and 6.3 show the policy testing results. The fuel cost without load shedding is also provided. We observe that in the case of low and medium wind integration, wind spilling does not result in a significant benefit. However, for high wind integration, the cost of operation is significantly lower when wind spill is allowed and load shed does not happen, whereas demanding the wind energy to be fully integrated leads to both an inefficient dispatch (high fuel costs) and an increased load shedding.

In figure 6.2, the reason of the more economical dispatch can be seen: the extra flexibility enabled by optimizing the wind output allows for a higher utilization of the cheap nuclear plants.

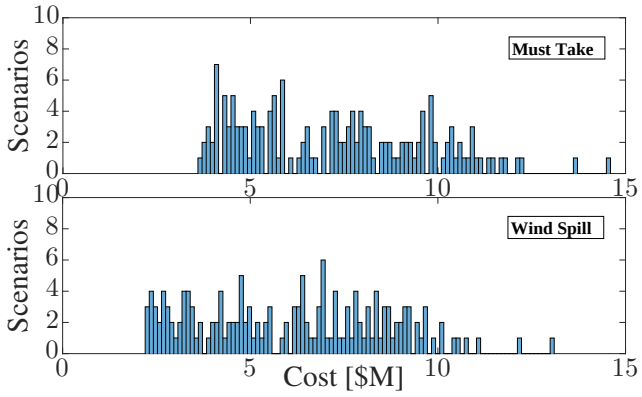

Figure 6.3: Histogram for the scenarios of stochastic unit commitment for the two policies in the high integration case. The variance of the scenario costs remains approximately the same (approximately equal to 6) for both policies, but the scenarios are spread around a lower mean for the wind spill case.

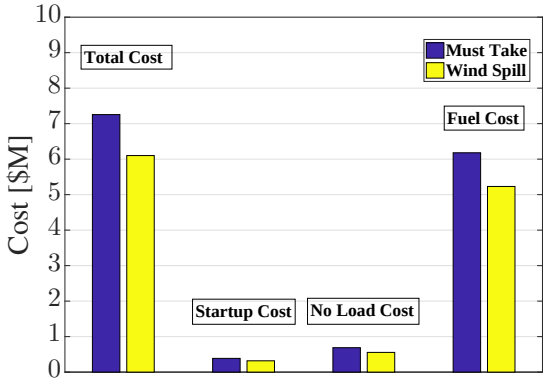

Figure 6.4: Comparison of the total cost, startup cost, no load cost and fuel cost for the two policies in the high integration case. Note that the bulk savings are obtained from the lower fuel costs due to the higher nuclear utilization.

Figure 6.3 shows the empirical distribution of the costs for the different scenarios of the stochastic unit commitment in the high integration case for the two policies. Finally, figure 6.4 shows the cost breakdown in the high integration case.

6.6 Conclusions

The main objective of this work is to convey that wind resources, and renewables in general, should be treated, to the extent possible, as any other resource for the unit commitment problem. Renewable integration is vital to achieve environmental goals, but it often competes with ensuring the secure and reliable operation of the grid due to the variability and stochasticity of the available

wind power. However, current wind turbines are capable to control their output power setpoint within the limits allowed by wind availability. By exploiting this capability a safer and more economic grid operation can be ensured.

In order to explicitly exploit the extent of controllability of wind generation, a stochastic unit commitment approach is employed to determine the dispatch of wind generation for a number of possible scenarios. Two cases, one in which wind is treated as a must-take resource and one that the wind output setpoint is also optimized, are considered for three integration scenarios in a reduced California test case. A clear benefit for the second strategy is obtained only in the high integration case.

At this point it is important to repeat with a critical view some of the assumptions of the current study, to initiate discussion and motivate a set of questions for future research. Firstly, the unit commitment problem as we formulated it did not include an objective term for the reduction of emissions. Including such a term would of course reduce the wind spilling benefits. However, the weight of such a term is at this point not as objective and universal as the operational costs of conventional generators and its value is still a source of debate, so for that reason it was omitted. Various study cases could of course extend our current results for the existence of such a term. Secondly, the results are based on a reduced system developed based on an earlier version of the WECC system. For that reason, we cannot claim that the results could generalize in a similar fashion for the full system as is, however the system used still provides a useful test case and most of the logic that was described could carry on. Thirdly, a major contributing factor in wind shedding is congestion. One could argue that if renewable generation integration increases, then the transmission system will also be enhanced to accommodate for it. However, changing the existing transmission system is accompanied by extra costs and the benefit from that could only be to accommodate some rare instances for which spilling some wind generation could also relieve the stress for the system. Since the focus at this point is not planning and investment on the transmission system, enhancements to it are not considered.

Finally, one could question the usefulness of solving the SUC problem at high precision. After all, the number of necessary scenarios to solve is not specified, and the error in capturing uncertainty could very well be higher than the precision level of the solution. However, at this point the plain UC problem is solved with very high precision every day since there are economic implications of these solutions. For example, NYISO eventually solves the UC problem at $\$200$ precision, and even though the solution they get is not necessarily the optimal for the problem they are solving, the heuristics and refinements they use (such as gradually fixing binary variables) are standardized to provide a high precision approximation. This kind of precision is necessary since commitment of small gas units, for example, depends on it and perturbations could lead to very different commitments. So, if the way to generate scenarios is precisely modeled and standardized, these levels of precision are indeed necessary in solving the SUC problem as well.

Regarding policy implications of adopting the proposed strategy, active wind spilling based on market operations can allow for a more efficient allocation (increased total welfare for the society), which could translate to benefits for the customers (in the form of reduced bills). The conventional generators will also be benefited, since they will not be the ones to fully carry the burden from renewable integration. In the current form of the SUC objective, clean energy generation will

be diminished. However, introducing a price for carbon in the objective that reflects economic welfare would resolve the problem; until such a price is set any economic comparison of the tradeoffs between clean energy and economic dispatch is by default hard anyway. Furthermore, since wind generation will be decreased, investments on wind resources may be discouraged. If this is found to be the case, an initial lump transfer investment incentive could be a preferred way to deal with it than actively introducing frequent economic inefficiencies in the day ahead markets or than compensating the wind generators for their spilled energy (unless this is committed as a reserve).

Chapter 7

Future Research Directions

7.1 Abstract

Throughout the completion of this dissertation, there were many times where future research directions opened up but were not explored, either because they were out of the scope of the ongoing research, or not within the interests of the funding source, or simply due to a shortage of time. We devote this short chapter to briefly state such directions.

7.2 Black Start Allocation

Ac Power Flows

During the restoration of the power system, the system operates under extreme conditions, outside the normal region of operation. Considerations such as reactive power compensation and the Ferranti effect become important. On top of that, common convex relaxations are often unsuitable, since they lead to fictitious reactive power compensation [8], when reactive power is exactly one of the most important modeling concerns. For the restoration problem around known black starts, we made an effort to handle the complexity of the ac problem with a detailed approximation of the ac power flows in [9].

When the problem is the black start allocation (BSA) on the grid instead, the characteristics of the generators and the positions of them in the underlying graph of the system become more important, which is why simplified power models can give satisfactory allocation results (even if the resulting restoration sequences found by the optimization need some modifications to become ac feasible). For example, as described in chapter 2, using the simplified model presented, we were still able to extract ac feasible restoration sequences by slightly modifying the optimization output. Of course, the ideal scenario would be to incorporate a detailed power formulation within the BSA framework. Since switching variables are also associated with the branches, an ac transmission switching model is necessary.

Ideas from [9] can be used in the BSA case as well, but the fact that the positions of black start generators are not fixed will lead to an additional number of cuts since the restoration now can potentially expand around any node with a generator. Another practical approach would be to find a black start allocation using a simplified model and then fix the black start units to solve a simpler restoration problem. If the resulting restoration plan is not acceptable, we can resolve the original simplified problem excluding the allocation obtained (for example, by using a "No-Good-Cut" as in chapter 4). In any case, a successful approach will most likely utilize a number of computational techniques to reach an acceptable solution and would be an interesting research direction.

Heuristics

It has been relatively clear to us after working with black start models that (at least using our formulations of the problem) commercial solvers are struggling to find feasible solutions to them. This is also described in chapter 2. Even using the heuristics developed, the resulting solutions obtained are often not very close to optimality (at least, that was observed for the smaller systems which we can actually solve to 1% optimality). On the contrary, after applying the strengthening described in chapter 3, fairly good relaxation bounds are usually obtained for these problems. This essentially hints that in order to further improve the computational behavior of the problem, the bulk of further work should focus on heuristics, especially for cases where the solver can not improve on the feasible MIP starts (such as for the case of the 2000 bus Texas system of chapter 3). In this dissertation we mainly use heuristics to obtain MIP starts and initialize the optimization. However, system aware local heuristics, or rounding heuristics after solving the linear programming relaxation of a node can also be implemented and used to potentially improve the performance.

Towards Scalable Stochastic Black Start Allocation

Chapter 4 introduced a model for stochastic black start allocation. Uncertainty in this model was due to the different possible outages or due to possible unavailability of components. There are multiple extensions to this model. Uncertainty due to renewable sources can be included, even though the current practice at least in California is to disconnect renewables after a blackout. Furthermore, the partial outage scenarios were randomly generated. A more elaborate study could generate scenarios based on historical outages, earthquake or fire data, or some other causes of blackouts. Finally, our model was simplified and implemented only for a small scale system as a proof of concept - the resulting optimization was still intractable without the decomposition employed. Large scale systems will require additional work for solving the subproblems - specifically, heuristics should to be used to obtain feasible black start allocation solutions for the case where the initial outage state is treated as an input. This can lead to an extension of the heuristic described in chapter 2.

Formulation Improvements

The improved formulations used for BSA in chapter 3 seemed to already provide fairly tight bounds, so we decided not to attempt further formulation improvements at that point. However, the connection to the rooted maximum weight independent subgraph problem from the literature discussed in chapter 3 might yield additional formulation and computational improvements. We discovered this connection relatively late during this particular project, so we did not fully utilize the breadth of existing work in graph theory. The theoretical and computational research for this and a few related problems is presented in section 3.9. A few constraints from the literature may be adaptable to our problem and yield bound improvements, such as the inequalities of [12].

In addition, the formulations used in chapter 3 include only simplified versions of the active and reactive power requirement. These simplifications are made in papers that attempt to solve a centralized black start allocation problem over a restoration time horizon in the literature, in order to obtain tractable models (as discussed in chapter 3). Using a more detailed model (such as the one we considered in chapter 2) may give rise to further formulation improvements we have not explored. We should also note that, even though the comparative strength of the formulations holds in every case, the actual performance of different formulations in practice also depends on the objective used - so in a power system where different restoration priorities impose a different objective than the one we considered in chapter 3, the comparative behavior of the different formulations may change and different sets of valid inequalities may become important.

Microgrids

One final future direction we would still wish to pursue is to see if we can extend our algorithmic approaches to provide grid resiliency services by microgrids, as in [127]. This would include allocating microgrids or hybrid (renewable and storage) systems as black start resources. The current guidance (at least in California) is that microgrids or hybrid installations are not used for restoration. However, as increasingly many such systems with significant capacity and often storage capabilities get introduced into the power grid, using them could provide a partial, cost efficient restoration solution.

7.3 Flexible Wind Dispatch

Carbon Impact

While we observed an economic benefit from curtailing wind generation in the computations of chapter 6, the study of that chapter did not take into account the carbon footprint that this curtailment implies. Of course, the actual dollar value of that quantity is not something the scientific community unanimously agrees on. However, estimates for the environmental cost of carbon do exist and an additional analysis on how much the results change when a carbon penalty is included in the objective would be interesting.

Test Systems

The computations of chapter 6 can also be extended in two important ways, as far as the test systems are concerned. First, policy decisions must be evaluated on the actual system they will be applied to. The benefits from wind curtailment will highly depend on the generation mix, the existing grid flexibility, the positions of renewable generation, and the graph structure. Therefore, a different conclusion may be drawn for a different system. Secondly, the system used may vary with different renewable integration scenarios as well as with the policy used (must take vs flexible wind integration). More precisely, high renewable integration scenarios may also be combined with grid enhancements (such as upgrades of line capacities) to alleviate congestion. These grid enhancements may not be as drastic if wind curtailment policies are in place. Since grid enhancement is also associated with costs, a combined study could be performed to evaluate the benefit from allowing wind curtailment.

Bibliography

[1] Flexible resources help renewables. California ISO, 2016.

[2] Curtailment fast facts. California ISO, 2017.

[3] M. Adibi, R. Kafka, S. Maram, and L. M. Mili. On power system controlled separation. *IEEE Transactions on Power Systems*, 21(4):1894–1902, 2006.

[4] S. Ahmed. A scenario decomposition algorithm for 0–1 stochastic programs. *Operations Research Letters*, 41(6):565–569, 2013.

[5] E. Álvarez-Miranda, I. Ljubić, and P. Mutzel. The maximum weight connected subgraph problem. In *Facets of Combinatorial Optimization*, pages 245–270. Springer, 2013.

[6] E. Álvarez-Miranda, I. Ljubić, and P. Mutzel. The rooted maximum node-weight connected subgraph problem. In *International Conference on AI and OR Techniques in Constriant Programming for Combinatorial Optimization Problems*, pages 300–315. Springer, 2013.

[7] I. Aravena and A. Papavasiliou. An asynchronous distributed algorithm for solving stochastic unit commitment. Technical report, Université catholique de Louvain, Center for Operations Research and Econometrics (CORE), 2016.

[8] I. Aravena, D. Rajan, and G. Patsakis. Mixed-integer linear approximations of ac power flow equations for systems under abnormal operating conditions. In *Power and Energy Society General Meeting (PES), 2018 IEEE*. IEEE.

[9] I. Aravena, D. Rajan, G. Patsakis, and S. Oren. A scalable mixed-integer decomposition approach for optimal power system restoration. Technical report, Optimization Online, 2019.

[10] A. Atamturk and V. Narayanan. Submodular function minimization and polarity. *arXiv preprint arXiv:1912.13238*, 2019.

[11] T. Athay, R. Podmore, and S. Virmani. A practical method for the direct analysis of transient stability. *IEEE Transactions on Power Apparatus and Systems*, (2):573–584, 1979.

[12] M. D. Biha, H. L. Kerivin, and P. H. Ng. Polyhedral study of the connected subgraph problem. *Discrete Mathematics*, 338(1):80–92, 2015.

[13] A. B. Birchfield, T. Xu, K. M. Gegner, K. S. Shetye, and T. J. Overbye. Grid structural characteristics as validation criteria for synthetic networks. *IEEE Transactions on power systems*, 32(4):3258–3265, 2016.

[14] L. Bird, J. Cochran, and X. Wang. Wind and solar energy curtailment: experience and practices in the united states. *US National Renewable Energy Laboratory, NREL/TP-6A20-60983*, page 3, 2014.

[15] G. E. Box, G. M. Jenkins, G. C. Reinsel, and G. M. Ljung. *Time series analysis: forecasting and control*. John Wiley & Sons, 2015.

[16] S. Boyd, S. P. Boyd, and L. Vandenberghe. *Convex optimization*. Cambridge university press, 2004.

[17] D. J. Burke and M. J. O'Malley. Factors influencing wind energy curtailment. *IEEE Transactions on Sustainable Energy*, 2(2):185–193, 2011.

[18] California ISO. Black start and system restoration Phase 2. `https://www.caiso.com/informed/Pages/StakeholderProcesses/Blackstart_SystemRestorationPhase2.aspx`, 2017. [Online; accessed Aug-2017].

[19] P. Carpentier, G. Gohen, J.-C. Culioli, and A. Renaud. Stochastic optimization of unit commitment: a new decomposition framework. *IEEE Transactions on Power Systems*, 11(2):1067–1073, 1996.

[20] M. Carrión and J. M. Arroyo. A computationally efficient mixed-integer linear formulation for the thermal unit commitment problem. *IEEE Transactions on Power Systems*, 21(3):1371–1378, 2006.

[21] R. Carvajal, M. Constantino, M. Goycoolea, J. P. Vielma, and A. Weintraub. Imposing connectivity constraints in forest planning models. *Operations Research*, 61(4):824–836, 2013.

[22] A. Castillo. Microgrid provision of blackstart in disaster recovery for power system restoration. In *Smart Grid Communications, 2013 IEEE International Conference on*, pages 534–539. IEEE, 2013.

[23] A. Castillo. Risk analysis and management in power outage and restoration: A literature survey. *Electric Power Systems Research*, 107:9–15, 2014.

[24] B. Chen, C. Chen, J. Wang, and K. L. Butler-Purry. Sequential service restoration for unbalanced distribution systems and microgrids. *IEEE Transactions on Power Systems*, 33(2):1507–1520, 2018.

[25] C. Chen, J. Wang, F. Qiu, and D. Zhao. Resilient distribution system by microgrids formation after natural disasters. *IEEE Transactions on smart grid*, 7(2):958–966, 2016.

[26] K. Cheung, D. Gade, C. Silva-Monroy, S. M. Ryan, J.-P. Watson, R. J.-B. Wets, and D. L. Woodruff. Toward scalable stochastic unit commitment. *Energy Systems*, 6(3):417–438, 2015.

[27] Y.-T. Chou, C.-W. Liu, Y.-J. Wang, C.-C. Wu, and C.-C. Lin. Development of a black start decision supporting system for isolated power systems. *IEEE Transactions on Power Systems*, 28(3):2202–2210, 2013.

[28] J. H. Chow. *Time-scale modeling of dynamic networks with applications to power systems*, volume 46. Springer-Verlag, 1982.

[29] J. H. Chow. *Power system coherency and model reduction*. Springer, 2013.

[30] W. S. Cleveland. Robust locally weighted regression and smoothing scatterplots. *Journal of the American statistical association*, 74(368):829–836, 1979.

[31] C. Coffrin and P. Van Hentenryck. Transmission system restoration with co-optimization of repairs, load pickups, and generation dispatch. *International Journal of Electrical Power & Energy Systems*, 72:144–154, 2015.

[32] Y. Colombani and S. Heipcke. Multiple models and parallel solving with Mosel, February 2014. *Avalaible at: http://community. fico. com/docs/DOC-1141*.

[33] M. Conforti, G. Cornuéjols, G. Zambelli, et al. *Integer programming*, volume 271. Springer, 2014.

[34] E. Cotilla-Sanchez, P. D. Hines, C. Barrows, S. Blumsack, and M. Patel. Multi-attribute partitioning of power networks based on electrical distance. *IEEE Transactions on Power Systems*, 28(4):4979–4987, 2013.

[35] G. Csardi, T. Nepusz, et al. The igraph software package for complex network research. *InterJournal, complex systems*, 1695(5):1–9, 2006.

[36] P. Damcı-Kurt, S. Küçükyavuz, D. Rajan, and A. Atamtürk. A polyhedral study of production ramping. *Mathematical Programming*, 158(1-2):175–205, 2016.

[37] J. Deane, G. Drayton, and B. Ó. Gallachóir. The impact of sub-hourly modelling in power systems with significant levels of renewable generation. *Applied Energy*, 113:152–158, 2014.

[38] P. Demetriou, M. Asprou, and E. Kyriakides. A real-time controlled islanding and restoration scheme based on estimated states. *IEEE Transactions on Power Systems*, 2018.

[39] L. Deng, B. F. Hobbs, and P. Renson. What is the cost of negative bidding by wind? a unit commitment analysis of cost and emissions. *IEEE Transactions on Power Systems*, 30(4):1805–1814, 2015.

[40] B. Dilkina and C. P. Gomes. Solving connected subgraph problems in wildlife conservation. In *International Conference on Integration of Artificial Intelligence (AI) and Operations Research (OR) Techniques in Constraint Programming*, pages 102–116. Springer, 2010.

[41] L. Ding, F. M. Gonzalez-Longatt, P. Wall, and V. Terzija. Two-step spectral clustering controlled islanding algorithm. *IEEE Transactions on Power Systems*, 28(1):75–84, 2013.

[42] L. Ding, Z. Ma, P. Wall, and V. Terzija. Graph spectra based controlled islanding for low inertia power systems. *IEEE Transactions on Power Delivery*, 32(1):302–309, 2017.

[43] T. Ding, K. Sun, C. Huang, Z. Bie, and F. Li. Mixed-integer linear programming-based splitting strategies for power system islanding operation considering network connectivity. *IEEE Systems Journal*, 2015.

[44] T. Ding, K. Sun, Q. Yang, A. W. Khan, and Z. Bie. Mixed integer second order cone relaxation with dynamic simulation for proper power system islanding operations. *IEEE Journal on Emerging and Selected Topics in Circuits and Systems*, 7(2):295–306, 2017.

[45] M. T. Dittrich, G. W. Klau, A. Rosenwald, T. Dandekar, and T. Müller. Identifying functional modules in protein–protein interaction networks: an integrated exact approach. *Bioinformatics*, 24(13):i223–i231, 2008.

[46] F. Dörfler and F. Bullo. Kron reduction of graphs with applications to electrical networks. *IEEE Trans. on Circuits and Systems*, 60(1):150–163, 2013.

[47] E. Ela and D. Edelson. Participation of wind power in lmp-based energy markets. *IEEE Transactions on Sustainable Energy*, 3(4):777–783, 2012.

[48] A. Esmaeilian and M. Kezunovic. Prevention of power grid blackouts using intentional islanding scheme. *IEEE transactions on industry applications*, 53(1):622–629, 2017.

[49] European Union. Directive 2009/28/ec of the european parliament and of the council of 23 april 2009 on the promotion of the use of energy from renewable sources and amending and subsequently repealing directives 2001/77/ec and 2003/30/ec. *Official Journal of the European Union*, 5:2009, 2009.

[50] N. Fan, D. Izraelevitz, F. Pan, P. M. Pardalos, and J. Wang. A mixed integer programming approach for optimal power grid intentional islanding. *Energy Systems*, 3(1):77–93, 2012.

[51] S. Fattahi, M. Ashraphijuo, J. Lavaei, and A. Atamtürk. Conic relaxations of the unit commitment problem. *Energy*, 134:1079–1095, 2017.

[52] Federal Energy Regulatory Commission. Grid Reliability and Resilience Pricing Docket Nos. RM18-1-000, Grid Resilience in Regional Transmission Organizations and Independent System Operators AD18-7-000. Technical report, 2018.

[53] S. Fink, C. Mudd, K. Porter, and B. Morgenstern. Wind energy curtailment case studies. *NREL subcontract report, NREL/SR-550*, 46716, 2009.

[54] N. Fountas, N. Hatziargyriou, C. Orfanogiannis, and A. Tasoulis. Interactive long-term simulation for power system restoration planning. *IEEE Transactions on Power Systems*, 12(1):61–68, 1997.

[55] F. Friend. Cold load pickup issues. In *Protective Relay Engineers, 2009 62nd Annual Conference for*, pages 176–187. IEEE, 2009.

[56] D. Gade, G. Hackebeil, S. M. Ryan, J.-P. Watson, R. J.-B. Wets, and D. L. Woodruff. Obtaining lower bounds from the progressive hedging algorithm for stochastic mixed-integer programs. *Mathematical Programming*, 157(1):47–67, 2016.

[57] A. Gholami and F. Aminifar. A hierarchical response-based approach to the load restoration problem. *IEEE Transactions on Smart Grid*, 8(4):1700–1709, 2017.

[58] M. Golari, N. Fan, and J. Wang. Two-stage stochastic optimal islanding operations under severe multiple contingencies in power grids. *Electric Power Systems Research*, 114:68–77, 2014.

[59] M. Golari, N. Fan, and J. Wang. Large-scale stochastic power grid islanding operations by line switching and controlled load shedding. *Energy Systems*, 8(3):601–621, 2017.

[60] R. Golden and B. Paulos. Curtailment of renewable energy in california and beyond. *The Electricity Journal*, 28(6):36–50, 2015.

[61] A. Golshani, W. Sun, Q. Zhou, Q. P. Zheng, and Y. Hou. Incorporating wind energy in power system restoration planning. *IEEE Transactions on Smart Grid*, 2017.

[62] C. Guéret, C. Prins, and M. Sevaux. Applications of optimization with Xpress-MP. *contract*, page 00034, 1999.

[63] M. Haouari, S. B. Layeb, and H. D. Sherali. Tight compact models and comparative analysis for the prize collecting Steiner tree problem. *Discrete Applied Mathematics*, 161(4-5):618–632, 2013.

[64] M. Hedayati-Mehdiabadi, K. W. Hedman, and J. Zhang. Reserve policy optimization for scheduling wind energy and reserve. *IEEE Transactions on Power Systems*, 33(1):19–31, 2018.

[65] M. Hedayati-Mehdiabadi, J. Zhang, and K. W. Hedman. Wind power dispatch margin for flexible energy and reserve scheduling with increased wind generation. *IEEE Transactions on Sustainable Energy*, 6(4):1543–1552, 2015.

[66] K. W. Hedman, R. P. O'Neill, E. B. Fisher, and S. S. Oren. Optimal transmission switching with contingency analysis. *IEEE Transactions on Power Systems*, 24(3):1577–1586, 2009.

[67] H. Heitsch and W. Römisch. A note on scenario reduction for two-stage stochastic programs. *Operations Research Letters*, 35(6):731–738, 2007.

[68] D. Hochbaum. Polynomial time algorithms for ratio regions and a variant of normalized cut. *IEEE Transactions on pattern analysis and machine intelligence*, 32(5):889–898, 2010.

[69] D. S. Hochbaum. The pseudoflow algorithm: A new algorithm for the maximum-flow problem. *Operations research*, 56(4):992–1009, 2008.

[70] D. S. Hochbaum. A polynomial time algorithm for Rayleigh ratio on discrete variables: Replacing spectral techniques for expander ratio, normalized cut, and cheeger constant. *Operations Research*, 61(1):184–198, 2013.

[71] Y. Hou, C. C. Liu, K. Sun, P. Zhang, S. Liu, and D. Mizumura. Computation of milestones for decision support during system restoration. *IEEE Transactions on Power Systems*, 26(3):1399–1409, Aug 2011.

[72] Y. Hou, C.-C. Liu, K. Sun, P. Zhang, S. Liu, and D. Mizumura. Computation of milestones for decision support during system restoration. In *Power and Energy Society General Meeting, 2011 IEEE*, pages 1–10. IEEE, 2011.

[73] ISO New England. Schedule 16 - Blackstart standard rate report. `https://www.iso-ne.com/isoexpress/web/reports/billing/-/tree/schedule-16---blackstart-standard-rate-report`, 2016. [Online; accessed Aug-2017].

[74] Y. Jiang, S. Chen, C.-C. Liu, W. Sun, X. Luo, S. Liu, N. Bhatt, S. Uppalapati, and D. Forcum. Blackstart capability planning for power system restoration. *International Journal of Electrical Power & Energy Systems*, 86:127–137, 2017.

[75] R. Kafka. Review of PJM restoration practices and NERC restoration standards. In *Power and Energy Society General Meeting-Conversion and Delivery of Electrical Energy in the 21st Century, 2008 IEEE*, pages 1–5. IEEE, 2008.

[76] L. Kane and G. W. Ault. Evaluation of wind power curtailment in active network management schemes. *IEEE Transactions on Power Systems*, 30(2):672–679, 2015.

[77] M. E. Khodayar, M. Shahidehpour, and L. Wu. Enhancing the dispatchability of variable wind generation by coordination with pumped-storage hydro units in stochastic power systems. *IEEE Transactions on Power Systems*, 28(3):2808–2818, 2013.

[78] K. Kim and V. M. Zavala. Algorithmic innovations and software for the dual decomposition method applied to stochastic mixed-integer programs. *Mathematical Programming Computation*, pages 1–42, 2017.

[79] S. Koch, S. Chatzivasileiadis, M. Vrakopoulou, and G. Andersson. Mitigation of cascading failures by real-time controlled islanding and graceful load shedding. In *Bulk Power System Dynamics and Control (iREP)-VIII (iREP), 2010 iREP Symposium*, pages 1–19. IEEE, 2010.

[80] P. V. Kokotovic, B. Avramovic, J. H. Chow, and J. R. Winkelman. Coherency based decomposition and aggregation. *Automatica*, 18(1):47–56, 1982.

[81] A. Kyriacou, P. Demetriou, C. Panayiotou, and E. Kyriakides. Controlled islanding solution for large-scale power systems. *IEEE Transactions on Power Systems*, 33(2):1591–1602, 2018.

[82] A. Kyriacou, S. Timotheou, M. P. Michaelides, C. Panayiotou, and M. Polycarpou. Partitioning of intelligent buildings for distributed contaminant detection and isolation. *IEEE Transactions on Emerging Topics in Computational Intelligence*, 1(2):72–86, 2017.

[83] D. D. Le, G. Gross, and A. Berizzi. Probabilistic modeling of multisite wind farm production for scenario-based applications. *Sustainable Energy, IEEE Transactions on*, 6(3):748–758, 2015.

[84] H. F. Lee and D. R. Dooly. Decomposition algorithms for the maximum-weight connected graph problem. *Naval Research Logistics (NRL)*, 45(8):817–837, 1998.

[85] R. M. Lee, M. J. Assante, and T. Conway. Analysis of the cyber attack on the Ukrainian power grid. *SANS Industrial Control Systems*, 2016.

[86] J. Li, C.-C. Liu, and K. P. Schneider. Controlled partitioning of a power network considering real and reactive power balance. *IEEE Transactions on Smart grid*, 1(3):261–269, 2010.

[87] S. Liao, W. Yao, X. Han, J. Wen, and Y. Hou. Two-stage optimization method for network reconfiguration and load recovery during power system restoration. In *Power & Energy Society General Meeting, 2015 IEEE*, pages 1–5. IEEE, 2015.

[88] S. Liu. Phase I.A. Stochastic study testimony of Dr. Shucheng Liu on behalf of the California Independent System Operator Corporation, 11 2014.

[89] S. Liu, Y. Hou, C.-C. Liu, and R. Podmore. The healing touch: Tools and challenges for smart grid restoration. *IEEE power and energy magazine*, 12(1):54–63, 2014.

[90] S. Liu, R. Podmore, and Y. Hou. System restoration navigator: A decision support tool for system restoration. In *Power and Energy Society General Meeting, 2012 IEEE*, pages 1–5. IEEE, 2012.

[91] W. Liu, Z. Lin, F. Wen, and G. Ledwich. A wide area monitoring system based load restoration method. *IEEE Transactions on Power Systems*, 28(2):2025–2034, 2013.

[92] Z. Liu, A. Clark, P. Lee, L. Bushnell, D. Kirschen, and R. Poovendran. A submodular optimization approach to controlled islanding under cascading failure. In *Proceedings of the 8th International Conference on Cyber-Physical Systems*, pages 187–196. ACM, 2017.

[93] M. Lydia, S. S. Kumar, A. I. Selvakumar, and G. E. P. Kumar. A comprehensive review on wind turbine power curve modeling techniques. *Renewable and Sustainable Energy Reviews*, 30:452–460, 2014.

[94] K. Meeusen. Phase I.A. Stochastic study testimony of Dr. Karl Meeusen on behalf of the California Independent System Operator Corporation, 11 2014.

[95] J. Minkel. The 2003 Northeast Blackout–Five Years Later. *Scientific American*, 13, 2008.

[96] J. M. Morales, R. Minguez, and A. J. Conejo. A methodology to generate statistically dependent wind speed scenarios. *Applied Energy*, 87(3):843–855, 2010.

[97] G. Morales-España, J. M. Latorre, and A. Ramos. Tight and compact milp formulation for the thermal unit commitment problem. *IEEE Transactions on Power Systems*, 28(4):4897–4908, 2013.

[98] P. Moutis, S. A. Papathanassiou, and N. D. Hatziargyriou. Improved load-frequency control contribution of variable speed variable pitch wind generators. *Renewable Energy*, 48:514–523, 2012.

[99] S. I. Nanou, G. N. Patsakis, and S. A. Papathanassiou. Assessment of communication-independent grid code compatibility solutions for VSC–HVDC connected offshore wind farms. *Electric Power Systems Research*, 121:38–51, 2015.

[100] T. Nishikawa and A. E. Motter. Comparative analysis of existing models for power-grid synchronization. *New Journal of Physics*, 17(1):015012, 2015.

[101] G. Oggioni, F. H. Murphy, and Y. Smeers. Evaluating the impacts of priority dispatch in the european electricity market. *Energy Economics*, 42:183–200, 2014.

[102] B. Pal and B. Chaudhuri. *Robust control in power systems*. Springer Science & Business Media, 2006.

[103] A. Papavasiliou and S. S. Oren. Stochastic modeling of multi-area wind production. In *12th International Conference on Probabilistic Methods Applied to Power Systems*, 2012.

[104] A. Papavasiliou and S. S. Oren. Multiarea stochastic unit commitment for high wind penetration in a transmission constrained network. *Operations Research*, 61(3):578–592, 2013.

[105] A. Papavasiliou, S. S. Oren, and R. P. O'Neill. Reserve requirements for wind power integration: A scenario-based stochastic programming framework. *IEEE Transactions on Power Systems*, 26(4):2197–2206, 2011.

[106] A. Papavasiliou, S. S. Oren, and B. Rountree. Applying high performance computing to transmission-constrained stochastic unit commitment for renewable energy integration. *IEEE Transactions on Power Systems*, 30(3):1109–1120, 2015.

[107] Patrick J. Kiger. Blackouts: A history. National Geographic: `http://channel.nationalgeographic.com/american-blackout/articles/blackouts-a-history/`, 2013. [Online; accessed Aug-2017].

[108] G. Patsakis, I. Aravena, and S. Oren. Black Start Allocation for Power System Restoration Data. Zenodo. http://doi.org/10.5281/zenodo.3842167, May 2020.

[109] G. Patsakis, I. Aravena, and D. Rajan. A stochastic program for black start allocation. In *Proceedings of the 52nd Hawaii International Conference on System Sciences*, 2019.

[110] G. Patsakis, P. Karamanakos, P. Stolze, S. Manias, R. Kennel, and T. Mouton. Variable switching point predictive torque control for the four-switch three-phase inverter. In *2013 IEEE International Symposium on Sensorless Control for Electrical Drives and Predictive Control of Electrical Drives and Power Electronics (SLED/PRECEDE)*, pages 1–8. IEEE, 2013.

[111] G. Patsakis, S. Nanou, and S. Papathanassiou. Fault ride through of VSC-HVDC connected offshore wind farms: a simplified model. *EWEA 2015 annual event*, 2015.

[112] G. Patsakis and S. Oren. A combinatorial algorithm for large-scale power system islanding. In *2019 IEEE Milan PowerTech*, pages 1–6. IEEE, 2019.

[113] G. Patsakis and S. Oren. The hidden cost of priority dispatch for wind power. In *Proceedings of the 52nd Hawaii International Conference on System Sciences*, 2019.

[114] G. Patsakis, D. Rajan, I. Aravena, and S. Oren. Strong mixed-integer formulations for power system islanding and restoration. *IEEE Transactions on Power Systems*, 34(6):4880–4888, 2019.

[115] G. Patsakis, D. Rajan, I. Aravena, J. Rios, and S. Oren. Optimal black start allocation for power system restoration. *IEEE Transactions on Power Systems*, 33(6):6766–6776, 2018.

[116] J. Phillips, M. Finster, J. Pillon, F. Petit, and J. Trail. State energy resilience framework. Technical report, Argonne National Lab.(ANL), Argonne, IL (United States), 2016.

[117] B. Pierpont, D. Nelson, A. Goggins, and D. Posner. The path to low-carbon, low-cost electricity grids. 2017.

[118] PJM. *PJM Manual: System Restoration*, 6 2017. Rev. 24.

[119] S. Poudel and A. Dubey. Critical load restoration using distributed energy resources for resilient power distribution system. *IEEE Transactions on Power Systems*, 34(1):52–63, 2019.

[120] Z. Qin, Y. Hou, C.-C. Liu, S. Liu, and W. Sun. Coordinating generation and load pickup during load restoration with discrete load increments and reserve constraints. *IET Generation, Transmission & Distribution*, 9(15):2437–2446, 2015.

[121] F. Qiu and P. Li. An integrated approach for power system restoration planning. *Proceedings of the IEEE*, 2017.

[122] F. Qiu, J. Wang, C. Chen, and J. Tong. Optimal black start resource allocation. *IEEE Transactions on Power Systems*, 31(3):2493–2494, 2016.

[123] D. Rehfeldt and T. Koch. Combining np-hard reduction techniques and strong heuristics in an exact algorithm for the maximum-weight connected subgraph problem. *SIAM Journal on Optimization*, 29(1):369–398, 2019.

[124] K. Ryan, D. Rajan, and S. Ahmed. Scenario decomposition for 0-1 stochastic programs: Improvements and asynchronous implementation. In *Parallel and Distributed Processing Symposium Workshops, 2016 IEEE International*, pages 722–729. IEEE, 2016.

[125] N. Saraf, K. McIntyre, J. Dumas, and S. Santoso. The annual black start service selection analysis of ERCOT grid. *IEEE Transactions on Power Systems*, 24(4):1867–1874, 2009.

[126] K. P. Schneider, E. Sortomme, S. Venkata, M. T. Miller, and L. Ponder. Evaluating the magnitude and duration of cold load pick-up on residential distribution using multi-state load models. *IEEE Transactions on Power Systems*, 31(5):3765–3774, 2016.

[127] K. P. Schneider, F. K. Tuffner, M. A. Elizondo, C.-C. Liu, Y. Xu, and D. Ton. Evaluating the feasibility to use microgrids as a resiliency resource. *IEEE Transactions on Smart Grid*, 8(2):687–696, 2017.

[128] S. Sharma. ERCOT black start enhancements. Electric Reliability Council of Texas: `http://www.ercot.com/content/wcm/key_documents_lists/108699/06._ERCOT_BlackStart_Enhancements.pptx`, 2017. [Online; accessed Aug-2017].

[129] J. Shi and J. Malik. Normalized cuts and image segmentation. *IEEE Transactions on pattern analysis and machine intelligence*, 22(8):888–905, 2000.

[130] A. Solomon, D. M. Kammen, and D. Callaway. The role of large-scale energy storage design and dispatch in the power grid: a study of very high grid penetration of variable renewable resources. *Applied Energy*, 134:75–89, 2014.

[131] Q. Spaen, D. S. Hochbaum, and R. Asín-Achá. Hnccorr: A novel combinatorial approach for cell identification in calcium-imaging movies. *arXiv preprint arXiv:1703.01999*, 2017.

[132] W. Sun, C.-C. Liu, and R. F. Chu. Optimal generator start-up strategy for power system restoration. In *Intelligent System Applications to Power Systems, 2009. ISAP'09. 15th International Conference on*, pages 1–7. IEEE, 2009.

[133] W. Sun, C.-C. Liu, and S. Liu. Black start capability assessment in power system restoration. In *Power and Energy Society General Meeting, 2011 IEEE*, pages 1–7. IEEE, 2011.

[134] W. Sun, C.-C. Liu, and L. Zhang. Optimal generator start-up strategy for bulk power system restoration. *IEEE Transactions on Power Systems*, 26(3):1357–1366, 2011.

[135] S. Takriti, J. R. Birge, and E. Long. A stochastic model for the unit commitment problem. *IEEE Transactions on Power Systems*, 11(3):1497–1508, 1996.

[136] J. A. Taylor and F. S. Hover. Convex models of distribution system reconfiguration. *IEEE Transactions on Power Systems*, 27(3):1407–1413, 2012.

[137] F. Teymouri, T. Amraee, H. Saberi, and F. Capitanescu. Towards controlled islanding for enhancing power grid resilience considering frequency stability constraints. *IEEE Transactions on Smart Grid*, 2017.

[138] P. Trodden, W. Bukhsh, A. Grothey, and K. McKinnon. MILP formulation for controlled islanding of power networks. *International Journal of Electrical Power & Energy Systems*, 45(1):501–508, 2013.

[139] P. A. Trodden, W. A. Bukhsh, A. Grothey, and K. I. McKinnon. Optimization-based islanding of power networks using piecewise linear ac power flow. *IEEE Transactions on Power Systems*, 29(3):1212–1220, 2014.

[140] A. Tuohy, P. Meibom, E. Denny, and M. O'Malley. Unit commitment for systems with significant wind penetration. *IEEE Transactions on power systems*, 24(2):592–601, 2009.

[141] N. I. A. C. (US). *Critical infrastructure resilience: Final report and recommendations*. National Infrastructure Advisory Council, 2009.

[142] K. Van den Bergh, K. Bruninx, E. Delarue, and W. Dâhaeseleer. A mixed-integer linear formulation of the unit commitment problem. *KU Leuven Energy Institute Working Paper WP EN2013-11. Online: http://www. mech. kuleuven. be/en/tme/research/energy_environment/Pdf/wpen2013-11. pdf*, 2013.

[143] L. S. Vargas, G. Bustos-Turu, and F. Larraín. Wind power curtailment and energy storage in transmission congestion management considering power plants ramp rates. *IEEE Transactions on Power Systems*, 30(5):2498–2506, 2015.

[144] J. P. Vielma. Mixed integer linear programming formulation techniques. *Siam Review*, 57(1):3–57, 2015.

[145] J. Vondrák. Optimization of submodular functions: Tutorial-lecture i. 2012.

[146] C. Wang, V. Vittal, and K. Sun. OBDD-based sectionalizing strategies for parallel power system restoration. *IEEE Transactions on Power Systems*, 26(3):1426–1433, 2011.

[147] C. Wang, B. Zhang, Z. Hao, J. Shu, P. Li, and Z. Bo. A novel real-time searching method for power system splitting boundary. *IEEE Transactions on Power Systems*, 25(4):1902–1909, 2010.

[148] D. Wang, X. Gu, G. Zhou, S. Li, and H. Liang. Decision-making optimization of power system extended black-start coordinating unit restoration with load restoration. *International Transactions on Electrical Energy Systems*, 2017.

[149] X. Wang and V. Vittal. System islanding using minimal cutsets with minimum net flow. In *Power Systems Conference and Exposition, 2004. IEEE PES*, pages 379–384. IEEE, 2004.

[150] Y. Wang, A. Buchanan, and S. Butenko. On imposing connectivity constraints in integer programs. *Mathematical Programming*, 166(1-2):241–271, 2017.

[151] L. A. Wolsey and G. L. Nemhauser. *Integer and combinatorial optimization*, volume 55. John Wiley & Sons, 1999.

[152] G. Xu and V. Vittal. Slow coherency based cutset determination algorithm for large power systems. *IEEE Transactions on Power Systems*, 25(2):877–884, 2010.

[153] B. Yang, V. Vittal, and G. T. Heydt. Slow-coherency-based controlled islanding—a demonstration of the approach on the august 14, 2003 blackout scenario. *IEEE Transactions on Power Systems*, 21(4):1840–1847, 2006.

[154] Y. T. Yang, B. Fishbain, D. S. Hochbaum, E. B. Norman, and E. Swanberg. The supervised normalized cut method for detecting, classifying, and identifying special nuclear materials. *INFORMS Journal on Computing*, 26(1):45–58, 2013.

[155] H. You, V. Vittal, and X. Wang. Slow coherency-based islanding. *IEEE Transactions on Power Systems*, 19(1):483–491, 2004.

[156] N.-P. Yu, C.-C. Liu, and J. Price. Evaluation of market rules using a multi-agent system method. *IEEE Transactions on Power Systems*, 25(1):470–479, 2010.

[157] L. Yutian, F. Rui, and V. Terzija. Power system restoration: a literature review from 2006 to 2016. *Journal of Modern Power Systems and Clean Energy*, 4(3):332–341, 2016.

[158] Y. Zhou, W. Hu, Y. Min, Q. Zhou, and M. Li. MILP-based splitting strategy searching considering island connectivity and voltage stability margin. In *Power and Energy Society General Meeting (PESGM), 2016*, pages 1–5. IEEE, 2016.

[159] R. D. Zimmerman. MATPOWER 4.0 b4 User's manual. *Power Syst Eng Res Cent*, pages 1–105, 2010.

[160] R. D. Zimmerman, C. E. Murillo-Sánchez, and R. J. Thomas. Matpower: Steady-state operations, planning, and analysis tools for power systems research and education. *IEEE Transactions on power systems*, 26(1):12–19, 2011.